ON-LINE INSTRUMENTATION FOR LATEX PRODUCTION

By

PAUL D. GOSSEN, B.A.Sc., M.Eng.

A Thesis

Submitted to the School of Graduate Studies

in Partial Fulfilment of the Requirements

for the Degree

Doctor of Philosophy

McMaster University

June 1991

components. PCA of the UV spectra was able to detect outliers among the calibration samples, whether they were anomolous latex samples or poor spectra of good latex. PCA could also detect structure in the data, clustering similar samples together on plots of the data plotted in the reduced space of the principal components.

The UV spectra were used to predict the compositions of major latex constituents and the mean particle diameter using multivariate calibrations calculated by Partial Least Squares. The models were evaluated based on their prediction error, calculated by crossvalidation. The predictions of the weight fractions of styrene monomer, poly(styrene), total styrene, and total monomer were very good: PRESS/(n-1) was between 0.09 and 0.11. The models for mean diameter were excellent (PRESS/(n-1) = 0.03) for a group of samples with narrow particle size distributions of similar breadth. For the latex with broad size distributions, the model was not significantly different from the random model. The models for water and methyl methacrylate compositions were significant, but not good enough to be used for an analyzer.

There are some points of interest in the raw instrument responses. The first is this system's exceptional immunity to noise. The spectrometer resolution was limited only by the quantization error in the analog-to-digital conversion. The second operating region was chosen because in exhibits some of the oscillations in latex properties that are characteriztic of higher solids vinyl acetate emulsion polymerizations. In this region, the densitometer was able to resolve oscillations with peak-to-peak differences of 0.0007 g/ml. The densitometer data was not filtered, and the spectrometer took a 10 second averaging filter for each data point.

All the information in Fig. 5.3.1 is used in the calculations of solids fraction and mean diameter in Fig. 5.3.2. Both these quantities are also compared to off-line analyses done on samples taken during the run. Solids fraction was measured off-line by gravimetry: drying and weighing latex samples. Volume weighted mean diameter was measured using the Nicomp 370 Dynamic Light Scattering (Section 2.3). In the calculations of the on-line results a single parameter, the density of the aqueous phase, was adjusted to bring on-line solids fraction in line with off-line gravimetry. Particle diameter was then calculated with no further parameter adjustment.

Refering to Fig. 5.3.2, on-line particle sizing results seem to exhibit much less variation than off-line dynamic light scattering. In fact, the on-line results are so stable, that the sensitivity of the particle sizer to process changes could be called into question. Later, Run 8 will provide a dramatic demonstration of the sensitivity of the technique while also pointing out that much of the variation in the volume weighted mean from DLS can be attributed to two phenomena. First the volume weighting is not the native unit of the instrument. It is calculated from the intensity weighted mean and standard deviation, and tends to be less stable than the native, intensity weighted DLS diameter. Secondly, the latex was unbuffered and somewhat unstable. Samples coagulated within days, which contributes much noise in off-line measurements. Run 8 solves this dilema by comparing on-line DLS results with on-line turbidity.

ON-LINE INSTRUMENTATION FOR LATEX PRODUCTION

DOCTOR OF PHILOSOPHY (1991)
(Chemical Engineering)

McMASTER UNIVERSITY
Hamilton, Ontario

TITLE: On-line Instrumentation for Latex Production

AUTHOR: Paul Gossen, B.A.Sc. (University of Waterloo)
M.Eng. (McMaster University)

SUPERVISORS: Prof. J.F. MacGregor
Prof. R.H. Pelton

NUMBER OF PAGES: xviii, 212

ABSTRACT

The availability of fast, reproducible on-line instrumentation plays a critical role in paving the way for improvements in the productivity and product quality of industrial processes. In the polymer latex industry, one of the primary reasons for the lack of adequate instrumentation is that the traditional on-line sensors for density, viscosity, light scattering and absorption seldom respond to only one property; instead, their response is a function of many latex properties. If, however, these sensors respond differently to latex property changes, a novel approach to instrumentation is to use information from several of them to infer several quality variables simultaneously.

This thesis applies this concept to two latex systems. The first is the continuous emulsion polymerization of poly(vinyl acetate). A density meter and the single wavelength UV turbidity of a diluted sample are used to track solids fraction and mean particle size on a pilot scale reactor. The sensor-latex property relationships are derived from a mechanistic understanding of the system. The standard deviation of the solids fraction measurement is 0.8% of value, for the mean diameter, it is 3%. The second process is the batch copolymerization of styrene and methyl methacrylate (MMA). Two spectrometers, covering a wavelength range from 190 nm to 1800 nm were used to predict the weight fractions of water, styrene and MMA monomer, poly(styrene), and poly(MMA). The standard deviations of the composition measurements were between 0.2 and 1.2 weight percent. The sensor-latex property relationships were arrived at by an empirical, multivariate calibration.

The important implications of these results are that: (1) the number of sensors that could be considered for on-line analyzers is greatly increased; and (2) this methodology may be successful for previously intractable instrumentation problems. Also, potentially any latex property that can be measured in the laboratory can be included in the calibration, provided the property of interest has a reproducible effect on the response of the sensor.

ACKNOWLEDGEMENTS

For their contributions to this thesis, I would like to thank:

my supervisors, Dr. J.F. MacGregor and Dr. R.H. Pelton, for their insight, encouragement, and help throughout;

my collegues and coworkers in the Department of Chemical Engineering, for sharing their expertise and for discussing those things not yet at that stage. In particular I would like to thank Dora Kourti, Derrik Kozub, Nassar Ali, Kim McAuley, Jim Kresta, Gord Slater and Bill Warriner.

David Nicoli for providing us with prototypes of the on-line NICOMP® particle sizer, and assisting in its operation;

the Department of Chemical Engineering and the Ontario Centre of Materials Research for their financial support, and the McMaster Institute of Polymer Production Technology for the use of the laboratories and pilot plants;

my wife, Ruth, for enduring it all.

SUMMARY AND CONCLUSIONS

The availability of fast, reproducible on-line instrumentation plays a critical role in paving the way for improvements in the productivity and product quality of industrial processes. In the polymer latex industry, one of the primary reasons for the lack of adequate instrumentation is that the traditional on-line sensors for density, viscosity, light scattering and absorption seldom respond to only one property; instead, their response is a function of many latex properties. However, if these on-line sensors respond differently to latex property changes, a novel approach to instrumentation is to use information from several of these nonspecific sensors to infer several quality variables simultaneously.

This thesis successfully applies this concept to two latex systems. The first is the continuous emulsion polymerization of poly(vinyl acetate). A density meter and the single wavelength UV turbidity of a diluted sample are used to track solids fraction and mean particle size. The relationships between the sensor responses and the properties of the latex are derived from a thorough, mechanistic understanding of the phenomena involved. The second process is the batch copolymerization of styrene and methyl methacrylate (MMA). Ultraviolet and near-infrared spectra were used to predict the weight fractions of water, styrene monomer, MMA monomer, poly(styrene), and poly(MMA). In this case, the relationships between the sensor responses and the latex properties were arrived at by an empirical, multivariate calibration.

In the case of vinyl acetate homopolymer, Mie theory gives a relationship between the specific turbidity of the latex sample and the weight average of the particle size distribution. The

specific turbidity is the turbidity divided by the mass of polymer in the sample. What is required from an on-line instrument based on this theory, then, is a measurement of the polymer fraction in a diluted latex sample, and the UV turbidity at one wavelength for that diluted sample. Chapter 3 outlines the design, construction, and testing of an analyzer system based on the specific turbidity.

The solids fraction of the latex is calculated from a mass balance around the reactor, and an on-line measurement of the density of the latex. Density of latex is measured with a vibrating U-tube densitometer. Linear temperature compensation is sufficient to compensate for temperature variation from 18 to 26°C. The standard deviation of the density measurement is 0.89×10^{-4} g/ml. To calculate solids fraction from a density measurement on a continuous reactor, these properties of the latex must be known: density and inlet concentration of all constituents in the feed streams; all feed flow rates; polymer density. The density of the aqueous phase is difficult to characterize, so it was chosen as the adjustable parameter used to align solids fraction from densitometry to laboratory results from gravimetric determinations.

The turbidity must be measured on a dilute latex sample for the relationship between turbidity and mean diameter to be valid. The dilution ratio must be known and reproducible so that the polymer fraction information measured in the concentrated latex stream is preserved. A sampler-diluter was designed and constructed to extract a latex sample from the process stream, dilute it by a known amount, then send the diluted latex to a spectrometer. Accurate dilution metering was achieved by using a sampling valve that sampled reproducible volumes, then diluting it in a tank in which the total volume of sample plus diluent was carefully metered. The standard deviation of the dilution ratio was measured as 2.34×10^{-4}.

Incomplete mixing in the metering tank is an issue that still needs to be addressed. Early prototypes included a stirrer in the mixing tank, but that was eliminated to streamline the design for in-plant installation. Using an L/D ratio of 3 for the tank and improving the distribution of diluent while the tank fills helps, but does not eliminate, the problem.

Since the relationship between the sensor responses and the latex properties known for this turbidity particle sizer, a detailed error propagation analysis can be carried out once the important sources of variation are quantified. Case studies reported in Chapter 4 show that the standard deviation in solids fraction is 0.7 to 0.9%. In general, the error associated with the density measurement decreases with increasing solids, whereas the contribution from mass balance uncertainty increases with increasing monomer fraction. The monomer conversion standard deviation is over 10%, almost exclusively as the result of mass balance uncertainty. The mean diameter relative error is 3%. The largest contribution is from uncertainty in the dilution ratio of the sampler-diluter.

In Chapter 5, the above on-line particle size analyzer is tested during several runs on a pilot scale continuous reactor producing poly(vinyl acetate) latex. The experimental runs confirm the accuracy and reproducibility of the on-line solids fraction and particle sizing analyzer. They also demonstrate the advantages of automated on-line measurements over off-line laboratory analysis, and the stable operation and flexibility of a continuous seed latex reactor. The experimental runs encompass operating regions that produced seed latexes with a mean particle diameter of 70 to 210 nm at 7 to 15% solids. Each of the runs included changes in the operating conditions to evaluate the ability of the analyzers to follow process changes. Some of the observations made from the pilot plant experiments are:

1) The sampler/diluter operated continuously for 100 cycles at 5 minute intervals without any problems. To date, it has operated flawlessly for over 500 cycles without need for maintenance.

2) The one adjustable parameter used to align on-line solids fraction measurements with off-line gravimetric determinations was sufficient to allow on-line solids to track the off-line determinations within one run. Large changes in the reactor conditions between runs required changes in the adjustable parameter.

3) On-line mean diameter measurements from turbidity were verified either by off-line or simultaneous on-line Dynamic Light Scattering measurements. When mixing in the dilution tank is good, the mean particle diameter can be calculated from dilute transmittance without resorting to any additional adjustable parameters once the solids fraction in the concentrated latex is known. In runs where there was no mixing in the dilution tank, poor mixing resulted in a constant bias in the transmittance readings that was compensated for by using the transmittance path length as an adjustable parameter.

4) On-line particle sizing by turbidimetry resolved step changes in mean diameter on the order of 10 nm. Off-line particle sizes by DLS consistently showed higher variance than on-line results, but on-line particle sizes by DLS and turbidity have comparable variances.

The remainder of the thesis focuses on more complex, copolymer latex systems. In these systems, the compositions of the major polymer constituent must be known in addition to the solids fraction and particle diameter. The methodology employed is the multivariate calibration of optical spectra. The relationship between the sensor responses and the latex properties is empirically determined. This has the very important implication that transducers can be used even when the complete sensor-property relations are not known, and that any sensor can be used, as long as it responds reproducibly to the changes in the properties of the latex. Two spectrometers were evaluated. They covering a wavelength range from 190 nm in the ultraviolet, to 1800 nm in the near-infrared.

For the multivariate calibration, a set of latex samples was made with a range of property variations. The properties of these samples must be carefully characterized, and the optical spectra are measured by the analyzers. Principal Component Analysis and Partial Least Squares are then used to construct an outlier detection and calibration model that can predict the properties of the latex from the optical spectrum.

In Chapter 8, ultraviolet/visible light spectra from 190 to 820 nm are evaluated as a technique for measuring composition and particle diameter in a styrene/methyl methacrylate latex. In this region of the optical spectrum, the latex constituents absorb only below 350 nm. The absorption peaks overlap, and their maxima tend to shift depending on the molecular environment of the constituent. Furthermore, light scattering is an important and very nonlinear mechanism for the attenuation of the incident beam.

Two data sets are analyzed. Calibration Set A has small particles, around 30% solids. Calibration Set B has larger particle with a broader distribution, around 50% solids. The latex is

diluted 1/2000 and 1/20,000 to make the 10 mm thick samples transparent to the spectrometer beam, and to ensure a linear relationship between the turbidity ($\ln(1/T)$) and the polymer concentration in the non-absorbing region (>350 nm) of the spectrum. Principal Component Analysis (PCA) then reduces the high dimensional, colinear space of UV absorbances to a smaller dimensional, more easily interpreted set of variables. Over 98% of the variance in the original data could usually be explained by the first 2 or 3 principal components. PCA of the UV spectra can detect outliers among the calibration samples, whether they are anomalous latex samples or poor spectra of good latex. PCA also detects structure in the data, clustering similar samples together on plots in the reduced space of the principal components.

The UV spectra are used to predict the compositions of major latex constituents and the mean particle diameter using multivariate calibrations calculated by Partial Least Squares. The models are evaluated based on their prediction error, calculated by crossvalidation. The weight fractions of styrene monomer, poly(styrene), total styrene, and total monomer are predicted very well: prediction error standard deviations are between 0.2 and 0.5 weight percent. The models for mean diameter are very good only for Calibration Set A, the group with narrow particle size distributions of similar breadth. Water and methyl methacrylate compositions were not well predicted for any samples by the UV spectra.

Chapter 9 reports on results of multivariate calibration of NIR spectra. Spectra are taken with a transflectance fibre optic probe with a 3 mm gap in the range 900 to 1800 nm. Calibration Set A is translucent for this optical path length of 6 mm. PLS calibration models of the NIR spectra of Set A yield excellent predictions of mean particle diameter, and of the concentrations of all the major components (water, poly(styrene), poly(MMA), styrene, MMA).

Calibration Set B is opaque to the NIR spectrometer probe with a path length of 6 mm, so only light scattered by the sample reaches the detector. PLS calibration models of the NIR spectra

of Set B are very poor. When the latex is diluted by a factor of 100 to make it more transparent, The resulting calibration models for water and total styrene are good because of the high molar absorbance of these species, but none of the other models gives better prediction.

A third, small calibration set made up of commercial poly(styrene-butadiene) latex was evaluated using the NIR spectrometer with a transflectance fiber optic probe with a 1 mm gap. This latex is similar to Calibration Set B. Light could be transmitted through the 1 mm gap, increasing the amount of light received at the detector. The PLS calibration models give good results for poly(styrene) prediction, but poor results for particle diameter. The results imply that NIR spectrometer can be used for measuring concentration of bulk constituents in latex provided that the signal-to-noise ratio is adequate. For industrial applications, the solutions that should be pursued include increasing the light transmitted to the sample and the reflected light collected from the sample by using more fibres in the fibre bundle between the spectrometer and the probe. Detector configurations that maximize the reflected light collected from the sample should also be investigated.

Chapter 10 examines methodologies for combining some of the sensors discussed above to improve their predictive performance. A multiblock variant of the Partial Least Squares (PLS) algorithm is compared to methods based on the more familiar PLS1. First, the multiblock PLS method is shown to be a convenient framework for comparing competing PLS models, although it is sensitive to the scaling of the data. Then, UV and NIR spectra of Chapters 8 and 9 are combined using both multiblock PLS and ordinary PLS1. The predictive performance of the calibrations does not improve, and tends to be worse than the better of the two spectrometers. Contrary to expectation, combining UV spectra with density did not yield better predictions for either mean diameter or styrene concentration. Combining NIR spectra with density did yield better prediction of the water content of the latex, but this was not at a statistically significant level with the small

sample size used for this study. The conclusion of this chapter is that, in a multivariate calibration framework, if two sensors give very similar information about a sample, combining the data from both the sensors will not give better results than using the better of the two alone.

In summary, this work shows that multivariate sensors can be combined in either a mechanistic or empirical framework to measure properties of a latex that would otherwise be very difficult or impossible to measure on-line. The empirical framework is well suited to dealing with very complex and nonlinear relationships between the sensor response and the latex properties that need not be completely described by a mechanistic relationship. The important implications of this are: (1) the number of sensors that could be considered for on-line analyzers is greatly increased; and (2) the methodology may be successful for previously intractable instrumentation problems. Finally, potentially any latex property that can be measured in the laboratory can be included in the calibration, provided the property of interest has a reproducible effect on the response of the sensor.

Table of Contents

Table of Tables

Table of Figures

1

INTRODUCTION

The shifts in global economic power during the last decades have made it increasingly clear that the long term economic health of a nation is strongly tied to the global competitiveness of that country's manufacturing industries. The focus of that competitiveness is the ability of manufacturing industries to add value to basic raw materials quickly and efficiently, with low cost and high quality. For the modern manufacturer, efficiency and quality are the paramount concerns. The need for very high efficiency is being driven by concern for the global environment, and the quest for quality, by the fiercly competitive, global marketplace.

Achieving these objectives requires a fundamental understanding of the industrial processes involved, and the ability to control these processes. In the chemical industry, both these criteria hinge on the availability of technology to monitor the important variables that affect the quality of the product and productivity of the process. Polymer production, unfortunately, is notorious for poor product quality control because of insufficient understanding of the fundamental chemistry and the difficulty in monitoring most of the important quality variables on-line. Most measurements of quality variables require expensive and time consuming laboratory tests, involving long delays between the time a measurement is taken and the time the measurements are returned to the plant operators. These long deadtimes greatly hamper the ability of operators or control computers to make timely adjustments in the process conditions to get product quality back on target once off.

Beyond improving the performance of existing polymerization processes, the availability of a fast, reproducible on-line analyzer technology would help in overcoming a major stumbling

block in the move from batch processes to the efficiency and sophistication of continuous reactor technology. The need for on-line instrumentation is dictated by the higher productivity and increased variability and complexity of continuous processes.

Obviously, then, the absence of on-line instrumentation is a major stumbling block to monitoring quality, to developing feedback control, and to improving the sophistication of process technology in the polymerization industry.

1.1 On-Line Instrumentation

The distinction between on-line analyses and those typical of a quality control or analytical laboratory is an important one. First, since the aim is to use the on-line analyzer in a feedback loop, the entire system must be automated, operating without human intervention. As a result, all analyzer systems are composed of three parts: (1) a sampler, which takes a sample of the process; (2) a transducer, which translates the physical properties of the process sample into useable data; and (3) data analysis, to get relevant information from the data.

Although writers differ on the criteria for the design of an analyzer system, they (Smith and Klie, 1976; Davis, 1990; Care-Brion, 1990; Trop, 1989) are unanimous in their assertion that the number one priority is analyzer system reliability. This takes precedence over reproducibility, sensitivity, accuracy, and cost. The concept of reliability is best grasped by articulating what contributes to analyzer system failure. Trop (1989) reports a survey of AT&T production engineers. They ranked reliability as the most important feature for an on-line system, and said that the following contributed to poor reliability: (1) frequent re-calibration; (2) frequent routine maintenance; (3) complexity; (4) difficult to troubleshoot problems. Davis (1990), writing on his experience with ICI Chemicals and Polymers, also stresses reliability. There are two classes of analyzer failure, he says: those to do with hardware, and those to do with people. Of the hardware

problems, poor analyzer design, complexity, and poor sampling ranked highly. People problems involved lack of training and commitment, or a shortage of technicians. These can be linked back to complexity, the need for frequent maintenance, or difficulty in troubleshooting problems.

With this background, it is easier to see why there is a conspicuous absence of on-line analyzers in polymer - and particularly in latex - production. Implementation is fraught with series of roadblocks in each of the three analyzer subsystems: sampling, transducers, and data analysis. Much of the difficulty has to do with the nature of latex itself.

1.2 Latex

Water based polymer latexes are the basis for a wide array of products such as paints, adhesives, and rubber. Latex is a suspension of submicron polymer particles in water. The particles are typically between 200 and 1000 nm, and the solids fraction can range anywhere from 25 to 60% by weight. There are many advantages to producing polymers in latex form. Latex viscosity is independent of polymer molecular weight, so high molecular weight polymer can be produced and the suspension still have the viscosity of water. The water acts as a heat transfer medium for highly exothermic polymerization reaction, and the low viscosity enhances heat transfer, even at high conversion. This helps in cooling the highly exothermic polymer reactions.

In many cases, the latex is used as is in coating or adhesive applications, or when the polymer is to be mixed with water based slurries, as in many paint, paper, or construction material applications. In rubber production, the polymer in the latex is coagulated and the water dried off to produce the final product. Because latex is a water based process, the cost, safety, and environmental drawbacks of using organic solvents in the polymerization process are avoided. This provides much impetus for continued research into new applications for latexes.

The simplest recipes for the production of latex call for monomer and water, a water soluble initiator, and an emulsifier. When the reactants are heated to the reaction temperature, the initiator dissociates into free radicals, starting the reaction. The emulsifier serves the triple purpose of: (1) emulsifying the monomer in the water phase; (2) forming micelles that are the locus for particle nucleation during the reaction; and (3) stabilizing the resulting polymer particles. Most latex recipes also call for other components in small amounts to act as pH modifiers for enhanced stability and various electrolytes for viscosity modification.

Many properties affect the final performance of the latex in its chosen application. The ones focussed on in this thesis are: particle size distribution; solids fraction; fraction monomer conversion; and, in copolymer systems, the composition of copolymer. The particle size distribution greatly affects the polymerization rate, latex stability and viscosity, and processing variables like film forming properties. Solids and monomer fraction are important variables in the productivity of the process; while copolymer composition is critical in determining the properties of the polymer itself.

Some of the challenges facing the development of on-line analyzers are now more easily understood. First, latex is a very complex system: not only can several monomers and their copolymers be present, but they are dispersed in water with much surfactant present. The monomer can be in any of the several phases: in the water; in polymer particles; or, early in the polymerization, in a monomer droplet phase. The particles in a latex system are small relative to the wavelength of light, making them very effective scatterers, which accounts for the characteristic opaque, milky white appearance of latex. Thus, the response of most conceivable sensors can result from simultaneous changes in several latex properties. In the past, this has severely limited the combination of latex process and sensor transducers that were amenable to on-line analyzer applications. This aspect of the problem is discussed below; but another, more basic problem is often responsible for the failure to implement on-line analyzers for latex systems: that of sampling a process stream which has often been designed primarily to coagulate, coat, form films, or adhere to surfaces.

1.3 Sampling

Though seldom an area of research, sampling is a critical concern for industrial applications. Davis (1990) reports that 85% of analyzer breakdowns are the fault of the sampling system. Sampling and sample conditioning is the part of the analyzer system that isolates some hopefully representative part of the process stream and does the gross preparations, like filtering and degassing, to make the sample acceptable for the more sensitive transducers.

Sampling is broadly lumped into two categories: *in situ* and extractive. While *in situ* implies that the sensing element is in direct contact with the process steam, it does still sample only a small fraction of that stream. In fact, in the case of optical probes, which have an energy penetration of only a few millimeters in some latexes, the *in situ* probe may even take a less representative sample than an extractive system. Extractive systems, on the other hand, are costlier and may be more maintenance intensive. In either case, latexes are the bane of any sampler because of their tendency to coat, adhere, or coagulate in a shear field. The issue of sampling, therefore, cannot be ignored in any proposed design of an analyzer system for latex.

1.4 Multivariate, Nonspecific Sensors

Aside from sampling, another one of the primary reasons for the lack of adequate instrumentation for latex systems is the complexity of the polymer systems themselves. The traditional on-line sensors for density, viscosity, and light attenuation seldom respond to one quality variable; instead, their response is a function of many of the latex sample properties. In cleaner chemical processes, this problem is often overcome by effecting a physical separation of the product constituents, as in chromatography. That solution, however, is impractical in latex systems for the same reasons that have hamstrung the design of on-line samplers: the polymer quickly plugs the apparatus, necessitating frequent cleaning and maintenance.

Fortunately, all of the above on-line sensors will respond differently to latex property changes. A novel approach to instrumentation, therefore, is to use information from several nonspecific sensors to infer several product properties simultaneously. The first benefit of this approach is that the sensors can now be chosen with a stronger emphasis on those criteria which would ensure their success in a process environment: robust construction, ease of operation, simplicity, safety, and low cost. The deconvolution of sensor data is no longer done at the sampling stage nor at the transducer; instead, it is deferred to the data analysis stage.

The interpretation of the data from multiple sensors can be accomplished in two ways. In simple, single monomer systems, a tractable theoretical relationship between the sensor response and the properties of interest may exist. The sensor response can then be simply combined in a set of simultaneous equations and the underlying latex properties calculated. For more complex copolymer latexes, fundamental sensor-property relations are often intractable. Here, we resort to empirical, multivariate calibration models. The sensor-property relation is built up empirically using a number of samples that have been carefully characterized in the laboratory. This is an attractive approach for a number of reasons. Recent developments in multivariate calibration techniques allow very large, collinear measurement vectors to be used in the empirical modelling; so, at least theoretically, the number of sensors that can be used is unlimited. This paves the way for the use of optical spectrometry, since there are now, commercially available, spectrometers that can scan large wavelength ranges. Optical spectrometers provide one of the most cost effective ways of getting a large number of sensor responses for a sample, and are a frequent candidate for on-line sensors because of their robustness, mechanical simplicity, and non-intrusiveness. Scanning spectrometers are capable of delivering absorbance readings at hundreds of wavelengths from the ultraviolet to the near infrared quickly and economically. Finally, potentially any quality variable or latex property that can be measured in the laboratory can be included in the calibration. All that is required is that the property of interest has a measurable effect on the response of at least one of the sensors.

1.5 Scope of This Work

The principal aim of this work is to develop and evaluate analyzers for important bulk properties in latex production. The approach taken is to select transducers that are already successfully applied in on-line environments and attempt to apply them, or combinations of them, to latex systems. The sensors used are a vibrating U-tube densitometer, a scanning ultraviolet spectrometer (190 to 820 nm), and a scanning near-infrared spectrometer (900 to 1800 nm).

The issue of sampling is addressed. An extractive sampler/diluter is designed, built, and tested for dilution of samples for the UV spectrometer. The NIR spectrometer uses a fibre optic probe to bring light to and from the samples. It is the data analysis step, however, that distinguishes latex applications from many conventional on-line analyzer applications. This thesis is divided into two parts, differentiated by the treatment of the transducer data.

Chapters 2 to 5 deal with the analyzers for production of vinyl acetate homopolymer latex. The transducer responses are related to the latex particle size, monomer conversion, and solids fraction by mechanistic relationships. Chapter 2 discusses the theory relating the transducer responses and these latex properties. Chapter 3 outlines the design and testing of an on-line, extractive sampler/diluter that dilutes the latex before it goes to the UV spectrometer. Chapter 4 gives a detailed error propagation analysis of the entire analyzer system, showing most of the critical sources of variation in the analyzer system. The sampler/diluter was designed to minimize variation wherever possible; nonetheless, the analysis points to some potential weaknesses of this mechanistically based analyzer systems. Chapter 5 reports the results of several continuous poly(vinyl acetate) seed reactor pilot scale runs with monomer conversion and particle size being measured on-line.

Chapters 6 to 10 cover analyzers for the copolymerization of styrene and methyl methacrylate. Here, the transducer responses are related to latex particle size, monomer conversion, solids fraction, and copolymer composition by empirical, multivariate models.

Chapter 6 discusses some basic theory of optical spectrometry and multivariate calibration. Chapter 7 explains in detail how the samples used in the calibration set were designed, made, and characterized. Chapter 8 reports the results of using the UV spectrometer as a sensor for the properties of the latex, and Chapter 9 does the same for the NIR spectrometer. Chapter 10 briefly discusses how the densitometer and the UV and NIR spectrometers could be combined to estimate the latex properties.

2

PARTICLE SIZING BY LIGHT SCATTERING: BACKGROUND AND THEORY

2.1 Particle Sizing from Turbidity

Turbidity is one of the easiest measurements to make in either a laboratory or plant environment. It involves measuring the attenuation of a beam of light through a sample, and requires only the most basic, single wavelength spectrometer. Because suspended particles scatter the incident light in all directions, the intensity of the scattered light can be measured at any angle in turbid media. The term turbidity, however, generally refers to the attenuation measured at 180° to the incident beam, .

Elucidation of the mechanisms and theoretical description of light scattering occupied some of the greatest experimental and theoretical physicists of the 19th century. The culmination of this effort was a completely general mathematical solution of the light scattering phenomenon around the turn of the century. Although usually ascribed to Mie, the solution was arrived at independently by many European physicists between 1890 and 1920 (Kerker, 1969).

The potential of using light scattering to measure the size of small particles was recognized very soon after the earliest theoretical description of the phenomenon by Rayleigh in 1871 (Kerker, 1969). The phenomenon was first applied to particle sizing in polymer colloids by Heller and coworkers (1957a, 1957b). They were also the first to propose using solutions to the light scattering function to estimate the parameters of the particle size distribution of a polydispersed colloid (Stevenson and coworkers (1961), Wallach and coworkers (1961)). Since then, turbidity

measurements have been used to measure particle size distributions with mixed success. Heller's group's exhaustive, and successful, experimental and theoretical studies were based on poly(styrene) latex with a refractive index 1.2 times that of water. That was a fortunate choice. Poly(vinyl acetate) latex, whose refractive index is only 1.1 times that of water, has been the source of many unsuccessful applications: Maxim and coworkers (1969) showed that for poly(vinyl acetate), the estimates of the parameters of the particle size distribution are so highly correlated as to be meaningless; Kiparissides (1978) calculated particle size distributions using turbidity at 7 wavelengths and did not get agreement between light scattering and liquid exclusion chromatography results; Zollars (1980) used an on-line instrument to show that turbidity tracked monomer conversion in a batch reactor, but did not yield any particle diameters that could be confirmed by some alternate technique.

Kourti (1989) finally resolved some of the theoretical problems surrounding the technique, showing that for particles like poly(vinyl acetate) with a low refractive index ratio, turbidity techniques can give a mean of the distribution, but can not be used in general to estimate the parameters of a particle size distribution. She got excellent agreement between mean diameters from turbidity, dynamic light scattering, electron microscopy, and hydrodynamic chromatography. The treatment below outlines the general theory for estimating particle size distributions from turbidity spectra, but focusses on Kourti's solution of the problems encountered when refractive index ratios approach unity.

In a dilute suspension of spherical particles with size distribution f(D), time average turbidity τ is given by:

$$\tau = -\frac{\ln(T)}{l} = N\int_0^\infty Q_{ext}\frac{\pi D^2}{4}f(D)dD \qquad (2.1.1)$$

where T is the measured transmittance, l the optical path length, N the number of particles per unit volume, and D the particle diameter. Q_{ext} is the light energy scattered per unit cross-sectional area

of a sphere, and is called the extinction coefficient. Q_{ext} can be calculated from rigorous Mie theory (van de Hulst (1957), Kerker (1969)) and is a complex function of two dimensionless ratios: (1) the refractive index of the sphere to that of the medium in which they are suspended,

$$m = \frac{n_p}{n_m} \tag{2.1.2}$$

and (2) the diameter of the spheres to the wavelength of the incident light in the suspending medium.

$$\alpha = \frac{\pi D}{\lambda_m} \text{ where } \lambda_m = \frac{\lambda_o}{n_m} \tag{2.1.3}$$

Wiscombe (1978, 1986, 1988) provides efficient, well documented and well tested computer code to calculate Q_{ext}. His code was used for the Q_{ext} calculations in this work.

Equation 2.1.1 cannot yet, however, be used to calculate particle size. The number concentration of particles, N, is still unknown and not at all easily measured. Two frequently used ways of circumventing this problem are to use either specific turbidity or turbidity ratios.

2.1.1 Specific Turbidity

The mass concentration of the polymer in suspension is given by:

$$C = N\rho_p \int_0^\infty \frac{\pi D^3}{6} f(D)dD \tag{2.1.1.1}$$

where ρ_p is the density of the polymer particle. The ratio of equation 2.1.1 to 2.1.1.1 is called specific turbidity, and can be rewritten:

$$\frac{\tau\rho_p}{C} = \frac{3\int_0^\infty Q_{ext} D^2 f(D)dD}{2\int_0^\infty D^3 f(D)dD} \tag{2.1.1.2}$$

The specific turbidity is independent of particle number concentration. Now, if τ and C are measured and the physical properties ρ_p, α, and m known, only parameters related to the size distribution remain to be estimated.

Many researchers (Wallach, Heller and Stevenson (1961), Kerker (1969), Zollars (1980), Kourti (1989)) choose the two parameter log-normal distribution to describe latex systems. In principle, a minimum of two measurements of specific turbidity at two wavelengths would allow us to solve equation 2.1.1.2 for the parameters of the distribution. As mentioned before, however, in cases where the refractive index ratio m is low the estimates of the parameters of a distribution are so highly correlated as to be meaningless (Maxim and coworkers (1969), Kourti (1989)). Poly(vinyl acetate), with $m = 1.1$, is such a case. Poly(styrene), with $m = 1.2$, is not. Nonetheless, turbidity can still yield important information for a poly(vinyl acetate) suspension if the following approach is used.

Monodispersed Approximation

For a monodispersed suspension, equation (2.1.1.2) becomes

$$\frac{\tau\rho_P}{C} = \frac{3Q_{ext}}{2D_m} \qquad (2.1.1.3)$$

where the subscripted diameter D_m indicates that this is a monodispersed approximation of a polydispersed colloid. Consider an exponential approximation for the Mie extinction coefficient at constant refractive index:

$$Q_{ext} = k_0 D^{\gamma-2} \qquad (2.1.1.4)$$

Substituting this approximation into equation (2.1.1.3) gives

$$\frac{\tau\rho_P}{C} = \frac{3}{2} D_m^{\gamma-3} \qquad (2.1.1.5)$$

Substituting the same approximation into equation (2.1.1.2) for specific turbidity of a polydispersed colloid gives

$$\frac{\tau\rho_P}{C} = \frac{3\int D^y f(D)dD}{2\int D^3 f(D)dD} \qquad (2.1.1.6)$$

Comparing the preceding expressions:

$$D_m^{y-3} = \frac{\int D^y f(D)dD}{\int D^3 f(D)dD} \qquad (2.1.1.7)$$

The important result of this expression is that, if the exponent y is roughly constant over the range of particle sizes in the suspension, the diameter calculated by the monodispersed approximation is related directly to the "$y3$" mean of the distribution.

Diameter Exponent

All that remains is to calculate the exponent y. The two limiting cases of very small and very large particles are easily calculated. For very small particles, Rayleigh scattering theory gives

$$Q_{ext} = \frac{8}{3}\left(\frac{m^2-1}{m^2+2}\right)\alpha^4 \qquad (2.1.1.8)$$

so $y = 6$. For very large particles, Q_{ext} is 2, so $y = 2$. Between these extremes, y is calculated by taking the logarithm of equation (2.1.1.4) and differentiating w.r.t. diameter:

$$\frac{d\ln(Q_{ext})}{d\ln(D)} = \frac{d\ln(Q_{ext})}{d\ln(\alpha)} = y - 2 \qquad (2.1.1.9)$$

The left side of this expression is easily calculated numerically from the subroutines used to calculate Q_{ext}. The results of this calculation are shown in Fig. 2.1.1. Kourti (1989) noted that for $m = 1.1$, $y = 4$ over a wide range of α characterizing submicron polymer latex if the incident beam has $\lambda_o = 400$ to 600 nm. Equation (2.1.1.7) then becomes

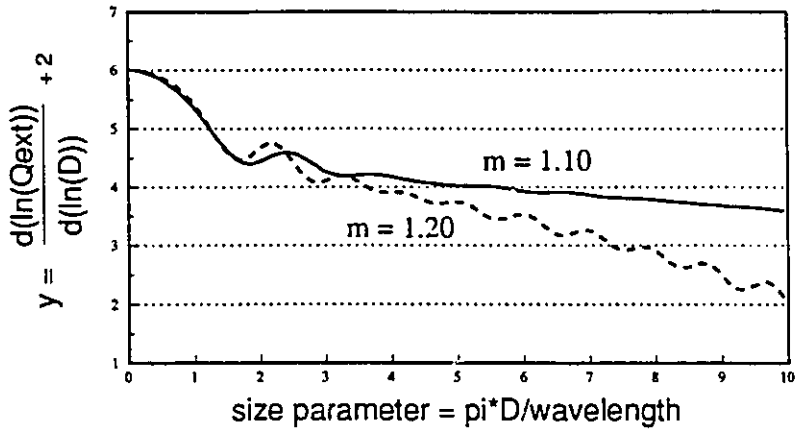

Fig. 2.1.1: Diameter Exponent y vs. Mie Size Parameter

$$D_m = \frac{\int D^4 f(D) dD}{\int D^3 f(D) dD} \qquad (2.1.1.10)$$

with the important result that, if the specific turbidity of the latex is measured at a single wavelength between 400 and 600 nm, D_m will give the weight average ($\overline{D}_{43}$) of the particle size distribution.

An interesting footnote to this discussion: the property of a system that makes it impossible to solve for the parameters of a particle size distribution is the same one that allows us to use the monodispersed approximation discussed above. Choosing different wavelengths at which to do the turbidity measurements simply changes the upper limit of α to which equation (2.1.1.6) is integrated. If the exponent y remains relatively constant throughout the applicable range of α changing the integration limits does not change the functional form of the integral. In other words, turbidity measurements at additional wavelengths give no additional information about the particle size distribution, accounting for the highly correlated estimate of distribution parameters recounted in the literature.

2.1.2 Turbidity Ratio

A second, more obvious way to get around the concentration dependence of equation (2.1.1) is to take the ratio of two turbidities measured at two different wavelengths.

$$\frac{\tau_1}{\tau_2} = \frac{\int_0^\infty Q_{ext,1} D^2 f(D) dD}{\int_0^\infty Q_{ext,2} D^2 f(D) dD} \qquad (2.1.2.1)$$

If $f(D)$ is a two parameter distribution, a minimum of two turbidity ratios would be needed to estimate the parameters. This requires three turbidity measurements at different wavelengths and was, in fact, the approach first taken by Stevenson and coworkers (1961) and Wallach and coworkers (1961). It still receives some attention in the literature (Garcia-Rubio, 1989).

This technique is subject to the same pitfalls as the specific turbidity technique when the refractive index ratio m approaches 1.0 (Kourit, 1989). To illustrate the reason for this, substitute the approximation of Q_{ext} in equation (2.1.1.3) into the above equation for turbidity ratio:

$$\frac{\tau_1}{\tau_2} = \frac{\int_0^\infty D^{y_1} f(D) dD}{\int_0^\infty D^{y_2} f(D) dD} \qquad (2.1.2.2)$$

Section 2.1.1 already explained that the exponent y is roughly constant over a large range of particle sizes for $m = 1.1$ when $\lambda_o = 400$ to 600 nm. This means that the turbidity ratio is approximately unity and, in the range of normally encountered experimental error, will yield no information on the particle size (Kourti, 1989). This major pitfall of the turbidity ratio technique for a large number of polymer latexes (including poly(vinyl acetate)) was the reason that the particle sizer designed in this work was based on the specific turbidity method.

2.2 Polymer Concentration from Density

Recall that the specific turbidity technique of particle sizing requires a measurement of the mass concentration of particles in a dilute latex suspension. The most convenient way to do this on-line is to measure the polymer concentration in concentrated latex and then dilute very accurately.

The theory for relating density to the extent of reaction in a system with a single reacting component is well known (Levenspiel, 1972). These ideas were first applied to monitoring latex reactors by Schork and Ray (1981) who demonstrated the technique with an on-line densitometer on a batch reactor. The equation they used for conversion, x, as a function of density is

$$x = \frac{v_0 - v_x}{v_0 - v_1} \qquad (2.2.1)$$

where $v_x = 1/\rho_x$ is the specific volume of the latex as measured by the densitometer. v_0 and v_1 are the specific volumes of the reactor contents at 0 and 100%, respectively. These can either be measured experimentally, or they can be calculated from

$$v_0 = X_o v_m + v_k \tag{2.2.2}$$

$$v_1 = X_o v_p + v_k$$

where X_o is the mass fraction of monomer in the reactor at $x = 0$, v_m and v_p are the specific volumes of monomer and polymer, respectively, and v_k is the specific volume of the constituents which do not change density on reaction. The mass fraction of polymer is then simply:

$$X_p = xX_o \tag{2.2.3}$$

When this technique is applied to a continuous reactor not at steady state, the contents of the reactor must be calculated using a dynamic mass balance. These calculations are outlined in detail in Chapter 3.

2.3 Particle Sizing by Dynamic Light Scattering

Dynamic Light Scattering (DLS) is another submicron particle sizing technique based on light scattering. It also goes by the names Photon Correlation Spectroscopy and Quasi-Elastic Light Scattering. It is discussed here because it the technique against which on-line turbidity is compared in this thesis. Aside from the advantage of experimental simplicity, the calculated particle diameter is independent of particle refractive index, concentration, and density. A prototype on-line DLS particle sizer (NICOMP Particle Sizing Systems) was used in parallel with turbidity in one experimental run. DLS, therefore, serves as a meaningful benchmark against which to compare a turbidity based instrument. The theoretical development below follows that of Stock and Ray (1985) with minor changes to accommodate the notation already introduced in this Chapter.

DLS differs from classical light scattering in that it measures the time variations of the scattered light caused by Brownian diffusion of the particles. These fluctuations can be observed if a dilute latex sample is illuminated with a laser beam, and a detector is placed at 90° to the incident beam. This detector is connected to a digital autocorrelator that records the intensity autocorrelation function:

$$G^{(2)}(t') = \lim_{N\to\infty}\left\{\frac{1}{N}\sum_{i=1}^{N} I(t_i)I(t_i+t')\right\} \tag{2.3.1}$$

$I(t_i)$ and $I(t_i+t')$ are the scattering intensities at times t_i and t_i+t', respectively. $t' = j\Delta t'$ is the time difference, with $\Delta t'$ corresponding to the time lag between correlator channels, and j=1..m to the channel number. This sum is taken over times ranging from several minutes to several hours. $G^{(2)}(t')$ is normalized to yield the net intensity autocorrelation function:

$$g^{(2)}(t') = \frac{G^{(2)}(t')}{G^{(2)}(\infty)} \tag{2.3.2}$$

$G^{(2)}(\infty)$ is simply the square of the time average intensity of the scattered light. $g^{(2)}(t')$ is related to the first order, or electric field, normalized autocorrelation function by:

$$g^{(2)}(t') = 1 + \beta[g^{(1)}(t')]^2 \tag{2.3.3}$$

β is a function of the experimental conditions and is not generally known, but it will be lumped with other estimated parameters, as discussed below.

If the latex solution is sufficiently dilute, so that there is neither particle interaction nor multiple scattering, $g^{(1)}(t')$ consists of the sum of exponentials

$$g^{(1)}(t') = \int_0^{\infty} G(\Gamma)\exp(-\Gamma t')d\Gamma \tag{2.3.4}$$

$G(\Gamma)d\Gamma$ is the fraction of the total intensity scattered by particles in the interval $d\Gamma$. Γ is the reciprocal mean decay time of an intensity fluctuation for a particle with diffusion coefficient D_t:

$$\Gamma = D_t\kappa^2 \tag{2.3.5}$$

where $$\kappa = \frac{4\pi n_m \sin(\theta/2)}{\lambda_0} \tag{2.3.6}$$

θ is the scattering angle, n_m the refractive index of the suspending medium and λ_0, the wavelength of the incident light *in vacuo*. For spherical particles in a Newtonian fluid, the diffusion coefficient of a particle is related to its diameter by the Stokes-Einstein equation:

$$D = \frac{k_b T}{\pi \eta D_t} \tag{2.3.7}$$

where k_b is the Boltzmann constant, η the viscosity of the suspending medium, and T the temperature.

The problem is now completely specified. In principle, all that is necessary to reconstruct the particle size distribution from $g^{(1)}(t')$ is to discretize the integral in equation (2.3.4) and estimate the weights $G_i(\Gamma)$. The objective function to be minimized is:

$$\chi^2 = \sum_{j=1}^{N} \{y(j\Delta t') - \hat{y}(j\Delta t')\} \tag{2.3.8}$$

where $$y(j\Delta t') = \{G^{(2)}(j\Delta t') - A\}^{1/2} \tag{2.3.9}$$

$$= (A\beta)^{1/2} g^{(1)}(j\Delta t')$$

In practice, however, the estimation of the weights $G(\Gamma)$ of equation (2.3.4) is an ill-conditioned problem (Burns, 1986). One of the simplest methods of overcoming this problem is to calculate only the leading moments of the particle size distribution. Called the Method of Cumulants, it was first proposed by Koppel (1972) and is especially suited to the applications in this work because turbidity also gives moments of the distribution.

Koppel realized that $g^{(1)}(t')$ was related to the moment generating function of $G(\Gamma)$:

$$M(-t';\Gamma) \equiv \int_0^{\infty} G(\Gamma) \exp(-\Gamma t') d\Gamma = g^{(1)}(t') \tag{2.3.10}$$

The cumulant generating function is therefore defined as:

$$K(-t';\Gamma) = \ln\{M(-t';\Gamma)\} = \ln|g^{(1)}(t')| \tag{2.3.11}$$

Approximating $K(-t';\Gamma)$ by a MacLauren series expansion

$$K(-t';\Gamma) = \sum_{m=1}^{\infty} k_m(\Gamma)\frac{(-t')^m}{m!} \tag{2.3.12}$$

gives the cumulants, $k_m(\Gamma)$, which are by definition:

$$k_m(\Gamma) = \frac{d^m}{d(-t')^m}K(-t';\Gamma)\Big|_{t'=0} \tag{2.3.13}$$

Comparison with the integral on the RHS of eq(2.3.10) yields:

$$k_1 = \bar{\Gamma}; k_2 = \mu_2; k_3 = \mu_3; k_4 = \mu_4 - 3\mu_2^2; \ldots \tag{2.3.14}$$

μ_m is the mth order central moment of the distribution:

$$\mu_m = \int_0^{\infty} G(\Gamma)(\Gamma - \bar{\Gamma})^m d\Gamma \tag{2.3.15}$$

The NICOMP model 370 particle sizer used in this work used a second order cumulants fit, so $\hat{y}(j\Delta t')$ in eq.(2.3.8) becomes:

$$\hat{y}(j\Delta t') = \hat{y}(t') = (A\beta)^{1/2}\exp\left(-\Gamma t' + \frac{1}{2}\mu_2 t'^2\right) \tag{2.3.16}$$

and $A\beta, \bar{\Gamma}$ and μ_2 are the parameters being estimated.

While the estimates of the leading moments of the distribution calculated by the Method of Cumulants are generally stable and accurate, their one drawback is that they are based on an intensity weighted distribution. A volume weighted mean would be preferable for a direct comparison to mean diameters from turbidimetry. In the case of the Nicomp 370, this is accomplished by assuming that the distribution of diffusion coefficients is Gaussian (Nicoli, 1987). The weights $G_i(\Gamma)$ for the intensity weighted distribution can be calculated from standard normal tables once the mean and variance are calculated from the cumulants.
Rayleigh-Gans-Debye theory states that

$$G_i \propto N_i K_i^2 D_i^6 \tag{2.3.17}$$

where $$K_i = 3\left\{\frac{\sin(2\kappa D_i) - 2\kappa D_i \cos(2\kappa D_i)}{2\kappa D_i^3}\right\}$$

Therefore, dividing each G_i by $K_i^2 D_i^3$ and re-normalizing will yield a particle size distribution with relative peak heights weighted by the particle volume, and the mean of that distribution will be the weight average diameter of the particle size distribution.

2.4 Nomenclature for Chapter 2

C	Mass concentration of particles in a latex.
D	Particle diameter.
D_m	Particle diameter calculated assuming monodispersed particle size.
D_i	Diffusion coefficient of particle.
k_b	Boltzmann constant.
l	Light path length for transmittance measurement.
m	Refractive index ratio n_m/n_p.
N	Particle number concentration in a latex.
n_p	Refractive index of the particles in a suspension.
n_m	Refractive index of the suspending medium.
Q_{ext}	Extinction Coefficient: light energy scattered per unit cross-sectional area.
t'	Lag time in an autocorrelation function
T	Transmittance.
T	Absolute temperature.
v_0	Latex specific volume at hypothetical 0% conversion.
v_1	Latex specific volume at hypothetical 100% conversion.
v_x	Latex specific volume in at conversion x.
x	Fraction monomer conversion.

α	Dimensionless particle size $\pi D/\lambda_m$
Γ	Reciprocal mean decay time of an intensity fluctuation in DLS.
η	Kinematic viscosity.
λ_o	Wavelength of light *in vacuo*.
λ_m	Wavelength of light in the suspending medium (continuous phase).
ρ_p	Particle density in a latex.
τ	Turbidity
θ	Scattering angle, forward scattering $\theta = 0$.

3

PARTICLE SIZING INSTRUMENT DESIGN AND CALIBRATION

This chapter outlines the design, testing, and calibration of the on-line conversion and turbidity particle size analyzer. The first section on the sample conditioning serves as an introduction to the instrument system process flow. The second section outlines the operation and calibration of the densitometer. There follows a brief discussion of the spectrometer. The last section is a detailed treatise on the design, operation and testing of the latex sampler-diluter designed for this analyzer system.

3.1 Sample Conditioning

Proper sample conditioning plays an important role in the success of any instrumentation system. One problem with sampling the effluent of the pilot scale continuous reactors was the presence of gas bubbles in the reactor outlet. These were attributed to nitrogen, used to degas the feedstock, coming out of solution on heating and during the polymerization of the monomer. Continuous streams of large bubbles wreak havoc with the densitometer operation and make it impossible to collect an accurate sample volume for the turbidity instrument.

The problems associated with bubbles in the reactor effluent were solved with the sample conditioning loop shown in Fig. 3.1. The reactor effluent flows into a funnel, where the gas bubbles are separated from the latex. Liquid level is maintained in the system by the siphon break at the exit from the sample loop.

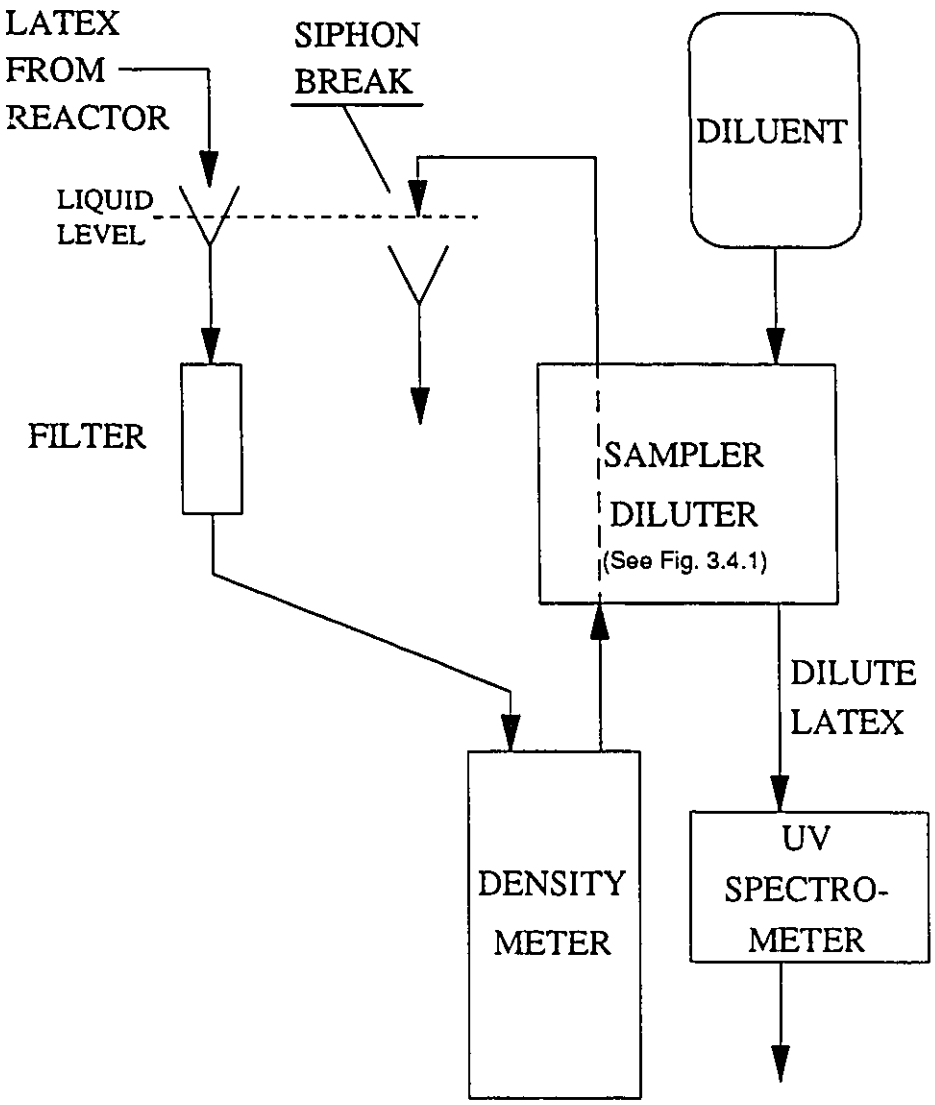

Fig. 3.1.1: Sample Conditioning Loop

3.2 Densitometer

Measuring the natural frequency of a tube filled with some sample is a fast, simple, and very accurate way of obtaining the density of the sample. Many commercial instruments are available, and they are commonly used in industry. A vibrating U-tube densitometer from Anton-Paar (model DPR YE) used in this study has fluid flowing continuously through a 3/8", U-shaped copper tube.

3.2.1 Theory

The natural frequency of an oscillating tube is given by

$$T = 2\pi\sqrt{\frac{M + \rho V}{c}} \tag{3.2.1.1}$$

where T is the period of oscillation, M the mass of the tube, ρ the density of the fluid in the tube, V the volume of the tube, and c the constant of elasticity of the system. Squaring this equation and rearranging gives

$$\rho = \frac{c}{4\pi^2 V}T^2 - \frac{M}{V} \tag{3.2.1.2}$$

Since the constants c, M and V are unknown, this equation is rewritten

$$\rho = AT^2 - B \tag{3.2.1.3}$$

and A and B are estimated using fluids of accurately known density.

Measurement of Frequency

The electronics in the densitometer measurement cell oscillate the U-tube with a gain limited excitation signal. This causes the oscillations to stabilize at their natural frequency. The period of the oscillator vibrations is measured by comparing it to a very accurate quartz oscillator. This measurement scheme is depicted graphically in Fig. 3.2.1 below.

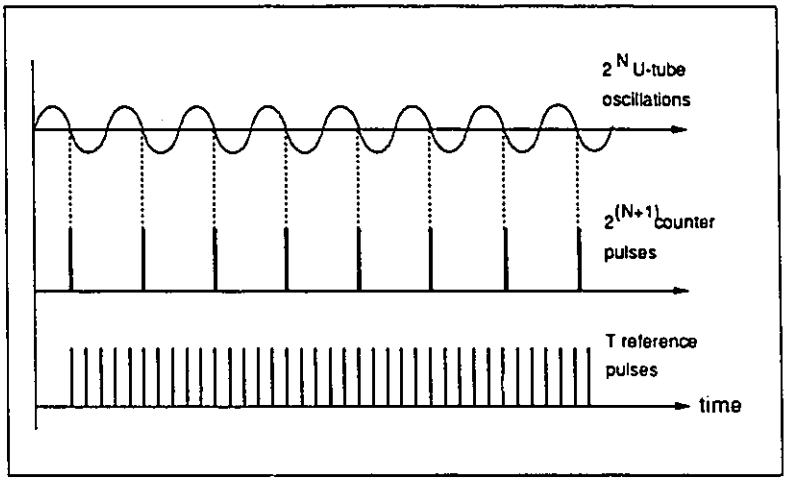

Fig. 3.2.1: **Measurement of Period of Oscillation**

2^N cycles of the U-tube oscillations are counted. The number of reference pulses from the quartz oscillator during these 2^N cycles is the densitometer's output T, which is proportional to the period of oscillation of the U-tube. The Anton-Paar DPR2000 module allows the user to select both the exponent N and the period of the reference oscillator, μ. The utility of this is outlined in the next section.

Densitometer Sensitivity

An important parameter in the design of a vibrating tube densitometer is the sensitivity. It plays a major role in determining the resolution of the densitometer. Taking the derivative of density w.r.t. period of oscillation in equation (3.2.1.2) and rearranging yields

$$d\rho = 2\left\{\frac{c}{4\pi^2 V}T^2 - \frac{M}{V} + \frac{M}{V}\right\}\frac{dT}{T} \qquad (3.2.1.4)$$

Recalling the definition of density from equation (3.2.1.2), and considering only small changes in density allows us to rewrite the above equation as

$$\Delta\rho = 2\left\{\rho + \frac{M}{V}\right\}\frac{\Delta T}{T} \qquad (3.2.1.5)$$

The ratio M/V is the instrument sensitivity. It can be estimated from measurements of the period of oscillation for two fluids of known densities. Consider equation (3.2.1.2) for two fluids at the same temperature with densities ρ_1 and ρ_2. With minimum algebra, it can be shown that

$$\frac{M}{V} = \left\{\frac{\rho_1 - \rho_2}{T_1^2 - T_2^2}\right\}T_2^2 - \rho_2 \qquad (3.2.1.6)$$

This estimate of the sensitivity can be used to calculate the achievable density resolution, $\Delta\rho$, from equation 3.2.1.5. As mentioned above, The Anton-Paar DPR2000 module allows the user to select both the exponent N and the period of the reference oscillator, μ, thereby setting the order of magnitude of T. This gives the user some flexibility in choosing the instrument's density resolution.

3.2.2 Calibration

The calibration of the densitometer is a two step process. Since both the density of the fluid and the elasticity constant of the U-tube are functions of temperature, some form of temperature compensation is necessary. The temperature compensation serves to reference all measurements to some common temperature at which the parameters of the density calibration equation (3.2.1.3) are estimated.

Three solutions were used as calibration standards. They were chosen to bracket the expected density range encountered in the pilot plant experiments. Their composition and densities are given in Table 3.2.1 below.

Temperature Compensation

The Anton Paar densitometer measures the temperature of the fluid using a platinum sensor welded to the outside of the U-tube. Figures 3.2.2 to 3.2.4 show how both temperature

	Density at 25°C [kg/m^3]	Period of Oscillation(T_c) at 25°C	Temperature Compensation Coefficient (C)
10 wt% 1-propanol in water	982.3	65249.2	8.55
deaerated water	997.05	65469.8	10.03
25 wt% acetic acid in water	1029 5	65955.9	6.02

THE TEMPERATURE COMPENSATION EQUATION FOR DENSITOMETER IS $T = C(t - t_0) + T_c$ WHERE $t_0 = 25°C$. C AND T_c ARE CALCULATED FROM t VS. T DATA BY LEAST SQUARES.

Table 3.2.1: Data for Densitometer Calibration

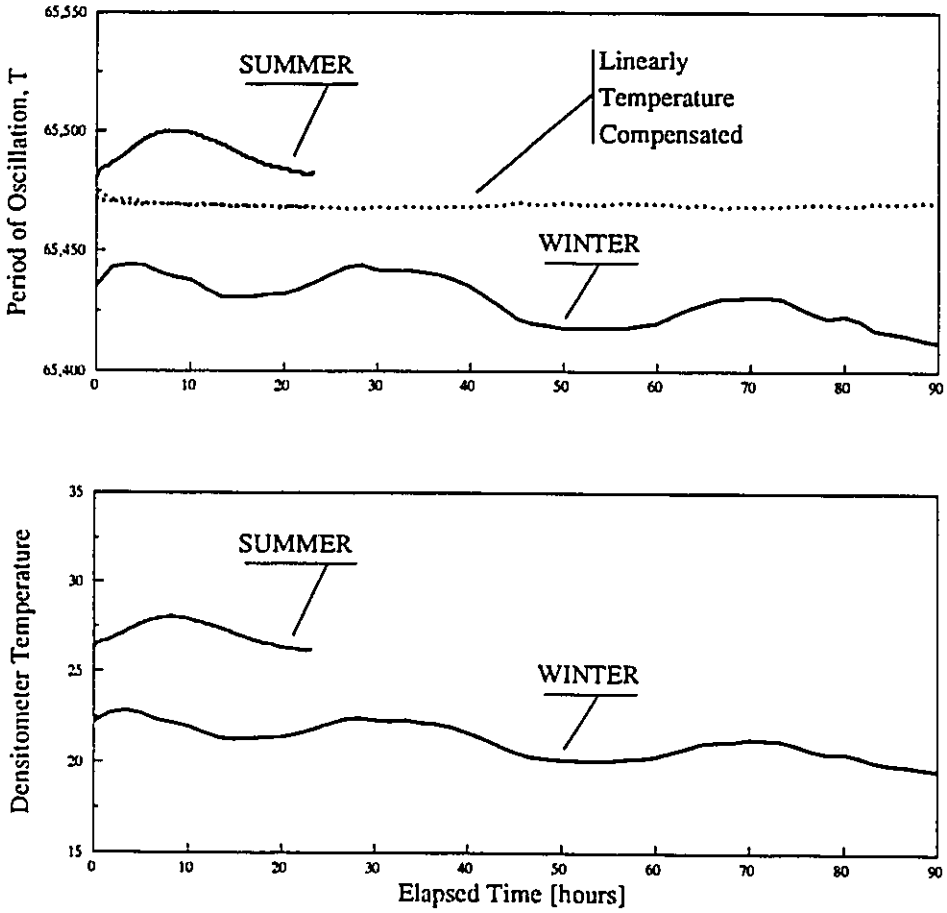

Fig. 3.2.2: Effect of Temperature on Densitometer Period of Oscillation for Water

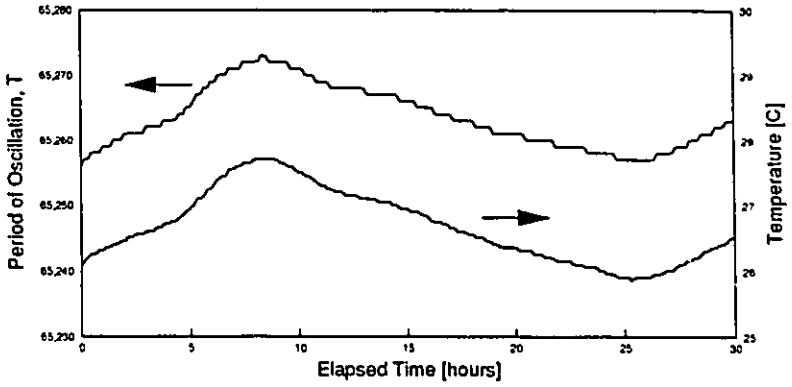

Fig. 3.2.3: Effect of Temperature on Densitometer Period of Oscillation for 10% n-Propanol in Water

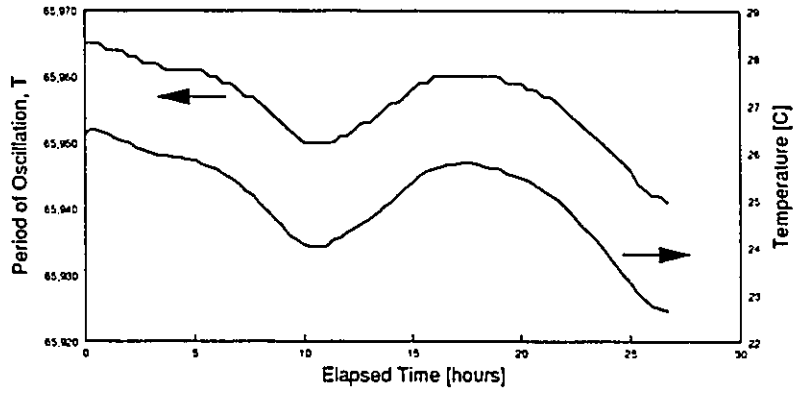

Fig. 3.2.4: Effect of Temperature on Densitometer Period of Oscillation for 25% Acetic Acid in Water

and period of oscillation vary for each of the calibration standards. Before this data can be used to calibrate the densitometer, these periods of oscillation must be referenced to some common temperature.

The Anton Paar DPR2000 temperature compensation assumes a linear relationship between the period of oscillation and the temperature:

$$T = C(t - t_0) + T_c \qquad (3.2.2.1)$$

The reference temperature t_0 is arbitrarily taken as 25°C. C and T_c are estimated from period vs. temperature data. The intercept T_c, then, is the period of oscillation referenced to 25°C. Table 3.1 gives these constants for the data of Figures 3.2.2 to 3.2.4.

Figure 3.2.2 also shows the temperature compensated period of oscillation for water. After temperature compensation, the standard deviation of T_c is:

$$\sigma_T = 0.86219 \qquad (3.2.2.2)$$

The temperature compensation parameters for pure water were used for on-line measurements with poly(vinyl acetate) latex because the latex was over 90% water.

Density Calibration

The parameters of the density calibration equation (3.2.1.3) are calculated from the density vs. period of oscillation data in Table 3.2.1. The calibration equation is:

$$(\rho - 1.002966) = D(T_c^2 \times 10^{-9} - 4.297977) \qquad (3.2.2.3)$$

where D = 0.508731 by least squares. The standard error of prediction for density in this model is

$$\sigma_\rho^c = 0.68 \times 10^{-4} \text{g/ml}$$

Note that, while the dependent variable in this calibration, T_c, has finite variance the values used in the calibration are the mean values of several hundred T_c's. Their variance will be very small, so least squares can be used.

The calibration equation can also be used to calculate the contribution of σ_ρ^T (eq. (3.2.2.2)) to the density variance:

$$(\sigma_\rho')^2 = \left(\frac{d\rho}{dT_c}\right)^2 (\sigma_T)^2 \qquad (3.2.2.4)$$

$$\sigma_\rho' = 0.57 \times 10^{-4} \text{ g/ml}$$

The total variance of the density measurement including calibration errors and temperature effects is:

$$\sigma_\rho = \sqrt{(\sigma_\rho')^2 + (\sigma_\rho^c)^2} \qquad (3.2.2.5)$$

$$= 0.89 \times 10^{-4} \text{g/ml}$$

3.3 Spectrometer

The spectrometer used for the particle sizer is a Bausch and Lomb Spectronic 20. The incident beam has a 20 nm bandwidth. The spectrometer was equipped with a cylindrical Pyrex flow-through cell (Fig. 3.3.1) and a 0-1 Volt D.C. analog output for on-line work.

The Spec 20 is not the ideal spectrometer for particle sizing by turbidimetry. In a series of papers, Heller and his coworkers (1956, 1957) emphasized that, for accurate turbidimetric readings, the incident beam should be as nearly perfectly collimated as possible and there should be several baffles in front of the photodetector to block light scattered at a shallow forward angle from the primary beam. Heller and coworkers (1957) noted, however, that these effects are not critical for particles in the range of 200 nm or smaller.

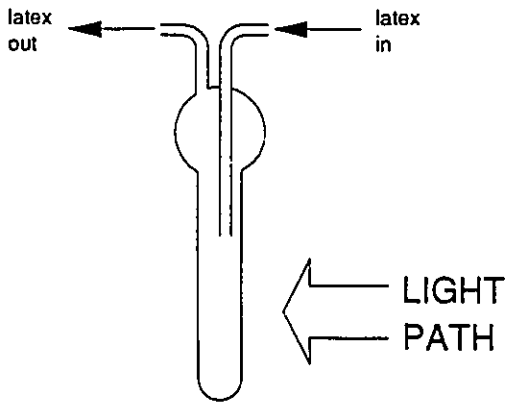

Fig. 3.3.1: Spec 20 Flow Through Sample Cell

3.4 Sampler-Diluter

A major stumbling block to the development of on-line instruments for latex is the tendency of the latex to coagulate and foul sampling systems. A further, stringent criterion for the sampler/diluter designed here for particle sizing by turbidimetery is that the latex concentration in the dilute suspension must be accurately known. The sampling and dilution steps must, therefore, be very accurate metered so that the solids fraction information of the concentrated latex, calculated from on-line densitometery, is preserved. Many of the sampler/diluter designs proposed in the literature for various latex instrumentation applications involve a continuous sample bleed with continuous, metered addition of diluent, then mixing before the sensing element (Zollars, 1980; Brandolin and Garcia-Rubio, 1990). The primary disadvantage to this approach is that it requires either flow indicators or metering pumps to accurately meter both latex and diluent. These are especially subject to fouling because of the high shear fields in the fluid. The hallmarks of the system described below are its mechanical simplicity, short cycle time, high accuracy, and a thorough cleaning of the sampling element after each sample.

3.4.1 Process Description

The sample valve and the dilution metering tank are the two main parts to the sampler-diluter (Fig. 3.4.1 to 3.4.3). Six solenoid valves interfaced to a programmable controller control the sampling and diluting sequencing. Diluent - usually water with 0.1 g/l sodium dodecyl sulphate - must be provided under a small positive pressure (1 ft. gravity head, in our case). The diluted latex flows out of the dilution and mixing tank either by gravity, or by applying pressurized air to the dilution tank.

The sampler is an ISOLOK® sampling valve (Model SAA-102-46-08, Bristol Equipment Company, Yorkville, IL) shown in Fig. 3.4.2. The sample valve can be threaded into the side of any pipe carrying latex. It does not obstruct the flow at any time during the sample cycle.

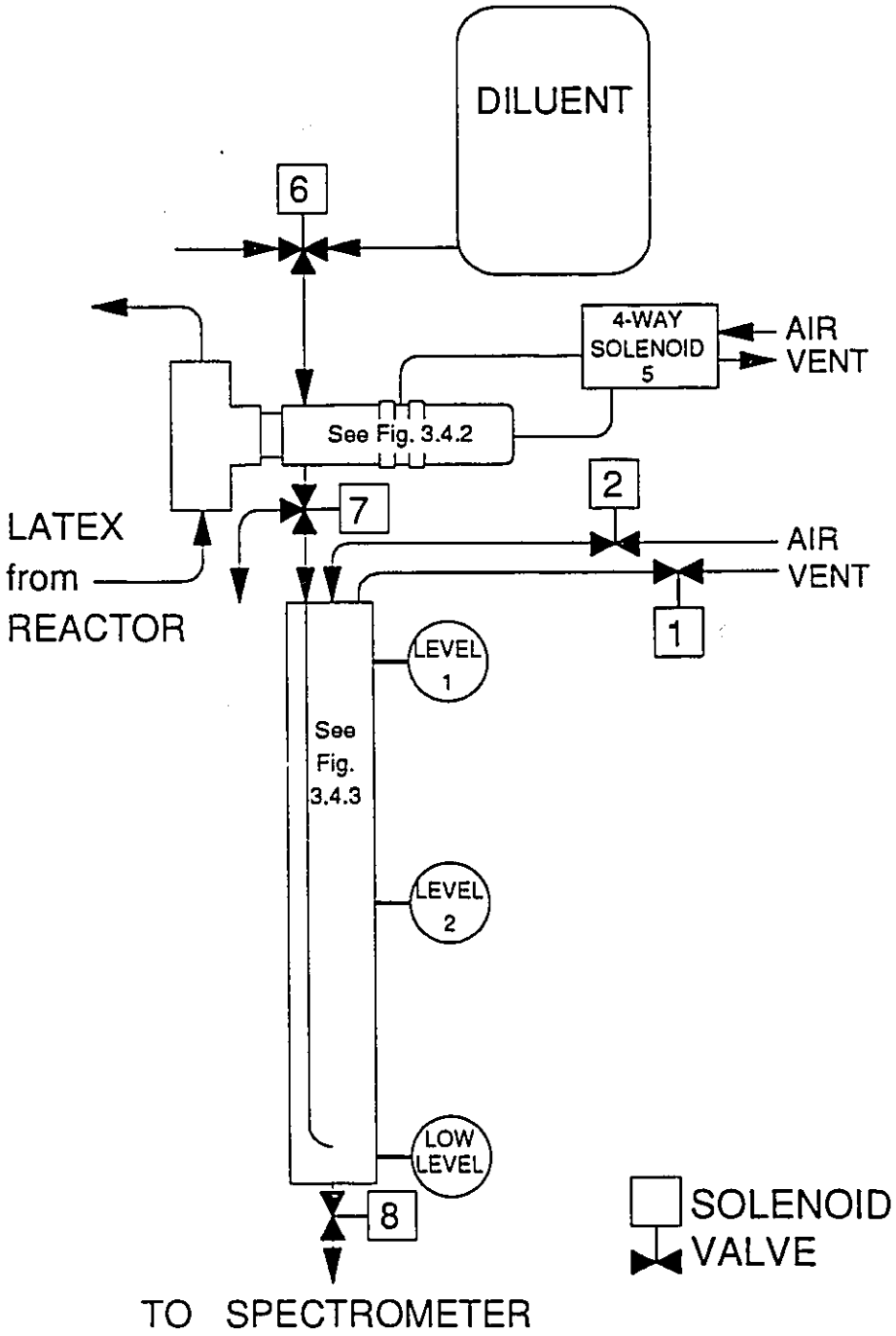

Fig. 3.4.1: Sampler-Diluter Process Flow Diagram

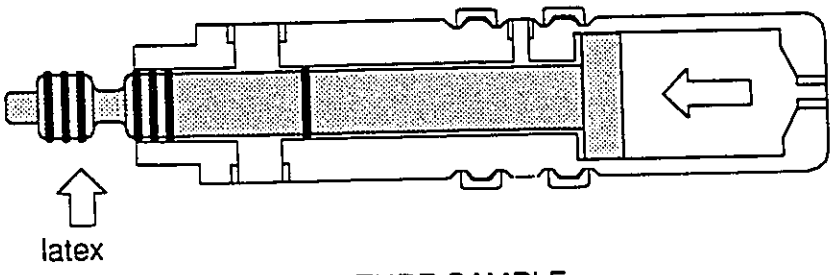

CAPTURE SAMPLE

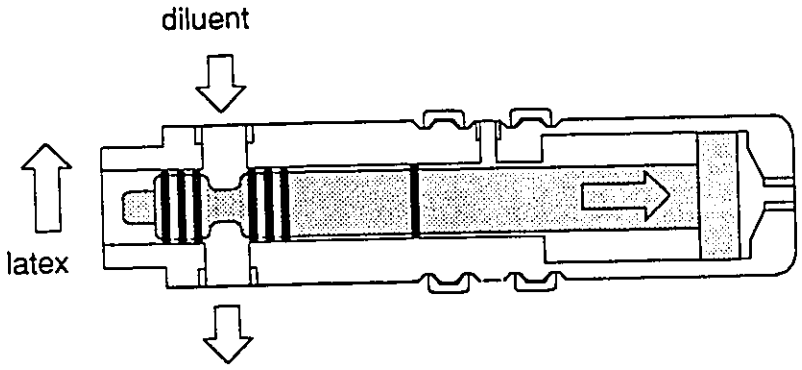

FLUSH SAMPLE

Fig. 3.4.2: ISOLOK® Sample Valve Operation

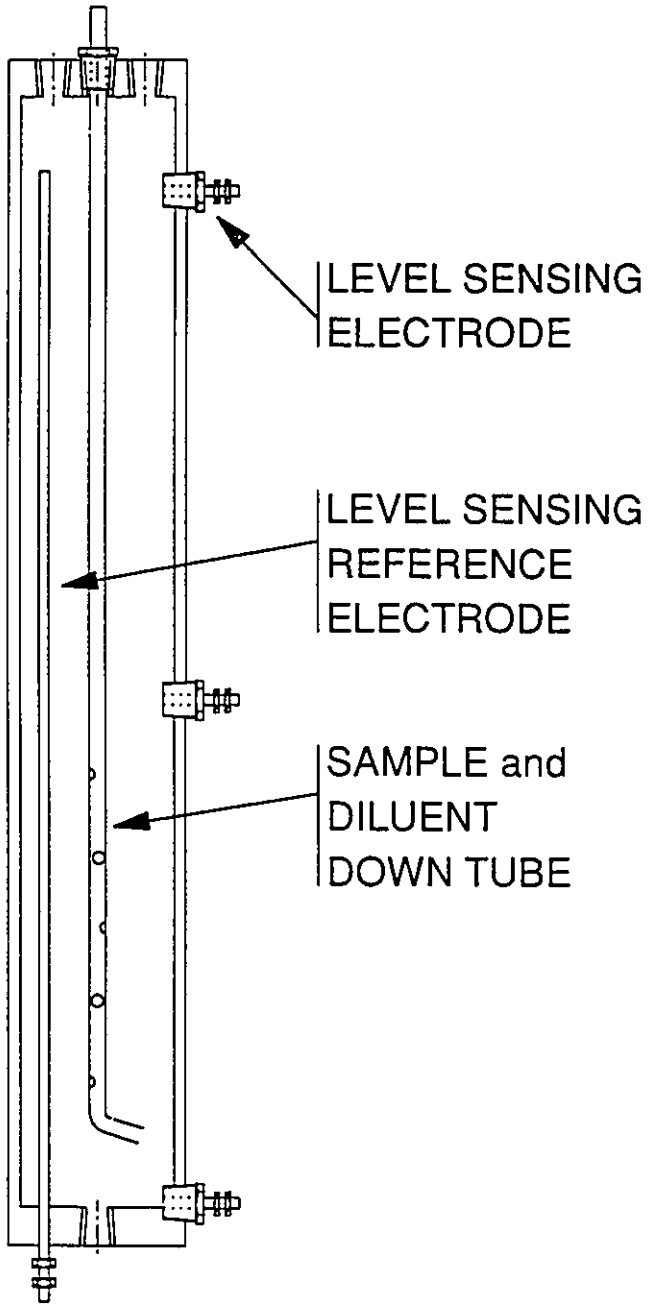

Fig. 3.4.3: Sampler-Diluter Dilution Tank

The sampling is done by a grooved rod that is pushed into the process stream by a double action air piston. Latex is flushed out of the sample chamber by the diluent when the rod is in its retracted position.

There are many advantages to using this valve. First, the sample volume is very reproducible because the sampling element is machined out of one piece of stainless steel. Furthermore, it need only be in the latex stream for several seconds at the beginning of each sample cycle, and is cleaned with diluent at the end of each sample cycle: buildup of latex on the sampling rod is eliminated.

The other principal feature of this system is the dilution tank (Fig. 3.4.3). Precise metering of dilution ratio is achieved by accurately measuring and controlling the volume sent to the tank. The volume is metered using level probes on the sides of the vessel. Several design features ensure accurate volume metering:

1) the level probes used are very sensitive resistive probes with a small sensing element (see Section 3.4.2);
2) latex and diluent enter the vessel via a down tube so that the rising surface of the liquid is not disturbed. This feature reduces level metering standard deviation by a factor of ten over letting the liquid enter the vessel through the top;
3) the high L/D ratio of the tank (from 3 to 6) ensures that errors in level measurements have a minimal effect on total volume metered. Unfortunately, while improving volume metering accuracy, the high L/D ratio is detrimental to good mixing of latex and diluent. This effect was offset somewhat by drilling holes in the down-tube below the lowest high level electrode. The results of this modification are discussed in detail in Section 3.4.3.

Refering to Fig. 3.4.1 for valve numbers, the sequence of events that comprise one sample cycle is:

1) The four-way solenoid valve 5 is energized, and the sampling valve extends to its sampling position.
2) Wait 15 s.
3) Valve 5 is deenergized, and the sampling rod retracts. Valves 6 and 7 open to flush the sample and diluent into the dilution tank until the liquid is sensed at the high level sensor.
4) Wait 10 s.
5) Valves 2 and 8 are opened and 1 is closed to drain the diluted latex to the spectrometer until liquid is no longer sensed at the low level sensor.

Every tenth cycle is a flush cycle that cleans the dilution tank and spectrometer cell, and provides a 100% transmittance reading for the spectrometer. The flush cycle is simply two sample cycles in a row with the latex sampling step eliminated.

3.4.2 Automation Hardware and Software

Programmable Controller

The implementation of the sequencing algorithm outlined above is a rather straightforward programmable controller application. The General Electric MicroGEM® Programmable Logic Controller (PLC) was used in this application. The controller provides eight contact closure outputs activated by software "relay coils". Twelve inputs sense contact closures in the field, and are powered by the controller's internal 24 VDC power supply.

The ladder diagram used to program the PLC is shown in Fig. 3.4.4. In this application, the program restarts the sample cycle at a preset interval given by timer D00. The hardware has also been configured to allow the sample cycle to be started by an external relay closure. This facilitates interfacing the sampler-diluter to a process computer.

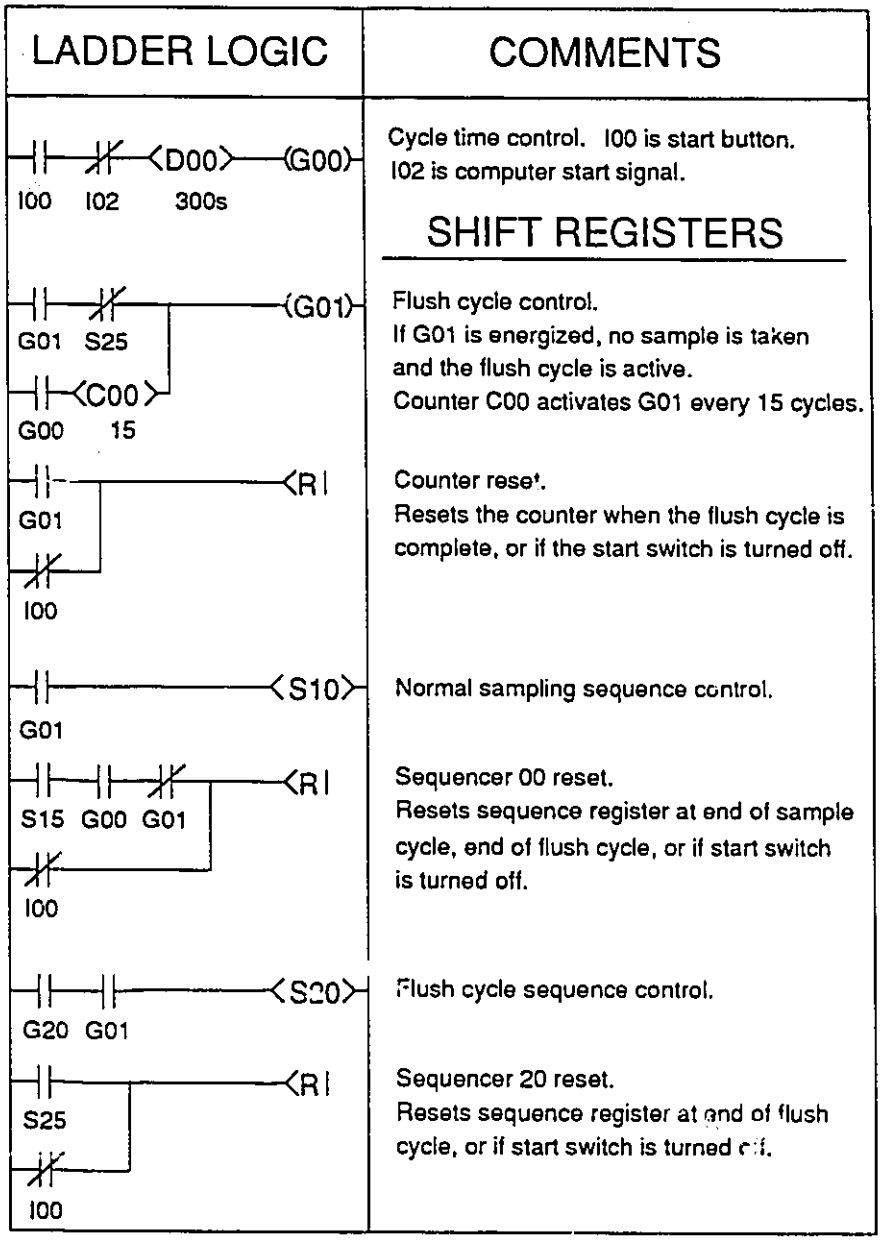

Fig. 3.4.4a: MicroGEM® Ladder Diagram

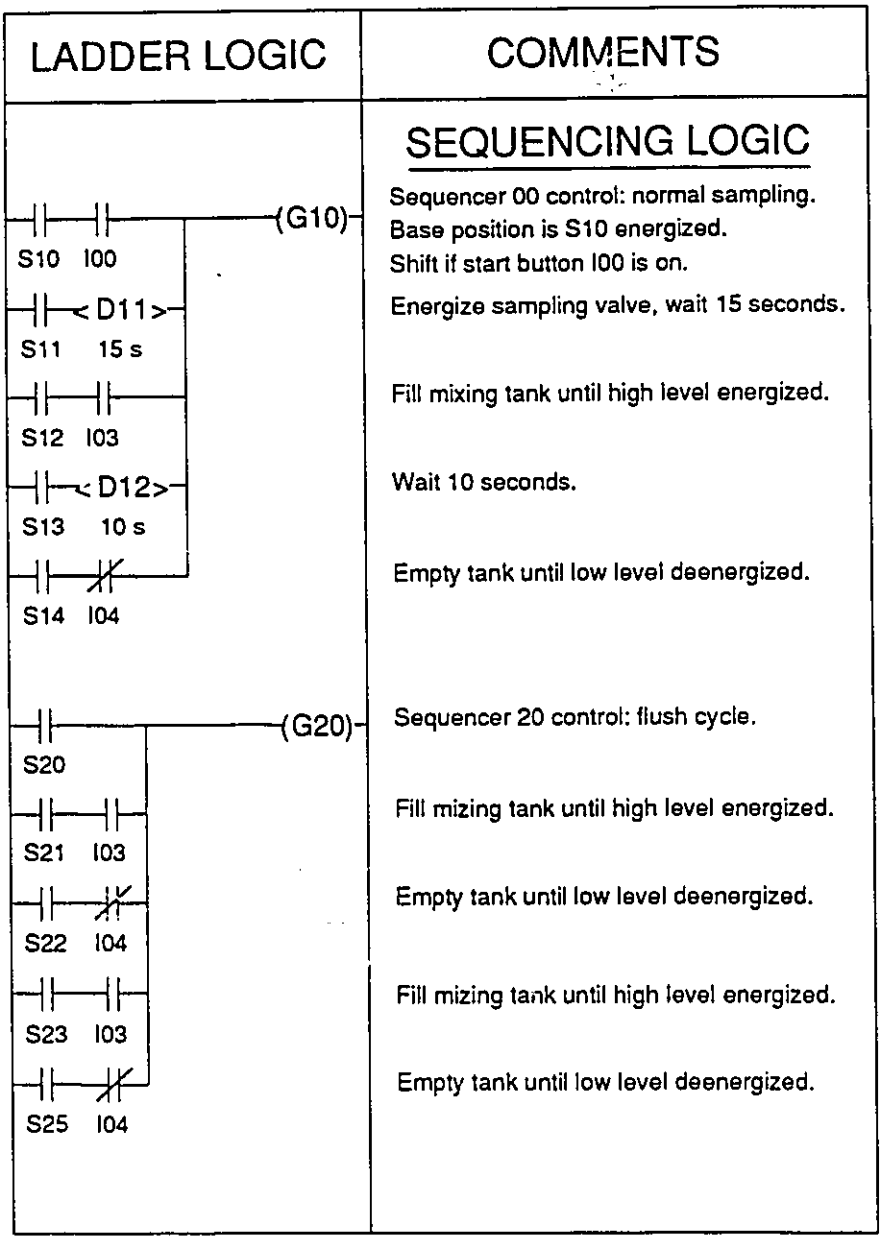

Fig. 3.4.4b: MicroGEM® Ladder Diagram

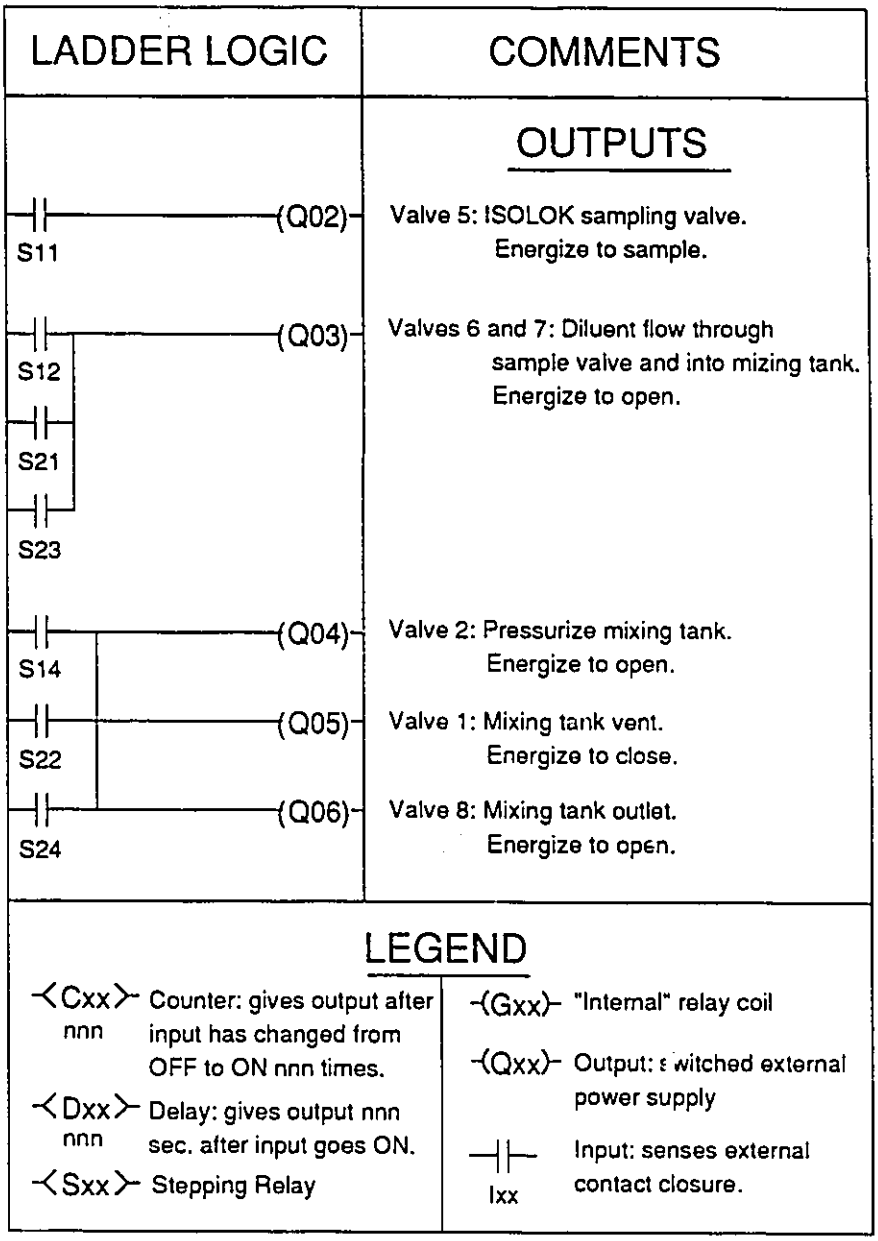

Fig. 3.4.4c: MicroGEM® Ladder Diagram

Level Sensors

To a great extent, the success of this sampler-diluter hinges on the design of very sensitive and accurate level sensors in the dilution tank. As these are of in-house design, they will be discussed in detail here.

The level sensors work on the basic principal of sensing a change in the electrical resistance of the path between the level sensing electrode and ground. The level sensing element is a no. 6 stainless steel screw insulated from the tank wall by a Teflon sheath (Fig. 3.4.5).

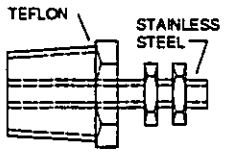

Fig. 3.4.5: Level Sensing Electrode

The electrode is connected to the level sensing electronics shown in Fig. 3.4.6 (designed and built by T. Papez and V.A. Cers of the Science and Engineering Electronics Shop at McMaster University). Inside the tank is a metal rod connected to the reference ground of the sensing circuitry. If the liquid in the tank is a conductor, when the liquid level reaches the electrode the base of transistor MPS8599 is pulled to ground, energizing the base of transistor MPS8099. The latter transistor is the contact closure that can be sensed as a programmable controller input.

The 2 kΩ potentiometers below the 70V rail serve to adjust the sensitivity of the electrodes, allowing the sensors to reject slow current leaks to ground caused by thin films on the electrodes.

3.4.3 Experimental Evaluation

Particle sizing by turbidimetry requires a reproducible and known dilution ratio so that the solids fraction of the diluted latex can be precisely calculated. The two factors in the tank design that affect this are dilution ratio reproducibility and mixing. These were measured by

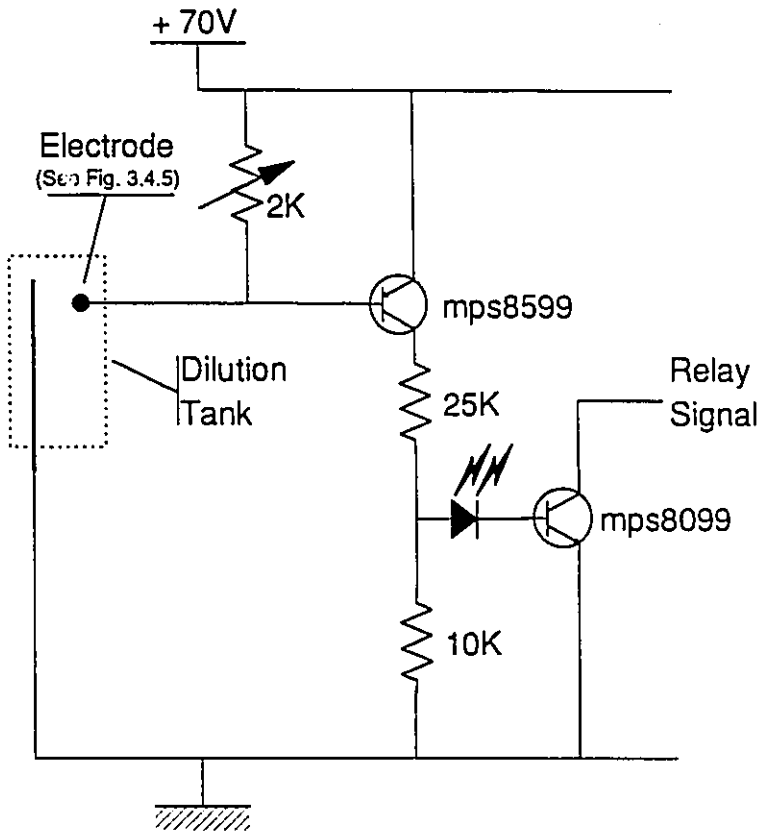

Fig. 3.4.6: Level Sensor Electronics
(Design: T.Papez, V.A.Cers, S.E.E.S., McMaster)

replacing the latex on the process side with a 0.5 g/L solution of a dye that is a strong UV absorber (Hodogaya Chemical Co.; Aizen Direct Yellow 86). Then, the sampler-diluter is run through a normal cycle.

Mixing

The diluted latex in the metering tank must be well mixed so that the dilution ratio can be known accurately. The degree of mixing was evaluated by connecting the Spec 20 spectrometer with a flow through cell to the sampler-diluter outlet, just as it would be for normal operation, and recording the transmittance at 395 nm as a function of time while the diluent metering tank is emptying.

This was done both for levels sensors 1 and 2 (see Fig. 3.4.3). The results are shown in Fig. 3.4.7. These graphs show transmittance vs. time for several cycles while the tank is emptying. The variation in transmittance is due to incomplete mixing in the dilution tank. As expected, the higher the L/D ratio, the worse the mixing. At the lower level sensor (Fig. 3.4.7a), the combination of a lower L/D ratio and holes in the side of the down tube decreased the peak-to-peak transmittance variation by 45% from the high level (Fig. 3.4.7b). The effect of incomplete mixing on the final particle size calculations is discussed in Chapter 5.

Dilution Ratio Calibration

For calibration of dilution ratio, dye again replaced latex on the process side. The diluted dye was collected in a large flask, mixed, and poured into sample vials for analysis. UV absorbance of the diluted dye at 394 nm was measured on a Hewlett-Packard hp8452a photodiode array spectrometer.

A calibration for dilution ratio vs. absorbance was obtained by making four diluted dye samples with a two stage dilution using volumetric pipettes and flasks. The absorbances of the calibration standards were measured several times. The data is in Table 3.4.1. It yielded the calibration equation

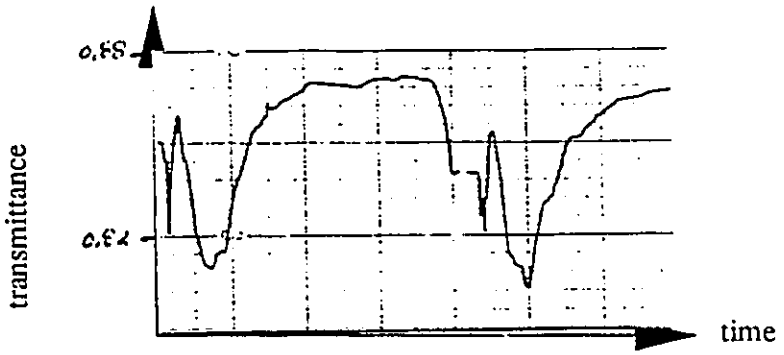

(a)

High Level 1
Metering Tank L/D = 6

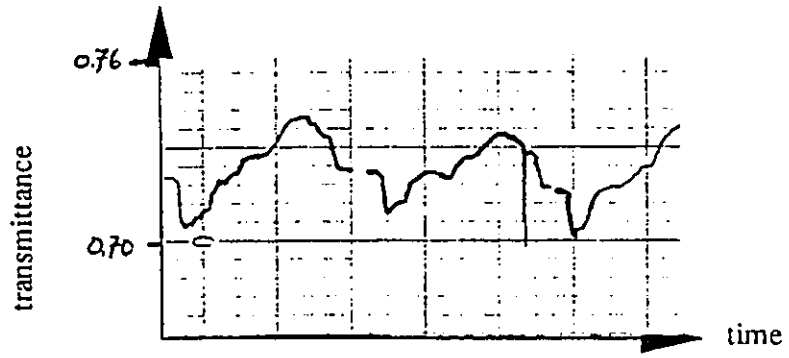

(b)

High Level 2
Metering Tank L/D = 3

Fig. 3.4.7: Dilution Tank Mixing - Dye Tests

Sample	Dilution Ratio	Absorbance @ 394 nm
water	0	-0.00002 0.00003 -0.00001 0.00078 0.00004 -0.00082 -0.00045 -0.00028 0.00073
A	1/250	0.07753
A A C C C C D	1/100	0.18313 0.19898 0.18469 0.19676 0.17838 0.18362 0.18777

Table 3.4.1: Dilution Ratio vs. Dye Absorbance Data

	Absorbance	Mean and Std. Dev.
Dilution Tank Level 1	0.08029 0.08032	$\bar{a}$ = 0.080305 s = 2.120 x 10^{-5}
Dilution Tank Level 2	0.16460 0.17299 0.16053 0.16290 0.16838 0.16356	$\bar{a}$ = 0.165493 s = 4.482 x 10^{-5}

Table 3.4.2: UV Absorbances for Dye Diluted by Sampler-Diluter

	Number of Samples	Mean Absorbance	Standard Deviation (σ_a)	Estimated Dil Ratio ($\hat{R}$)	Standard Error of $\hat{R}$
Dil Level 1	2	0.080305	2.1200 x 10^{-5}	0.0042771	±2.824 x 10^{-6}
Dil Level 2	6	0.165493	4.4817 x 10^{-3}	0.0088142	±3.915 x 10^{-6}

Table 3 ... ution Ratio Calculations

$$a = 18.7757R \tag{3.4.1}$$

where a is the absorbance, R the dilution ratio. The residual standard deviation is

$$s = 1.2596 \times 10^{-4} \text{ AU.}$$

Absorbances of diluted dye from the sampler-diluter are reported in Table 3.4.2. The dilution ratio calculations are summarized in Table 3.4.3.

When analyzing the variability of the dilution ratio calculated from these absorbances, a distinction must be made. The standard error of the dilution ratio prediction $\hat{R}$ is the uncertainty arising from the calibration equation. It is calculated following standard procedures for inverse regression (Draper and Smith, 1981), and shows that using the dye is a very accurate method of determining dilution ratio. The more important value for a process instrument, however, is the reproducibility of the dilution ratio metering. It is calculated directly from the standard deviation of the sample absorbances for Dilution Level 2 in Table 3.4.3 using the formula

$$(\sigma_R)^2 = \frac{(\sigma_a)^2}{(18.7757)^2} \tag{3.4.2}$$

$$\sigma_R = 2.389 \times 10^{-4}$$

or 2.9% of the dilution ratio. From the design of the sampler/diluter, you would expect the standard deviation of the volume metered in the tank, V_m, to be independent of level, and the error in latex sample volume to be roughly constant. This expectation has been confirmed by experiments. The variance of V_m can be very accurately measured by repeatedly collecting and weighing the effluent of the mixing tank. If water is used, mass in grams is approximately equal to volume in millilitres. Measured this way, the standard deviation of the metered volume is

$$\sigma_{V_m} = 0.414ml$$

The variance of the latex sampling step is then easily calculated using

$$\left(\frac{\sigma_{V_S}}{V_S}\right)^2 = \left(\frac{\sigma_R}{R}\right)^2 - \left(\frac{\sigma_{V_M}}{V_M}\right)^2$$

$$= 7.4 \times 10^{-4} - 8.1 \times 10^{-7}$$

$$\frac{\sigma_{V_S}}{V_S} = 2.7\%$$

clearly showing that the latex sampling step accounts for almost all the variance in the dilution ratio metering.

3.5 Nomenclature for Chapter 3

c	Constant of elasticity of densitometer U-tube.
a	UV Absorbance
C	Coefficient for linear temperature compensation of period of oscillation in densitometer.
D	Dilution tank dilution ratio = volume sample / total diluted volume.
M	Mass of densitometer U-tube.
t	Temperature, degrees C.
T	Period of oscillation of densitometer U-tube.
T_c	Period of oscillation of densitometer U-tube after temperature compensation.
V	Volume contained by densitometer U-tube.
V_M	Volumer of sampler/diluter mixing tank [ml]
V_S	volume of latex extracted in sample loop [ml]
ρ	Density.
σ_T	Standard deviation of temperature compensated period of oscillation signal from densitometer.
σ'_ρ	Standard deviation of density measurement attributable to temperature fluctuations.

σ_p^c Standard deviation of density measurement attributable to calibration equation error of prediction.

σ_D Standard deviation of dilution ratio, reproducibility.

4

CALCULATIONS AND ERROR PROPAGATION ANALYSIS

The pilot scale reactor that was outfitted for the experimental evaluation of this system is described in detail in Chapter 5. To understand the calculations below, it suffices to know that the reactor is fed by four feed stream, each with its own metering pump. One of the feed streams is pure monomer, another, pure distilled water. The other two are mostly water, one with some initiator dissolved in it, and the other with emulsifier.

4.1 Solids and Particle Diameter from Measured Density and Transmittance

While simple in principle, the calculation of solids fraction and particle diameter is complicated by the need for an accurate, dynamic mass balance to infer the contents of the reactor in continuous operation, and by the number of physical properties that must specified. The details of these calculations are specific to the reactor used in these experiments, but the concepts are sufficiently general to apply to any continuous reactor system. The important point is to highlight the difficulties encountered in these types of calculations in continuous system as opposed to the reported simplicity of batch reactor applications (Schork and Ray, 1981).

Feed mass concentrations of monomer, water, initiator and soap are calculated from measured flowrates and known or estimated feed stream densities and reagent concentrations.

monomer: $$C_{in,M} = F_M \rho_M / F_{in}$$

aqueous phase: $$C_{in,Aq} = (F_W + F_I + F_S)\rho_{Aq} / F_{in} \qquad (4.1.1)$$

initiator: $$C_{in,I} = F_I C_{F,I} / F_{in}$$

emulsifier: $$C_{in,S} = F_S C_{F,S} / F_{in}$$

The symbols are defined at the end of the Chapter.

Note that the densities and feed concentrations of all the reaction recipe components must be known. The concentrations of electrolytes in the feed streams are known from weighings of reagents when the feed solutions were mixed. The density of monomer was measured using the densitometer, which is not as straightforward as it may seem. Recall that the densitometer is calibrated for 25°C, and the temperature compensation coefficients were estimated using water (Section 3.2.2). As the coefficient of thermal expansion of water is very different from that of vinyl acetate, those temperature compensation coefficients cannot be used. The procedure for measuring vinyl acetate density is:

1) Inject vinyl acetate into the densitometer and, with the temperature compensation turned off, take several reading of density at different temperatures.
2) Plot densitometer period of oscillations vs. temperature and extrapolate to 25°C.
3) Calculate the density at 25°C using the calibration equation (3.2.2.3).

The vinyl acetate density measured by this method was 0.9265 g/cm^3, compared to a literature value for pure vinyl acetate of 0.9317 g/cm^3 in the CRC Handbook (Weast, 1980).

The aqueous phase is a solution of potassium persulphate, sodium dodecyl sulphate, and vinyl acetate. It is impossible to precisely quantify its density because the amount of monomer and initiator in solution vary with extent of reaction, and most of the emulsifier is adsorbed onto the particle surface. The range of variation of this parameter can be constrained between that of pure water (0.9987 g/cm^3) and the density of the most concentrated electrolyte solution used in the experimental runs (1.015 g/cm^3). This was the single parameter adjusted to make the on-line solids fraction measurements coincide with laboratory determination by gravimetry.

The feed density is calculated from the inlet densities of each phase:

$$\rho_{in} = C_{in,M} + C_{in,Aq} \tag{4.1.2}$$

The residence time of the reactor is based on the outlet conditions given by the density measurement, ρ_x

$$\theta = \frac{V_R}{F_{in}} \cdot \frac{\rho_x}{\rho_{in}} \tag{4.1.3}$$

A dynamic mass balance is used to calculate outlet concentrations of organic phase (polymer and monomer), aqueous phase, initiator and emulsifier. The calculations are simplified by assuming that density is measured and that flow rate changes are made only at fixed time intervals. The solution of the dynamic mass balance in an interval t_0 to t_f with constant flow rates and known initial conditions is then easily done using z-transforms.

$$C_i(t_f) = C_{in,i} \cdot \frac{\rho_x}{\rho_{in}}(1 - e^{-\Delta t/\theta}) + C_i(t_0)e^{-\Delta t/\theta} \tag{4.1.4}$$

Then follow the straightforward calculations of weight fractions of organic phase, initiator, and emulsifier

$$X_i = \frac{C_i(t_f)}{\rho_x} \tag{4.1.5}$$

and specific volumes of hypothetical zero and 100% conversion latexes:

$$v_0 = \frac{X_O}{\rho_M} + \frac{(1 - X_O)}{\rho_{Aq}}$$
$$v_1 = \frac{X_O}{\rho_P} + \frac{(1 - X_O)}{\rho_{Aq}} \tag{4.1.6}$$

As explained before, the aqueous phase density was the only adjustable paremeter used to align on-line and off-line gravitimetric solids fraction determinations, and was able to account for any run-to-run variations. The polymer density is also an elusive quantity. The Polymer Handbook (Brandrup and Immergut, 1975) value for poly(vinyl acetate) is 1.1 g/ml. For a highly branched

polymer like poly(vinyl acetate), however, it is highly dependent on monomer conversion in the reactor. For the calculations in this work, a constant value of 1.2 g/ml was used as this allowed the aqueous phase density to vary in an acceptable range.

Monomer conversion is:

$$x = \frac{v_0 - v_x}{v_0 - v_1} \tag{4.1.7}$$

as is the solids fraction in the latex:

$$X_p = xX_O \tag{4.1.8}$$

$$X_{sol} = X_p + X_S + X_I \tag{4.1.9}$$

To summarize progress so far, the solids fraction of a homopolymer latex can be calculated on-line in a continuous reactor system using an on-line densitometer, measurements of all flowrates into the reactor, and knowledge of all constituent densities and electrolyte concentrations in the latex. Constituent densities are difficult to quantify, so in this case the aqueous phase density was the single parameter used to align on-line and off-line solids fraction measurements.

By this stage, calculating mean particle diameter from an on-line dilute latex transmittance measurement is relatively straightforward. Latex is sampled and diluted by the equipment detailed in Section 3.4. Diluted latex polymer mass fraction:

$$C = X_p \rho_x \cdot \frac{V_S}{V_M} \tag{4.1.10}$$

The calibration of the dilution ratio V_S/V_M is outlined in Section 3.4.3.

The sample turbidity is calculated from the transmittance:

$$\tau = \frac{-\ln(T)}{l} \tag{4.1.1}$$

For refractive indeces around m=1.1, the specific turbidity $\tau\rho_p/C$ is a known function of the weight average of the particle size distribution (see Chapter 2). The mean diameter is computed from the specific turbidity by a table lookup. The table of diameter vs. specific turbidity was generated at about 5 nm diameter intervals using computer programs supplied by Wiscombe (1976, 1986, 1988). Newton's method was used to efficiently search the table for diameter given a specific turbidity measurement. Linear interpolation was used if the measured specific turbidity fell between tabulated values.

The refractive index ratio used to calculate Mie extinction coefficients was m=1.095. This is about 1/2% below the Polymer Handbook (Brandrup and Immergut, 1975) value for poly(vinyl acetate), but Kourti (1989) found that it gave the best agreement between particle sizes measured by turbidity and those from dynamic light scattering and electron microscopy.

4.2 Error Propagation Calculations

Error propagation calculations provide insights into the effects of quantifiable variables on the final calculated variables. Not only do they provide an estimate of the reproducibility of the instrument output, they also point to areas for design improvements that reduce the instrument variance.

The theory is quite simple. For a linear function of n independent random variables

$$f(y) = a_0 + a_1 y_1 + \cdots + a_n y_n \tag{4.2.1}$$

the variance is given by

$$V(f) = a_1^2 \sigma_{y_1}^2 + \cdots a_n^2 \sigma_{y_n}^2 \tag{4.2.2}$$

This approach can be used for nonlinear functions $f(y)$ by simply approximating them with a first order Taylor series expansion, yielding

$$V(f) = \left(\frac{df}{dy_1}\right)^2 \sigma_{y_1}^2 + \cdots + \left(\frac{df}{dy_n}\right)^2 \sigma_{y_n}^2 \qquad (4.2.3)$$

The calculations for solids fraction and particle diameter described above are complex. The raw data enter often into those calculations. When deriving the expressions for error propagation, therefore, care must be taken to ensure that quantities enter independently; for example, a density measurement entering at one point in the calculations may be cancelled in the next line. It is necessary to cast the expressions in their most reduced forms to avoid artificially high variance estimates. This explains the lack of one-to-one correspondence between the expressions of this section and of those of the previous one.

The solids fraction and mean diameter variance are a function of the reaction recipe and the monomer conversion. It also depends on several sources of variation that were measured in the laboratory and reported in other sections of this work. These include: the absolute error of the density measurement, $V(\rho_x)$; the relative error of flowrate delivery by the metering pumps, $V(F_i)/F_i$; the error in the sampler/diluter dilution ratio metering, $V(R)$; and the absolute error in the transmittance reading, $V(T)$. The error propagation equations are, therefore, cast in terms of these variables.

Throughout the calculations, the densities of all the recipe components are assumed to be exactly known. This was done because the purpose of these calculations is to evaluate instrument variance that is attributable to quantifiable and controllable variation. Systematic bias that arises from errors in physical parameters are dealt with via the adjustable parameters discussed in Chapter 3.

A few notes: first, this is a steady state solution. Second, density ρ and specific volume v are both used below. One is simply the reciprocal of the other, and the choice as to which is used depends on notational convenience. On to the first step: calculate quantities directly related to the reaction recipe. The notation is explained at the end of the Chapter.

Total water flow:

$$F_{Aq} = F_I + F_S + F_W \tag{4.2.1}$$

$$V(F_{Aq}) = V(F_I) + V(F_S) + V(F_W) \tag{4.2.2}$$

Total mass flow:

$$M_{in} = \rho_M F_M + \rho_{Aq} F_{Aq} \tag{4.2.3}$$

$$V(M_{in}) = \rho_M^2 V(F_M) + \rho_{Aq}^2 V(F_{Aq}) \tag{4.2.4}$$

Total organic phase mass fraction:

$$X_O = \frac{\rho_M F_M}{M_{in}} \tag{4.2.5}$$

$$\frac{V(X_O)}{X_O^2} = \frac{V(F_M)}{F_M^2} + \frac{V(M_{in})}{M_{in}^2} \tag{4.2.6}$$

Initiator and emulsifier mass fractions (X_I and X_S) are similarly computed.

Hypothetical specific volume at 0 and 100% conversion:

$$v_0 = v_M X_O + v_{Aq}(1 - X_O) \tag{4.2.7}$$

$$v_1 = v_P X_O + v_{Aq}(1 - X_O) \tag{4.2.8}$$

$$V(v_0) = (v_M^2 + v_{Aq}^2) V(X_O) \tag{4.2.9}$$

$$V(v_1) = (v_P^2 + v_{Aq}^2) V(X_O) \tag{4.2.10}$$

Latex density depends on conversion, which must be specified for these calculations:

$$v_x = \frac{1}{\rho_x} = v_0 - x(v_0 - v_1) \tag{4.2.11}$$

$$\frac{V(v_x)}{v_x^2} = \frac{V(\rho_x)}{\rho_x^2} \tag{4.2.12}$$

Polymer weight fraction:

$$X_P = \frac{(v_M - v_{Aq})X_O - (v_x - v_{Aq})}{(v_M - v_P)} \tag{4.2.13}$$

$$V(X_P) = \left[\frac{v_M - v_{Aq}}{v_M - v_P}\right]^2 V(X_O) + \left[\frac{1}{v_M - v_P}\right]^2 V(v_x) \tag{4.2.14}$$

Conversion Error:

$$V(x) = \left[\frac{1}{v_0 - v_1}\right]^2 V(v_x) + \left[\frac{v_x - v_1}{(v_0 - v_1)^2}\right]^2 V(v_0) + \left[\frac{v_0 - v_x}{(v_0 - v_1)^2}\right]^2 V(v_1) \tag{4.2.15}$$

Solids Fraction:

$$X_{sol} = X_P + X_I + X_S \tag{4.2.16}$$

$$V(X_{sol}) = V(X_P) + V(X_I) + V(X_S) \tag{4.2.17}$$

Dilute latex polymer volume fraction:

$$C_P = X_P \cdot R \cdot \frac{v_P}{v_x} \tag{4.2.18}$$

where $$R = \frac{V_s}{V_m}$$

$$\frac{V(C_P)}{C_P^2} = \frac{V(X_P)}{X_P^2} + \frac{V(R)}{R^2} + \frac{V(v_x)}{v_x^2} \tag{4.2.19}$$

The turbidity error is:

$$\frac{V(\tau)}{\tau^2} = \left[\frac{1}{\ln T}\right]^2 \frac{V(T)}{T^2} \tag{4.2.1}$$

The specific turbidity vs. diameter relation is linear over a large region relevant to this system, so

$$\overline{D} \propto \frac{\tau}{C_P} \tag{4.2.1}$$

$$\frac{V(\overline{D})}{\overline{D}^2} = \frac{V(\tau)}{\tau^2} + \frac{V(C_P)}{C_P^2} \tag{4.2.1}$$

4.3 Error Propagation Case Studies

The questions answered by this case study are:

1) what is the effect of reaction recipe on the solids fraction and diameter uncertainty?

2) Are there any significant sources of error that could be reduced by design changes to the instrument system?

3) what is the contribution of uncertainy in flow rates? This is important because it is a variable that cannot be controlled in the design of the instrument system, and very precise flow metering is expensive.

Two reaction recipes were considered (Table 4.3.1): a 50% solids latex, and an 8% solids seed latex. The latter recipe is one typical of the ones used in the next Chapter for the experimental evaluation of the instrument system. Both recipes are base on actual pilot plant experiments. The high solids latex recipe was run using a 5 litre reactor, and the seed latex used a 500 ml one. This will not make any difference in the calculations that follow, however, since this analysis is based on relative errors in flow rates: its conclusions are independent of reactor size. Finally, the following calculations were all done assuming 100% conversion. All conversion dependant calculations reach a minimum there.

	High Solids Latex	Low Solids Latex
Water Flow [ml/min]	80.0	42.5
Initiator Flow [ml/min] (40 g KPS/l H_2O)	20.0	6.1
Emulsifier Flow [ml/min] (60 g SDS/l H_2O)	20.0	5.4
Monomer Flow [ml/min] (Vinyl Acetate)	120.0	5.0
Emulsifier Conc. [g/l H_2O]	10.0	6.0
Initiator Conc. [g/l H_2O]	6.7	4.5
Monomer Mass Percent	48.1	7.9

Table 4.3.1: Recipes for Reproducibility Case Studies

As mentioned earlier, several sources of variation were quantified experimentally. These are discussed in detail in the various sections devoted to each subsystem. The results were:

Densitometer standard deviation:

$$\sigma_\rho = 0.89 \times 10^{-4} \text{ g/ml}$$

Sampler/diluter dilution ratio standard deviation:

$$\sigma_R = 2.389 \times 10^{-4} \text{ at } R = 0.00881$$

Transmittance:

$$\sigma_T = 4.038 \times 10^{-3}$$

For each reaction recipe, two cases were calculated: one with no error in the flow rates, and another using a relative error in flow rate of 2.0%. This is realistic for this case study because economical vortex flow meters can consistently achieve this in their design range. This will help separate variation arising out of the instrument system design (and under the control of the designer) from the mass balance errors, which are the scourge of the chemical process industry.

Consider first the error propagation in the calculation of solids fraction (Table 4.3.2). Several important conclusions can be drawn from the results reported there. By studying the column for solids fraction variance, $V(X_{sol})$, it is clear that the effects of densitometer error are independent of reaction recipe; but, when mass balance error is taken into account, the uncertainty in solids fraction increases dramatically with increasing monomer fraction in the recipe. Furthermore, comparing results for the polymer fraction, $V(X_P)$, and $V(X_{sol})$ shows that this uncertainty is almost exclusively due to uncertainty in calculating the organic phase mass fraction, X_O. The result of this is summarized in the last column of Table 4.3.2, which shows the relative standard deviation in the solids fraction. When there are no flow metering errors, solids fraction measurements are more accurate for higher solids latex. If mass balance errors are taken into account, however, this trend is offset with the net result that relative solids fraction error stays roughly constant over a wide range of recipes. In all cases, the calculated standard deviation is under 1%, which is acceptable for this application.

Next, consider the variance of the mean diameter of the latex particle size distribution. The last three columns of Table 4.3.3 show that its standard deviation, calculated from dilute latex transmittance, is on the order of 3% for all cases considered. This variation embodies roughly

equal contributions from the variance of the turbidity reading and from the calculated polymer fraction in the diluted latex. The latter is dominated by uncertainty in the dilution ratio which, in turn, reflects mostly the latex sampling variance (Section 3.4.3). The variance in the transmittance measurement could be reduced to negligible proportions through a suitable averaging filter and finer resolution on the analog-to-digital conversion. Since the diameter standard deviation is within an acceptable range, nothing was done about either source of error.

Finally, recall from Chapter 3 that densitometry has been proposed as a means of measuring monomer conversion in a polymerization reactor (Schork and Ray, 1985). Table 4.3.4 show that, while this is straightforward in a system with no mass balance errors, flow metering errors of 2% on the inlet streams cause the standard deviation to be over 10% of the measured conversion, regardless of the monomer fraction in the recipe. Clearly, caution is called for when using densitometers to track conversion in continuous polymerization reactors.

		$\left(\frac{V(X_o)}{X_o^2}\right)^{\frac{1}{2}}$ (10^2)	$\left(\frac{V(X_S)}{X_S^2}\right)^{\frac{1}{2}}$ (10^2)	$\left(\frac{V(X_l)}{X_l^2}\right)^{\frac{1}{2}}$ (10^2)	$(V(v_x))^{\frac{1}{2}}$ (10^2)	$(V(X_P))^{\frac{1}{2}}$ (10^2) Note(1)	$(V(X_{sol}))^{\frac{1}{2}}$ (10^2) Note(2)	$\left(\frac{V(X_{sol})}{X_{sol}^2}\right)^{\frac{1}{2}}$ (10^2)
Low Solids	no flow error	0.0	0.0	0.0	0.009	0.04	0.04	0.40
	flow error	2.5	2.5	2.5	0.009	0.07	0.07	0.84
High Solids	no flow error	0.0	0.0	0.0	0.009	0.03	0.03	0.06
	flow error	2.3	2.3	2.3	0.009	0.36	0.36	0.74

$$Note(1): V(X_P) = \left[\frac{v_M - v_{Aq}}{v_M - v_P}\right]^2 V(X_O) + \left[\frac{1}{v_M - v_P}\right]^2 V(v_x)$$

$$\text{Note(2): } V(X_{sol}) = V(X_P) + V(X_l) + V(X_S)$$

Table 4.3.2: Solids Fraction Variance

		$\left(\frac{V(X_F)}{X_F^2}\right)^{\frac{1}{2}}$ (10^2)	$\left(\frac{V(R)}{R^2}\right)^{\frac{1}{2}}$ (10^2)	$\left(\frac{V(v_z)}{v_z^2}\right)^{\frac{1}{2}}$ (10^2)	$\left(\frac{V(C_F)}{C_F^2}\right)^{\frac{1}{2}}$ (10^2) Note (1)	$\left(\frac{V(\tau)}{\tau^2}\right)^{\frac{1}{2}}$ (10^2) (T=0.75)	$\left(\frac{V(D)}{D^2}\right)^{\frac{1}{2}}$ (10^2) Note (2)
Low Solids	no flow error	0.45	2.5	0.01	2.51	1.87	3.13
	flow error	0.84	2.5	0.01	2.64	1.87	3.23
High Solids	no flow error	0.06	2.5	0.01	2.47	1.87	3.10
	flow error	0.76	2.5	0.01	2.59	1.87	3.19

Note (1) $\frac{V(C_F)}{C_F^2}=\frac{V(X_F)}{X_F^2}+\frac{V(R)}{R^2}+\frac{V(v_z)}{v_z^2}$

Note (2): $\frac{V(D)}{D^2}=\frac{V(\tau)}{\tau^2}+\frac{V(C_F)}{C_F^2}$

Table 4.3.3: Particle Diameter Variance

		$\nu_0 - \nu_1$	$\left(\frac{V(\nu_x)}{(\nu_0-\nu_1)^2}\right)^{\frac{1}{2}}$ (10^2)	$(V(\nu_1))^{\frac{1}{2}}$ (10^2) Note (1)	$\left(\frac{V(\nu_1)}{(\nu_0-\nu_1)^2}\right)^{\frac{1}{2}}$ (10^2)	$(V(x))^{\frac{1}{2}}$ (10^2) Note (2)
Low Solids	no flow error	0.02	0.45	0.0	0.0	0.45
	flow error	0.02	0.45	0.26	1.84	13.2
High Solids	no flow error	0.12	0.06	0.0	0.0	0.06
	flow error	0.12	0.06	1.46	4.25	12.4

Note (1) $V(\nu_1) = (\nu_F^2 + \nu_{M_f}^2)V(X_O)$

Note (2) $V(x) = \left[\frac{1}{\nu_0 - \nu_1}\right]^2 V(\nu_x) + \left[\frac{\nu_x - \nu_1}{(\nu_0 - \nu_1)^2}\right]^2 V(\nu_0) + \left[\frac{\nu_0 - \nu_x}{(\nu_0 - \nu_1)^2}\right]^2 V(\nu_1)$

where $\nu_x = \nu_1$ at 100% conversion

Table 4.3.4: Monomer Conversion Variance

4.4 Nomenclature for Chapter 4

C_{in}	Inlet mass concentration [g/ml]
C_F	Feed stream mass concentration [g/ml]
C	Volume fraction polymer in diluted latex sample [ml/ml]
D	Particle diameter [nm]
F	Volumetric flow rate [ml/min]
l	Turbidity sample cell optical path length [cm]
M	Mass flow rate [g/min]
R	Sampler/diluter dilution ratio
T	Transmittance
v	Specific volume [ml/g]
$V(x)$	Variance of x
V_M	Volume of sampler/diluter mixing tank [ml]
V_S	Volume of latex extracted in sample loop [ml]
x	Fraction monomer conversion
X	Mass fraction

Greek Symbols

ρ	Density
σ	Standard deviation
τ	Turbidity

Superscripts and Subscripts

Aq	Aqueous
C	Continuous phase
I	Initiator
in	Reactor inlet
M	Monomer
O	Organic phase

out	Reactor effluent
P	Polymer
S	Soap or emulsifier
sol	Solids
W	Water

5

ON-LINE EXPERIMENTAL RESULTS

5.1 Continuous Seed Reactor

The on-line solids and particle size instrument were evaluated on a pilot scale, continous latex reactor. The reactor is a 500 ml, jacketed, stainless steel vessel. The feed enters via an inlet manifold through the vessel wall. The feedstock is stored in sealed, stainless steel tanks in which it is deaerated and blanketed with ultra high purity nitrogen because oxygen is a radical scavenger and poisons the reaction. It is pumped from the tanks to the reactor by four positive displacement pumps: one each for initiator solution, emulsifier solution, monomer, and water.

The reactor is both heated and cooled by steam heated water which circulates in the jacket. The temperature is controlled by an electronic PID controller manipulating the steam flow rate to the jacket. A pitched blade agitator mixes the reactor contents at 200 r.p.m.

Latex exits through an overflow tube in the head of the reactor vessel, with the result that there is no head space in the reactor. The densitometer, sampler/diluter, and spectrometer are attached to the reactor effluent line as shown in Fig. 3.1.1.

In the experiments below, the reactor was run to produce a poly(vinyl acetate) seed latex. The points that differentiate a seed reactor from "normal" CSTR operation are the low residence time (<10 minutes) and the low monomer fraction (<0.10) of the seed reactor. Recipes of this type have important industrial applications. The low solids latex is intended to be a seed latex produced at the beginning of a train of larger reactors. Seeding the first large reactor of a continuous latex reactor train has been shown to increase the productivity of the process (Nomura and Harada, 1981). More importantly, some commercially important latex systems, like vinyl acetate and vinyl

chloride, exhibit sustained, limit cycle oscillations in conversion and particle size when produced in CSTRs (Green et al., 1976, Kiparissides, 1978). These oscillations are inextricably tied to particle nucleation mechanisms in the reactor, but can be eliminated in operating regions producing low solids latex at low reactor residence times. If particle nucleation is restricted to the seed reactor in a continuous reactor train, oscillations can be eliminated in the entire train. This has been demonstrated both experimentally and theoretically in the continuous emulsion polymerization of vinyl acetate (Nomura and Harada, 1981; Pollock, 1983; Penlidis, 1986). Furthermore, if the recipe is such that no particle nucleation occurs in downstream reactors, the particle size distribution of the finished product is entirely specified by that of the seed latex and by the residence times of the downstream reactors. The net result is a very efficient process for latex production with fine control of latex properties.

The high productivity of this process, however, means that unless there is adequate on-line instrumentation to monitor the properties of the seed latex, a lot of off-spec product can be made in the time it take a production laboratory to analyse a sample. Monitoring its particle size is important for quality control of the final latex, and will give important lead time in manipulating downstream reactors to keep product quality on-spec. These experiments are the first demonstration of a fully instrumented, stable, continuous production of poly(vinyl acetate) seed latex.

Other, more practical advantages of dealing with a seed latex in these experiments include the relative ease of sampling and the ability to work with lower dilution ratios for turbidity measurements than would be required for high solids latex. These advantages do not, however, present any restrictions to the range of applicability of the instrument. The sampling apparatus has been tested up to 40% solids poly(styrene/MMA) latex, and no coagulation or coating for the sampling element was observed (Tremblay, 1991); and the required dilution ratio for linear turbidity-concentration behaviour can always be decreased by using thinner transmittance cells.

5.2 Reaction Recipes and Pump Calibration

There are three experimental runs reported in this section, and each consisted of at least two different operating regions that were designed to cover a range of conversion, particle size, stable and unstable operating regions. All three runs produced a poly(vinyl acetate) seed latex. As this latex was initially designed to be fed directly to another continuous reactor, there is no pH buffer in the recipe. Consequently, these latexes are not very stable and have a limited shelf life. All the flow rates, feed concentrations, and reaction temperatures are listed in Table 5.2.1.

The flow rates delivered by the pumps vary considerably with downstream load. This problem is minimized by designing the feed system so that the biggest load is across the check valves at the reactor inlet manifold. Accurate calibrations are then done by first setting a check valve release pressures to ensure that there was flow only on the downstroke of the pump. The flow rate can then be calibrated against pump speed and stroke using a bucket and stopwatch. Once calibrated, the checkvalves are not adjusted. Table 5.2.1 reports flow rates from calibrations done before and after each run. The standard deviations are the calculated from the residual sum of squares of the calibration curves.

5.3 Experimental Runs

Each of the experiments described below highlights a different aspect of the combined solids/particle size instrument system and of the continuous seed reactor. Each run also has experimental idiosynchracies that distinguish it from the others and demand a slightly different treatment of the data and calculations. For clarity, they will be discussed separately. A synopsis of the conclusions is presented at the end of the Chapter.

Process Variables	Std Dev	Run 6		Run 7			Run 8				
	[ml/min]	1	2	1	2	3	1	2	3	4	5
Water [ml/min]	0.51	15.7	22.3	19.2	25.8	25.8	11.8	4.1	22.8	26.6	4.0
Monomer [ml/min]	0.41	10.0	10.0	6.1	8.1	8.1	4.9	4.9	4.9	4.5	4.5
Initiator Sol'n [ml/min]	0.19	17.1	17.1	9.8	13.0	13.0	9.8	9.8	9.8	7.7	12.7
Emulsifier Sol'n [ml/min]	0.80	5.5	9.6	25.0	33.5	33.5	32.4	37.8	21.2	22.2	38.9
Emulsifier Conc.	in feed	8.6	11.9	10.4	10.4	10.4	6.0	7.3	3.9	3.9	7.0
[g/l H_2O]	in feed tank	60.5		22.5			10.0				
Initiator Conc.	in feed	20.1	15.7	4.1	4.0	4.0	4.5	4.3	4.1	3.1	5.1
[g/l H_2O]	in feed tank	45.0		22.5			22.5				
Monomer Mass Percent		10.5	15.2	9.4	9.3	9.3	7.7	8.1	7.8	6.7	7.0
Reactor Space Time [min]		10.1	8.2	8.1	6.0	6.0	8.2	8.6	8.3	8.0	8.1
Reactor Temperature [°C]		50	50	50	50	60	60	60	60	60	60

Table 5.2.1: Latex Reaction Recipes

5.3.1 Run 6

Being the earliest in this series of experimental runs, Run 6 used a different prototype for the latex sampler than subsequent runs. Instead of having the Isolok® sample valve pictured in Fig. 3.4.2, two three-way ball valves were used to trap a known volume in a sample side stream and send it to the mixing tank. The disadvantages of this system were that the flow paths were smaller, more torturous, more difficult to clean, and that it interrupted the flow when sampling and diluting the latex. One advantage of this prototype was that the design allowed for mixing of diluted latex before it was sent to the spectrometer, so any errors attributable to poor mixing were eliminated.

The feed and reactor conditions and the raw instrument responses are in Fig. 5.3.1. The run comprised two operating regions, chosen to yield very different latex and to demonstrate one stable and one less stable operating region. Few start-up transients are seen because the instruments were only started up after the reactor had been lined out at the first steady state.

The transmittance plot in Fig. 5.3.1 shows a downward step in transmittance just as steady state is reached in operating region 2. This happens because the dilution ratio was decreased at this point (something that can be accomplished with the flick of a switch) to keep the transmittance in an optimal region for signal-to-noise. This practice was abandoned for later runs, but does illustrate a useful point: the specific turbidity hardly changed with the switch in dilution ratio, evidence of the linear turbidity/concentration relationship in this range of dilution ratios.

The dilution ratios used were 1/342.51 in the first operating region and 1/379.14 in the second. The accuracy of the dilution ratio is comparable to that of the later prototype (Section 3.4.3). The aspect ratio of the mixing tank was the same as that of Level 2 in Fig. 3.4.1., but the contents were well mixed.

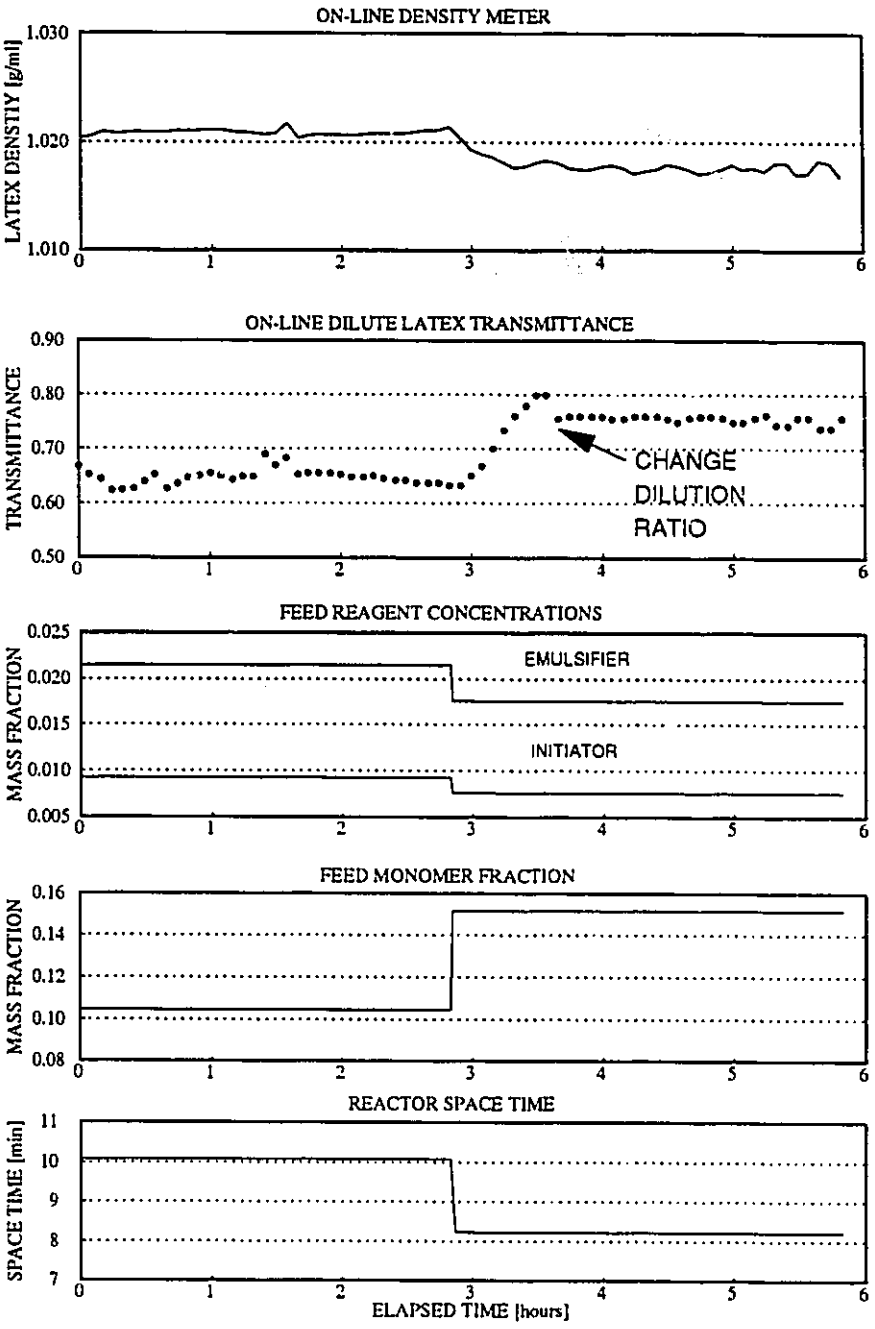

Fig. 5.3.1: Run 6 On-line Instrument Raw Data

There are some points of interest in the raw instrument responses. The first is this system's exceptional immunity to noise. The spectrometer resolution was limited only by the quantization error in the analog-to-digital conversion. The second operating region was chosen because in exhibits some of the oscillations in latex properties that are characteriztic of higher solids vinyl acetate emulsion polymerizations. In this region, the densitometer was able to resolve oscillations with peak-to-peak differences of 0.0007 g/ml. The densitometer data was not filtered, and the spectrometer took a 10 second averaging filter for each data point.

All the information in Fig. 5.3.1 is used in the calculations of solids fraction and mean diameter in Fig. 5.3.2. Both these quantities are also compared to off-line analyses done on samples taken during the run. Solids fraction was measured off-line by gravimetry: drying and weighing latex samples. Volume weighted mean diameter was measured using the Nicomp 370 Dynamic Light Scattering (Section 2.3).

In the calculations of the on-line results a single parameter, the density of the aqueous phase, was adjusted to bring on-line solids fraction in line with off-line gravimetry. Particle diameter was then calculated with no further parameter adjustment. The agreement between on-line and off-line results is excellent.

On-line particle sizing results seem to exhibit much less variation than off-line dynamic light scattering. In fact, the on-line results are so stable, that the sensitivity of the particle sizer to process changes could be called into question. Later, Run 8 will provide a dramatic demonstration of the sensitivity of the technique while also pointing out that much of the variation in the volume weighted mean from DLS can be attributed to two phenomena. First the volume weighting is not the native unit of the instrument. It is calculated from the intensity weighted mean and standard deviation, and tends to be less stable than the native, intensity weighted DLS diameter. Secondly, the latex was unbuffered and somewhat unstable. Samples coagulated within days, which contributes much noise in off-line measurements. Run 8 solves this dilema by comparing on-line DLS results with on-line turbidity.

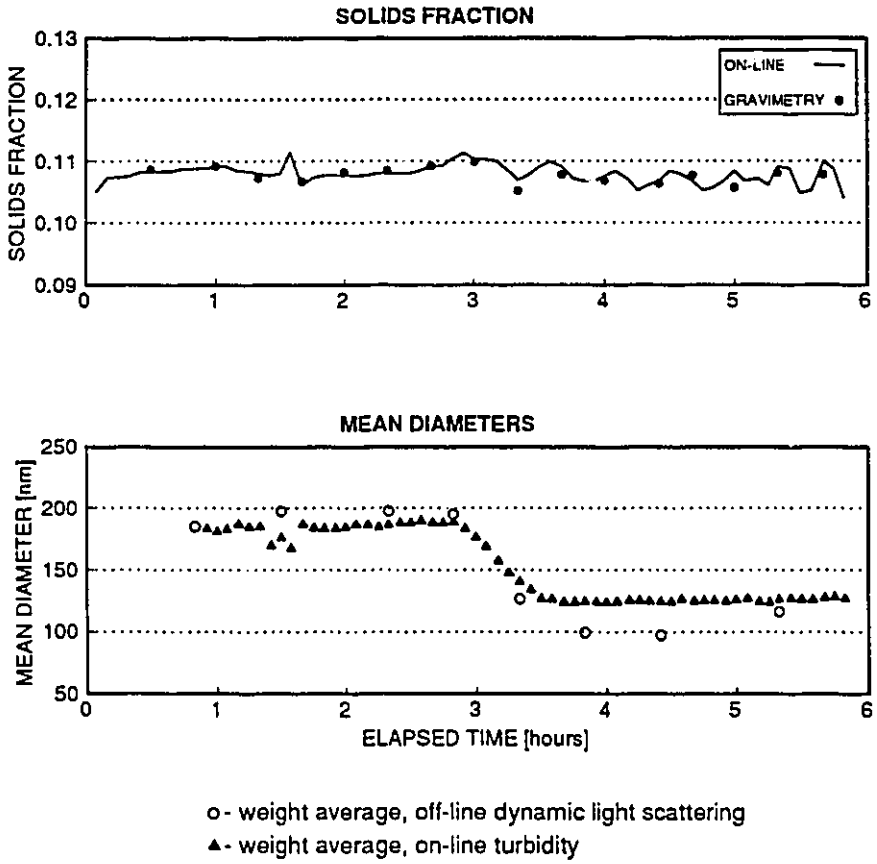

Fig. 5.3.2: Run 6 On-line Instrument Results

5.3.2 Run 7

Run 7 was the first run with the sampler-diluter prototype described in Section 3.4 using the dilution ratio corresponding to Level 2 in Fig. 3.4.1. The reactor conditions and raw instrument responses are shown in Fig. 5.3.3. There are three operating regions. The first two are designed to produce latex with similar mean diameter but different conversion by only changing the reactor space time. Between the second and third operating regions, only the reactor temperature was raised.

One unfortunate feature of this run was that latex samples were stored several weeks before being analysed for solids. Although radical scavenger (hydroquinone) was added to the samples when they were taken, the reaction apparently went to its limiting conversion in all sample vials. This conclusion is strongly supported by the fact that gravimetry showed no change in conversion between operating regions 2 and 3, when the reactor temperature was increased; whereas, the densitometer shows a large change in conversion which was confirmed during the run by a marked decrease in the odour of monomer in the sample vials and a visible increase in the turbidity of the latex.

Since off-line solids fraction data was not available, the density of aqueous phase was adjusted to align turbidity results and DLS volume weighted mean diameter (Fig. 5.3.4). The mean diameter results clearly follow start-up transients, the change between operating regions 2 and 3, and the lack of change between operating regions 1 and 2. The intensity weighted DLS mean diameters are show in Fig. 5.3.4 because they are refered to in the discussion of Run 8.

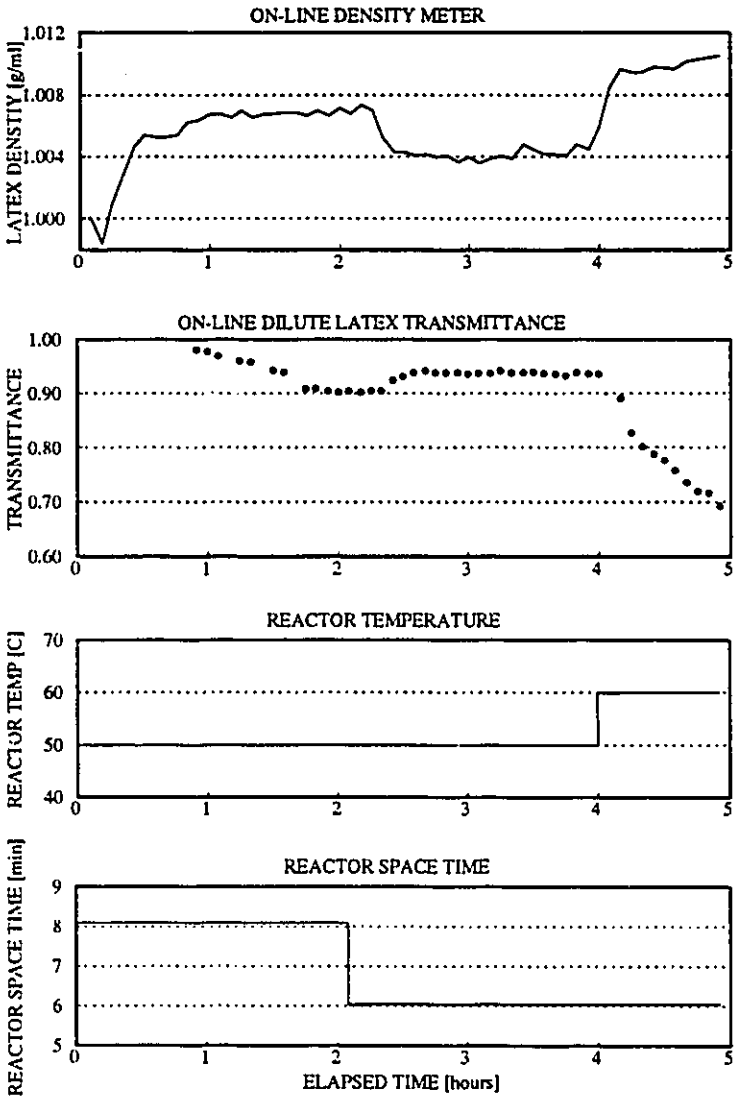

Fig. 5.3.3: Run 7 On-line Instrument Raw Data

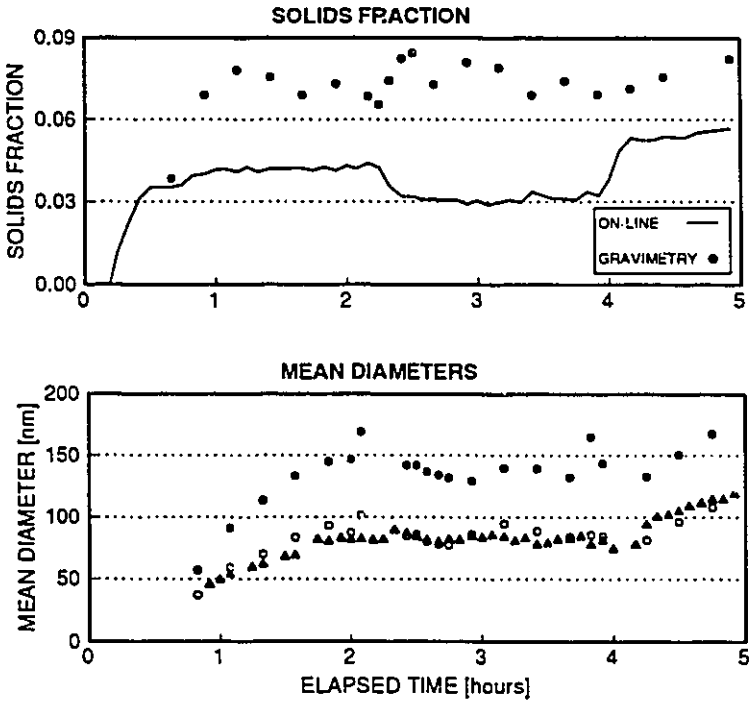

Fig. 5.3.4: Run 7 On-line Instrument Results

5.3.3 Run 8

Run 8 is the most dramatic run of this triplet. The feed conditions and raw instrument responses are shown in Fig. 5.3.5. The run was 10 hours long, and comprised 5 operating regions. The operation includes start-up transients, and attempted to cover as wide a range of operation as possible at one reactor temperature and space time.

The dilution ratio used corresponded to Level 1 in Fig. 3.4.1. Recall that this dilution ratio has some rather severe mixing problems because of the large L/D ratio of the tank (Section 3.4.3). This was compensated for by making the cell length in the turbidity calculation an additional adjustable parameter in the calculations. As before, the density of the continuous phase was adjusted to match on-line densitometer results with off-line gravimetry.

Turbidity results were compared with on-line dynamic light scattering using a Nicomp 370 particle sizer modified for on-line use. The Nicomp sampler-diluter is pictured in Fig. 5.3.7. For this run it sampled directly from a sample bleed off the reactor effluent just after the turbidity sampler-diluter. Filtered, deionized distilled water was used as the diluent for DLS.

The on-line DLS results are shown along with those of turbidity in Fig. 5.3.6. DLS samples were taken every 10 minutes, and the autocorrelator collected only 2 minutes of data for each sample. Nonetheless, intensity weighted DLS results show remarkable stability in the mean with only that small amount of data, and their reproducibility and sensitivity is on par with the turbidity based particle sizer. This is especially remarkable in that the broad particle size distributions produced by continuous reactors are a worst case scenario for dynamic light scattering particle sizers.

Fig. 5.3.6 also shows that the variation in volume weighted DLS means is greater than that of the intensity weighted means. The reason for this is that the volume weighted mean is a derivative quantity that depends on both the intensity weighted mean and breadth of the

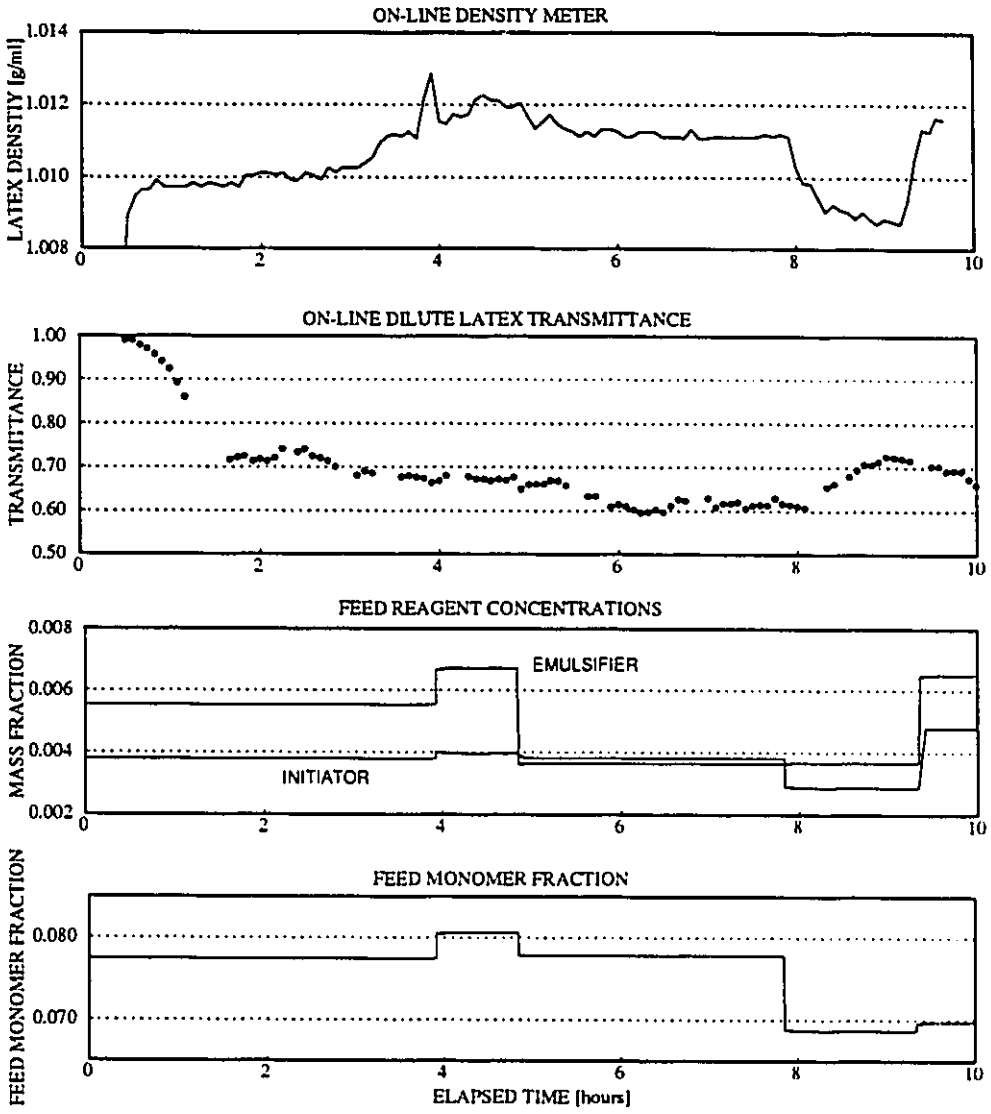

Fig. 5.3.5: Run 8 On-line Instrument Raw Data

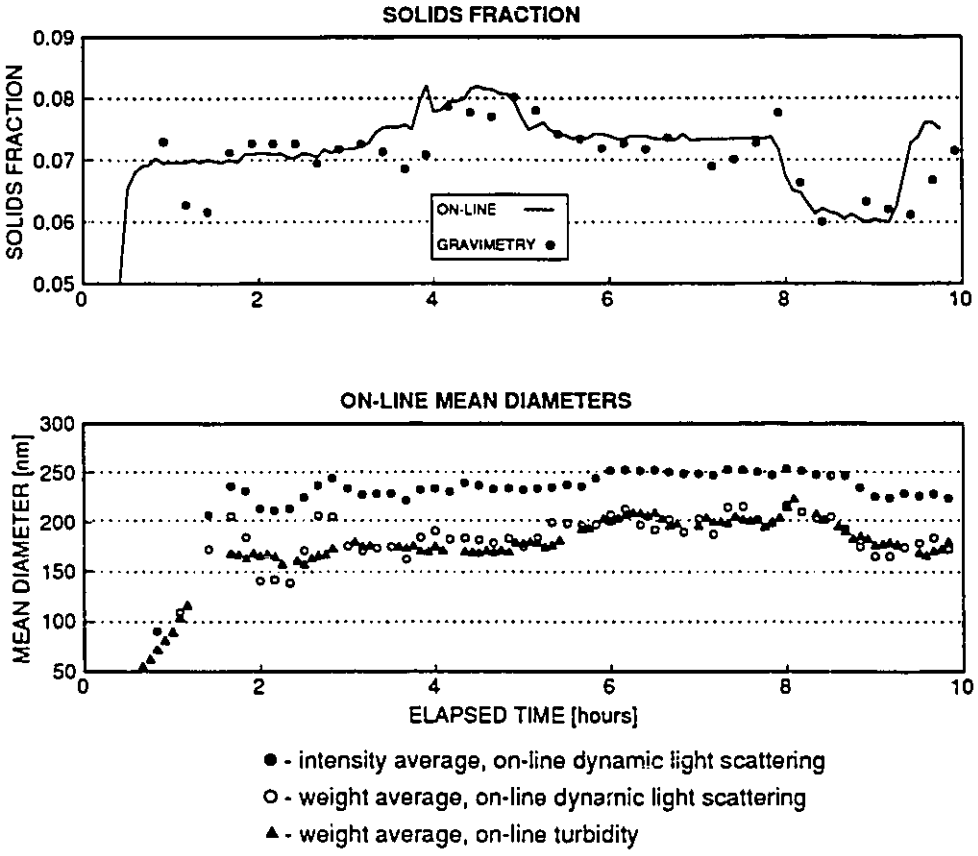

Fig. 5.3.6: Run 8 On-line Instrument Results

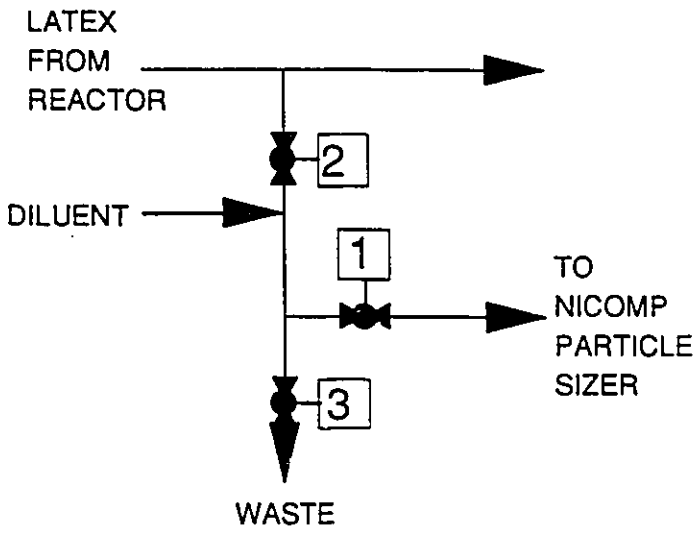

Fig. 5.3.7: Nicomp On-line Sampler-Diluter

distribution. While the intensity weighted mean is quick to converge to its final value, the breadth parameter is much less stable, and these instabilities manifest themselves in the calculation of the volume weighted mean.

Another important comparison to make is between the DLS intensity weighted mean diameters from Run 8 in Fig. 5.3.6 and those for Run 7 in Fig. 5.3.4. For comparable variation in mean diameters from turbidity, on-line DLS result in Run 8 have a much lower variance than than the off-line results in Run 7, even though the off-line results were calculated after taking from 10 to 100 times as much data as the on-line ones. The obvious conclusion is that the latex samples degrade very quickly, changing the particle size distribution and causing more sample-to-sample variation than the reactor actually produces.

5.4 Summary

The above experimental runs yielded much valuable information about the accuracy , reproducibility, and operation of the on-line solids fraction and particle sizing instrument designed in this work. They also demonstrate the advantages of automated on-line measurements over off-line laboratory analysis, and the stable operation and flexibility of a continuous seed latex reactor. Highlights of the previous section are:

1) The sampler/diluter operated continuously for 100 cycles at 5 minute intervals without any problems. To date, it has operated flawlessly for over 500 cycles without need for maintainance.
2) In an oscillatory operating region, the densitometer cleanly resolved density fluctuations with 0.0007 g/ml peak-to-peak variation.
3) A mixing tank L/D ratio of 6 adversely affects mixing. The result is a constant bias in the transmittance readings that was compensated for by using the transmittance path length as an adjustable parameter for Run 8.

4) Composition variation due to poor mixing is reduced by 45% by changing the L/D ratio from 6 to 3 and by drilling holes in the down tube below the level sensor.

5) When mixing in the dilution tank is good, the mean particle diameter can be calculated from dilute transmittance without resorting to any additional adjustable parameters once the solids fraction in the concentrated latex is known.

6) On-line particle sizing by turbidimetry resolved changes in mean diameter on the order of 10 nm.

7) Off-line particle sizes by DLS consistently showed higher variance than on-line results. On-line particle sizes by DLS and turbidity have comparable variance.

8) The continuous seed reactor produced latex with weight average diameters from 70 to 210 nm.

9) Stable seed reactor operation was achieved at monomer mass fractions from 0.670 to 0.105 and reactor space time from 6 to 10 minutes. Limit cycle oscillations were observed at a monomer fraction of 0.152 with and 8 minutes reactor space time.

6

OPTICAL SPECTROMETRY AND MULTIVARIATE CALIBRATION FOR COPOLYMER LATEX

The preceding chapters explained the design, construction, and evaluation of an on-line analyzer system that measured solids fraction and weight average particle diameter in a poly(vinyl acetate) homopolymer latex. Solids fraction was calculated from on-line density measurements in conjunction with a dynamic mass balance. Mean diameter was calculated from on-line solids fraction and on-line UV turbidity at one wavelength. Several conceptual points about that work bear highlighting because they serve as an introduction to the work to come by way of either analogy or contrast.

First, the relationships between the sensor responses and the properties of interest were derived from a thorough, mechanistic understanding of the physical phenomena involved. In both cases, a unique solution to these mechanistic relations was possible because they were being applied on a homopolymer system, thus restricting the degrees of freedom of the sensor-property relations so that all uncertainty in the parameters of these relations could be accounted for using only one adjustable parameter per property of interest. The second point to highlight is that each of the analyzers designed so far requires data from several "transducers" to calculate the latex property. Solids fraction was calculated using a densitometer plus a dynamic mass balance around the reactor. Mean diameter was calculated from this solids fraction plus the turbidity at one wavelength.

These conclusions can be contrasted to what will be presented below. The concept of multiple sensors is expanded, so the number of transducers will increase from a handful to several hundred. The sensor-property relations, in contrast, will be empirical. This has the very important

implication that transducers will be used even when the complete sensor-property relations are not known. The remaining work, therefore, focuses on picking robust transducers, suitable for industrial environments and readily available, and trying to determine what information can be obtained from these sensors in copolymer latex applications.

The discussion in Chapter 2 covered the application of UV/Vis spectrometry to measuring the particle size distribution (PSD) in latex. For homopolymers, the PSD and the monomer conversion are the primary properties of interest. Copolymer latexes present the additional complication of variation in polymer composition. An obvious place to look for appropriate on-line sensors for copolymer composition is in optical spectrometry.

6.1 Optical Methods For Copolymer Composition

6.1.1 Infrared

Infrared (IR) spectroscopy has been used for decades in both the qualitative and quantitative study of polymers. The IR region comprises wavelengths above 2.5 μm, where absorption is due to fundamental vibrations of the molecular bonds (Olsen, 1975). IR spectra have very sharp peaks that can be assigned to a particular vibrational mode of a bond in the polymer or monomer molecule. This aspect has made IR spectroscopy an important tool in elucidating the structure of polymer systems (e.g. Nyquist, 1987; Urban and coworkers, 1987a; Urban and Koenig, 1987b). More importantly for the matter at hand, IR spectroscopy has also found considerable application in the determination of copolymer composition. Quantitative applications generally require that at least one of the monomers present have some specific functional group that the other does not. This is not a big restriction, since comonomers are often chosen to have some specific functionality to modify the properties of the homopolymer. Calibration curves are then constructed relating the area under the single IR peak specific to

the concentration of the specific functional group, or using the ratio of the functional group peak to that of some internal standard (e.g. Sharabash and Guile, 1976; Brown and Glass, 1988; Fuller, Ritter and Draper, 1988).

Some of the advantages of IR spectroscopy include the sharp, very specific peaks and the insensitivity of the vibrational bands to their molecular environment. Infrared spectroscopy has, however, some serious drawbacks when used for quantitative work. The low power of the sources and the low sensitivity of the detectors gives the IR region low signal-to-noise ratio relative to other regions of the optical spectrum. Molar absorptivities are high, so the path length must be small. This is often accomplished by dissolving the polymer, then casting and drying a film for analysis. This presents a problem because polymers are often very difficult to dissolve, especially if there is some high molecular weight material present. Furthermore, glass does not transmit IR light, so other materials must be used. These drawbacks to IR spectroscopy for routine, quantitative analysis encouraged researchers to investigate other regions of the optical spectrum.

6.1.2 Ultraviolet

Ultraviolet spectroscopy has found much use in quantitative analytical chemistry because of its high sensitivity. Light absorption in the ultraviolet region is largely due to outer-electron transitions in the molecules, and as such is very affected by bonding (Olsen, 1975). In the region 179 to 340 nm, most of the absorption is due to $\pi \rightarrow \pi^*$ and $n \rightarrow \pi^*$ transitions. Any multiple bonds have π electrons, so they absorb here as do the non-bonding electrons of N,O,S, and halogens. In general, the more tightly an electron is held by its associated molecule, the more energy required for a transition, and the lower the wavelength of the absorption peak.

The presence of a very strong absorption peak for the styrene aromatic ring at 269.5 nm, far from the absorbing region of many of its comonomers, prompted several investigators to

try ultraviolet (UV) spectroscopy for composition of copolymers of styrene. In particular, UV absorption spectroscopy has received some attention in the past as a technique for measuring the copolymer composition of styrene-co-methyl methacrylate in chromatography applications. (Tobolsky et al., 1959; Gallo and Russo, 1974; Garcia-Rubio and Ro, 1985). The calibration technique is to purify the polymer samples by precipitation, dissolve them in and organic solvent, and then measure the absorbance at around 269 nm. While potentially very straightforward, investigators soon discovered that the absorptivity of styrene's aromatic ring was very dependent on its environment on the polymer backbone (Garcia-Rubio and Ro, 1985) and on the solvent in which it was dissolved (Gallo and Russo, 1974). The advent of inexpensive scanning UV spectrometers has sparked some new interest in this area because more sophisticated algorithms can be used to deconvolve the contribution of styrene functional groups in their various environments (Garcia-Rubio and Ro, 1985).

The theory of light scattering by polymer particles in latex was discussed in Chapter 2. The difficulties associated with reconstructing the particle size distribution of a latex from turbidity spectra were already discussed there. Some efforts have been made in recovering both the refractive index and the particle size distribution using UV spectroscopy (Rowell and Ford, 1981); but these techniques, though successful, involve taking turbidity readings at several angles. For on-line instruments we would like to use the same configuration as for the simpler, single wavelength turbidity meter used in the homopolymer case to take advantage of the commercially available diode array spectrometers, with their robustness, low cost, and ease of operation.

6.1.3 Near Infrared

The near-infrared (NIR) spectral region is generally defined as the wavelength range 800 to 2500 nm. Absorptions in the near-infrared are overtones and combinations of the fundamental mid-infrared molecular vibration bands. The energy transitions to the first, second

and third excitation states are progressively less likely to occur, so each overtone is successively weaker in intensity. This accounts for the characteristically low molar absorptivities that provide unique sampling advantages when using NIR spectra.

When dealing with organic compounds, the most prominant NIR bands are those related to O-H, C-H, and N-H groups. The frequencies of the fundamental stretch vibrations of these groups is in the mid-IR, so the first and second overtones occur in the near-IR. Combination bands, involving stretch plus one or more bending or rocking modes, also occur in this region. Many combinations occur, so the NIR region is complex, with many overlapping absorption bands.

The near infrared region got some early attention for measuring copolymer composition. Early applications were generally in the analysis of pressed copolymer samples, where the low molar absorptivity allowed for thicker samples than for IR spectroscopy. Emphasis was placed on the suitability of the method for fast in-plant analysis (Kaye, 1954). Aside from low molar absorptivity, NIR was seen to have the advantages of being in the glass transmission region, and having high energy sources (Miller and Willis, 1956; Foster, Row and Griskley, 1964).

These early results were largely ignored by the polymerization industry. It was left to the food and agriculture industry to realize the potential of NIR and pioneer much of the development of NIR instrumentation. Williams and Norris (1987) have published a definitive monograph on this technology. Their indexed bibliography has 954 references, over 800 of them in the agriculture and food industries. Stark and coworkers (1986) have written an excellent, concise review of the development of the field. Two aspects of NIR spectroscopy make it particularly attractive as an analytical technique for in-plant or on-line applications: (1) many analyses can be made using diffuse reflectance measurements on concentrated samples, requiring almost no sample preparation; and (2) NIR light can be transmitted by communication grade optical fibers, meaning the analyzer can be hundreds of meters away

from the process line that it is measuring. NIR technology is now quickly entering the chemical and polymerization industries. Some polymer applications have recently been reported in the literature (Miller, 1989; Taboudoucht and Ishida, 1989).

Water Based Systems

There are two strong water absorption bands in the NIR region: at 1940 nm and 1440 nm. The detection of water has, therefore, been one of the oldest applications of NIR spectroscopy (Weyer, 1985; Stark and coworkers, 1986). For the same reason, the use of NIR spectroscopy in systems that are predominantly water has been limited.

Recent applications to aqueous solutions have necessarily used full spectrum techniques (Buchanan and coworkers, 1988). An interesting approach is to remove the contribution of water to the spectrum by a least squares projection onto a plane that defines most of the water spectrum variation. This approach was used to do studies of the structure of styrene/acrylic acid in aqueous solution (Urban and coworkers, 1987a; Urban and Honigs, 1987b). It can also be used to remove unquantified interferences caused by compounds with known spectra (Devaux and coworkers, 1988a).

Remote Sensing with Fiber Optics

The availability of telecommunications grade fibre optic waveguides has opened the field to remote sensing spectroscopy. Optical fibres have good transmission efficiency in the range of 400 to 2200 nm, so applications have been limited to the visible and NIR regions. Early applications usually involved modifying a spectrometer to accommodate fibre optics. Now, fibre optic probes are available as integral parts of VIS/NIR instruments from several manufacturers.

One of the advantages of fibre optic probes is that they are intrinsically safe and can be used in explosive environments (Buchanan and Honig, 1987). They have also been used to analyze samples in radioactive environments (DeBold and van Hare, 1987). They also offer the

opportunity to do spectral measurements *in situ*, which may help avoid or minimize the difficult sampling problems associated with high-solids latex processes. Finally, many fibre optic probes can be multiplexed onto a single spectrometer, making it a very cost effective alternative to other on-line composition instruments.

6.2 Multivariate Calibration of Optical Spectra

The renaissance of interest in the NIR region of the spectrum is inextricably linked to the development of some sophisticated statistical techniques that deal with the many overlapping bands in the NIR region and with the nonlinearities introduced by using concentrated samples.

Commercial scanning spectrometers are now readily available for on-line use. In this work, two spectrometers provide absorbances digitized at 1516 wavelengths between 190 nm in the ultraviolet and 1800 nm in the near infrared. We can, therefore, at relatively low capital and operating cost, work in an environment rich in sensor data. While cost, availability, instrument sensitivity and reliability are the primary reasons for working in the UV to NIR spectral region (and the main criteria for any on-line instrument system), the major drawback is that throughout this region absorption peaks are very broad and nonspecific. This, in conjunction with the inherent complexity of latex systems and the nonlinearities associated with measurements made in concentrated suspensions, means that analytical sensor-property relations are intractable. Empirical, multivariate sensor calibration models are used to deal with this problem.

The methodology for constructing a multivariate calibration is to collect many samples covering the entire range of property variation that will be encountered during normal operation of the process. This is the calibration set. These samples are carefully analyzed by traditional laboratory methods for the properties of interest (polymer composition, particle size, residual monomer, etc.). The NIR or UV spectra of the samples are then taken and are related to the properties of interest using one of the statistical techniques described below. The properties of

unknown samples are estimated from their optical spectra using this calibration model. This methodology has several important implications. First, regardless of the accuracy of the spectrometer, the accuracy of the property prediction can never exceed that of the original laboratory measurement used to characterize the samples. Secondly, the calibration model will be invalid outside the range of sample properties in the calibration set, so the samples must exhaustively cover the range of variation that will be encountered by the analyzer.

Mathematically stated, the basic multivariate calibration problem is this: absorbances at many (say, $m = 1000$) wavelengths are measured. There are relatively few samples (say, $n = 50$) that have been carefully characterized and will be used to build the calibration model. The absorbances must be related to the concentrations of a number of constituents in the samples via the linear additive calibration model

$$y' = x'B \tag{6.2.1}$$

where x are the absorbances. In most of the multivariate calibration literature, y is a vector of analyte concentration . The model can, however, be generalized to any variable that is affected by the sensor responses in x. The coefficients of the model, B are estimated statistically. Spectra of n calibration samples are used to form the $n \times m$ matrix of dependent variables X. The p known properties of the samples form the $n \times p$ matrix Y. The standard multiple linear regression (MLR) approach to this problem is to estimate B by:

$$\hat{B} = (X'X)^{-1}X'Y \tag{6.2.2}$$

In spectroscopy, the variables in X are highly colinear, meaning $X'X$ is nearly singular and cannot be inverted. Furthermore, for most modern spectroscopy applications $n < m$, meaning, again, $X'X$ cannot be inverted. The approach taken to solve this problem is to reduce the column dimensionality of X while either: (1) preserving all the essential information in X; or (2) extracting only that information in X that is relevant to predicting Y; or (3) some compromise between (1) and (2) (Martens and Næs, 1987).

In many applications of NIR spectroscopy the data reduction is accomplished by using some subset of the NIR wavelengths as the predictors. Stepwise MLR or some variation thereof is used to select one to four wavelengths for each constituent of interest. The disadvantage of this method is that much of the information in a spectrum is discarded, and the ability to detect interferences is greatly diminished over full spectrum methods. In full spectrum methods, absorbances at every wavelength are used to calculate a reduced, well-conditioned form of X that can be used to estimate B in eq. 6.2.1.

Some researchers have used Fourier analysis to reduce and condition the spectral data. Fourier analysis is particularly applicable to interferometric spectrometers because the native spectra are taken in Fourier-space (Williams, 1989; Mittlefehldt and Gardella, 1989). Its many attractive features encouraged researchers to apply it to scanning spectrometers that collect data in wavelength-space (McClure and coworkers, 1984; Hoy and McClure, 1989). In this case, each spectrum is represented by the complex coefficients of its Fourier transform. The first reduction in the dimensionality of X is achieved because, as McClure and coworkers (1984) showed, only the first 99 terms of the Fourier expansion (the constant and 49 complex coefficients) can completely represent most NIR spectra.

Fourier transforms offer many signal processing advantages over working in wavelength space. The spectra can all be mean corrected by simply setting the constant term of the expansion to zero. Noise above a certain frequency can be filtered out by simply setting all terms in the Fourier expansion above that frequency to zero. The result is an ideal unit gain, zero phase shift filter. McClure and coworkers (1984) predicted compositions of sugar, nicotine, nitrogen, calcium, and potassium in tobacco using only the first 11 terms of the Fourier transform of reflectance NIR spectra. Finally, narrow bandpass filters can easily be designed in Fourier space to enhance identification of small spectral features adjacent to broad, interferent spectral bands (Davis and Kroutil, 1990).

In spite of all these advantages, Fourier transform analysis has not had the impact in the field of multivariate calibration as have the two matrix projection techniques described below. Part of the reason is that Fourier-space spectra are difficult to interpret and do not have the advantages of intuitive pattern recognition and outlier detection combined with the many tools for interpreting and troubleshooting that arise from the following calibration methods. In matrix projection techniques, the m sensor measurements are assumed to be a linear compound of $a < n < m$ latent factors:

$$X_{(n \times m)} = T_{(n \times a)} P_{(a \times m)} + E_{(n \times m)} \tag{6.2.3}$$

where $P = [p_1 \cdots p_a]'$ are the basis vectors, in the column space of X, of the a-dimensional space onto which X will be projected; and $T = [t_1 \cdots t_a]$ is the matrix of the projections of X on P. The calibration methods differ in the way P, the NIR loading matrix, is chosen. In principal component analysis (PCA), T and P are estimated simultaneously to give orthogonal latent vectors, p, that account for the maximum variation in X. Partial least squares (PLS) is an extension of PCA that maximizes the amount of the variation in Y that is explained by T. Martens and Næs (1987) succinctly summarize the difference between these two techniques by stating that PCA concentrates the data to their most dominant dimensions and PLS, to their most relevant ones.

6.2.1 Principal Component Analysis

Principal Component Analysis (PCA) is a powerful technique for analyzing multivariate data. Its properties are well known and well understood, and will be covered in some detail here for two reasons: the first is its utility in analyzing and finding structure in high-dimensional data; the second is that the concepts discussed here form the foundation for the discussion of other algorithms.

The classical derivation of PCA can be found in many introductory multivariate statistics textbooks (e.g. Chatfield and Collins, 1980). Given a multivariate variable

$$x' = [x_1, \ldots, x_m] \tag{6.2.1.1}$$

with mean μ and covariance matrix Σ, the objective of PCA is to find an orthogonal transformation to a variable

$$t' = [t_1, \ldots, t_m] \tag{6.2.1.2}$$

such that the individual variables in t are uncorrelated and ranked from 1 to m in order of decreasing variance. The transformation is of the form

$$x_{(m\times 1)} = t_1 p_{1,(m\times 1)} + \cdots + t_m p_{m,(m\times 1)} \tag{6.2.1.3}$$

$$x_{(m\times 1)} = t\mathbf{P}_{(m\times m)}$$

where the columns of $\mathbf{P}$ are the orthonormal basis vectors of the rotation that transforms x to t. The classical derivation has some important results and properties that will assist in interpretation of the results in subsequent Chapters:

1) the basis vectors in the transformed space, p_i, are the eigenvectors of the covariance matrix Σ;

2) the covariance matrix for the new variables, t_i, is $\Lambda = \text{diag}(\lambda_i)$ where λ_i are the eigenvalues of Σ ranked in descending order $\lambda_1 > \cdots > \lambda_m$;

3) By obvious extension, $\text{var}(t_i) = \lambda_i$;

4) The following are standard results of matrix algebra:

$$\Lambda = \mathbf{P}'\Sigma\mathbf{P}$$

$$\therefore \sum_{i=1}^{m} \text{var}(t_i) = \text{trace}(\Lambda) = \text{trace}(\Sigma) = \sum_{i=1}^{m} \text{var}(x_i) \tag{6.2.1.4}$$

The consequence of this final result is that we can define the fraction of the total variance of x explained by each of the principal components p_i:

$$\left\{\begin{array}{c}\text{fraction of}\\ \text{variance}\\ \text{explained by}\\ \text{component } i\end{array}\right\} = \frac{\text{var}(t_i)}{\sum_{i=1}^{m}\text{var}(x_i)} = \frac{\lambda_i}{\sum_{i=1}^{m}\text{var}(x_i)} \tag{6.2.1.5}$$

In our case, x is a very large vector of sensor measurements associated with a sample. Physical systems generally have many fewer underlying sources of variation than the number of sensors, so in practice the number of components that account for virtually all the variation

in x is very much smaller than m, the dimension of the measurement space. This is how the dimensionality of X is reduced: when the variance of the t-scores is no longer significantly different from the variance of noise, no more PCA dimensions are calculated, and X is approximated by:

$$X_{(n \times m)} = t_1 p'_{1,(1 \times m)} + \cdots + t_a p'_{a,(1 \times m)} \qquad (6.2.1.6)$$

$$X_{(n \times m)} = T_{(n \times a)} P_{(a \times m)} \text{ where } a \ll m$$

T can then be used in place of X in the sensor-property model (eq. 6.2.1 and 6.2.2).

The eigenvectors and eigenvalues of Σ can be calculated by the power method (Gerald and Wheatley, 1984; Golub and van Loan, 1990), which calculates them successively in order of decreasing λ_i. There are two practical problems associated with this approach:

1) when the column dimension of x is large ($m > 1200$ in our case) Σ is a huge matrix, too large for many small computers.

2) the approach does not deal with missing data.

It is in answer to the second problem than H. Wold introduced the NIPALS algorithm for PCA (H. Wold, 1966). NIPALS works on the data matrix X and is algebraically equivalent to the power method (Lorber and Kowalski, 1987) if Σ is calculated from the data; i.e. for mean zero data, if $\Sigma = X'X$. The algorithm is listed below:

1) mean center X

2) For $a = 1$ .. A, $E_0 = X$

2.1) choose t

2.2) While $\|t\|$ has not converged

2.2.1) estimate p by least squares using the current estimate for t: $p'_a = t'_a E_{a-1} / t'_a t_a$ (6.2.1.7)

2.2.2) normalize p: $p_a = \frac{p_a}{\|p_a\|}$ (6.2.1.8)

2.2.3) project X on p to calculate t. Note $p'p = 1$ except in the case of missing data, which is discussed below. $t_a = E_{a-1} p_a / p'_a p_a$ (6.2.1.9)

2.3) subtract the contribution of component just calculated from the X-residual to assure orthogonality of subsequent dimensions:

$$\mathbf{E}_a = \mathbf{E}_{a-1} - t_a p_a \qquad (6.2.1.10)$$

To deal with missing data, note that each element in p, p_j, is the slope of the linear relationship between the data in t and the corresponding column in X, x_j. For a mean centered data set, this line passes through the origin. The origin is therefore a point of zero leverage, so that the estimate of the coefficient p_j is independent of the number of points there. Hence, if any of the elements of column x_j is missing, that element and the corresponding element in t are set to zero while p_j is calculated. In the presence of missing data, step (2.2.1) above becomes:

2.2.1) For $j = 1..m$
  For i = 1..n
    if $x_{j,i}$ is a missing datum, then $x_{j,i} = t_i = 0$
    $p_j = t'x/t't$

A similar algorithm must be constructed for step (2.2.3) (eq. 6.2.1.9), noting that division of the right hand side of the expression by $p'p$ is necessary if there are missing data because some of the elements of p will be deleted and normality of p must be preserved in the projection.

This lays the foundation for all that follows. The use of PCA for analyzing and interpreting multivariate data will be clarified in the following chapters, but it is already apparent that PCA overcomes the problem of rank deficiency in the sensor matrix. PCA can reduce the dimensionality of a rank deficient matrix without a significant loss of information and the resulting matrix of principal component scores, T, can be used to replace X in a calibration model of the type in equations 6.2.1 and 6.2.2. With reference to eq. (6.2.1.6)

$$T = XP' \qquad (6.2.1.11)$$

and

$$\hat{B}_{PCA} = (T'T)^{-1}T'Y \qquad (6.2.1.12)$$

When the spectrum x of an unknown sample becomes available, the properties of that sample can be estimated from the model using the following prediction procedure:

1) Subtract the mean spectrum of the calibration set (from Step (1) of the calibration).

2) Calculate the PC scores: $t = xP'$ (6.2.1.13)

3) Calculate the sample properties: $y = \hat{B}_{PCA} t$ (6.2.1.14)

6.2.2 Partial Least Squares

When calculating an empirical relationship between X and Y, replacing X with the reduced matrix T from PCA has two important shortcomings:

1) the decomposition of the sensor matrix X is done with no consideration of the predictive power of the resulting principal component scores on the product properties of interest.

2) if more than one property is associated with each sample, PCR still predicts regression coefficients independently for each property. Redundant or correlated information in the property matrix Y is not used to advantage;

Partial Least Squares was developed to solve these deficiencies. The algorithm was first proposed by Herman Wold, and was a direct extension of his NIPALS algorithm for the calculation of principal components (H.Wold, 1966). It was shortly thereafter extended to the two-matrix canonical correlation problem and, in 1974, developed for multiblock, econometric path models (S. Wold and Kanetteh, 1989; Jöreskog and Wold, 1982). The emphasis in this early work was in "soft modelling": the elucidation of latent structures and of empirical relations between latent variables of data blocks.

There were some mistakes in the early formulations related to the orthogonality of subsequent dimensions. It was only in 1982 that the PLS algorithm was corrected to allow for multidimensional decompositions of data matrices (S. Wold and coworkers, 1982). PLS was introduced into the chemometrics literature in 1983 (Frank and coworkers, 1983; Lindberg and coworkers, 1983; Martens, 1985). Harald Martens' influential thesis on multivariate calibration (Martens, 1985) outlined applications of PLS to diffuse NIR reflectance, light transmission, and autoflorescence emission spectroscopy of grain and meat samples.

The PLS model for the measurement space that contains X is similar to that of PCA. PLS extends this approach to the property space Y, so that, for a calibration set with n samples:

$$X_{(n \times k)} = T_{(n \times a)} P_{(a \times k)} + E_{(n \times k)} \quad (6.2.2.1)$$

$$Y_{(n \times p)} = U_{(n \times a)} Q_{(a \times p)} + F_{(n \times p)} \quad (6.2.2.2)$$

PLS also constructs a linear "inner relation" relating the two

$$U = \mathbf{B} \cdot T \text{ where } \mathbf{B} = diag(b_i) \quad (6.2.2.3)$$

P and Q are the loading vectors of the a dimensional latent variable subspace, and T and U contain the projections of X and Y on those subspaces, respectively. Note that the matrices B above and B of eq. (6.2.1) are not one and the same. This slightly confusing notation is kept, however, to be consistent with a large body of the chemometrics literature.

The algorithm that calculates T, P, Q, and B is described below. Because q is not normalized, the inner relation is $\hat{U} = T$, so B is the identity matrix (Martens, 1985; Höskuldsson, 1988). Missing data is dealt with as in PCA. As in the NIPALS algorithm, this algorithm works by calculating the loading and score vectors for the ath dimension using the X residual matrix, E_{a-1}.

1) mean center X and Y

2) For $a = 1$ .. A, $E_0 = X$

2.1) choose u, usually the column in Y with the largest variance

2.2) While $\|t\|$ has not converged

2.2.1) $$w'_a = u'_a \mathbf{E}_{a-1} / u'_a u_a \quad (6.2.2.4)$$

2.2.2) $$w_a = w_a / \| w_a \| \quad (6.2.2.5)$$

2.2.3) $$t_a = \mathbf{E}_{a-1} w_a / w_a' w_a \quad (6.2.2.6)$$

2.2.4) $$q_a' = t_a' \mathbf{Y} / t_a' t_a \quad (6.2.2.7)$$

2.2.5) $$u_a = \mathbf{Y} q_a / q_a' q_a \quad (6.2.2.8)$$

2.3) $$p_a' = t_a \mathbf{E}_{a-1} / t_a' t_a \quad (6.2.2.9)$$

2.4) $$\mathbf{E}_a = \mathbf{E}_{a-1} - t_a p_a' \quad (6.2.2.10)$$

There have been some recent improvements in both the speed and memory requirements of this algorithm, especially for the case where Y is a column vector (Lorber and Kowalski, 1988; Manne, 1987). The above algorithm, however, best shows the relationships between the various vectors used by PLS and will be used both for calculations and as a basis for the theoretical discussions below.

When the spectrum $x_{(m \times 1)}$ of an unknown sample becomes available, the properties of that sample can be estimated from the PLS model:

1) Subtract the mean spectrum of the calibration set (from Step (1) of the calibration).

2) Calculate the scores for each PLS dimension ($a = 1..A, e_0 = x$):

$$t_a = e'_{a-1} w_a$$
$$e'_a = e'_{a-1} - t_a p'_a \qquad (6.2.2.11)$$

3) Calculate the sample properties:

$$\hat{y} = \sum_a t_a q'_a \qquad (6.2.2.12)$$

The regression vector B of equation (6.2.1) can also be calculated directly from the PLS calibration model vectors so the y can be calculated directly for the new x. The requisite formulae can be found in Lorber, Wangen and Kowalski (1987), Manne (1987), and Höskuldsson (1988).

Until recently, there had been few theoretical investigations into the convergence and statistical properties of PLS. Næs and Martens (1985) investigated some of the statistical properties of the loading vectors. Lorber and coworkers (1987) produced a proof of the convergence of PLS as it is applied to multivariate calibration using Singular Value Decomposition and the Power Method for calculating eigenvalues. Since then, several papers have emerged that attempt to explain PLS using both statistical (Helland, 1988) and linear algebra (Höskuldsson, 1988; Manne, 1987) frameworks.

Höskuldsson's (1988) geometric interpretation gives some useful insights into this algorithm . His interpretations are based on the fact that PLS is based on the singular value decomposition (SVD) of $X'Y$. Consider the first PLS dimension, where $E_0 = X$. The SVD gives:

$$X'Y = F\Lambda G' = \sum_{i=1}^{p} \lambda_i f_i g_i' \tag{6.2.2.13}$$

where $f_1 = w_1$ and $g_1 = q_1$. This result aids greatly in the interpretation of PLS, and helps in making judgements about certain applications. $Y'X$ is the $p \times m$ matrix of the projections of the columns of X on those of Y, and reflects the amount of the variation in X that can be explained by the variation in Y. The implications of this can be most easily understood by first considering the case where $p = 1$, i.e. only one Y variable is being modelled. In this case, $y'X$ is rank 1, and eq. 6.2.2.13 becomes

$$y'X = \lambda f_1 = \lambda w \tag{6.2.2.14}$$

where λ is a scalar. λw, then, weights each X-variable (column) by the ability of its projection on y to predict y. Since the scores t are calculated from projecting X on w, t's are scaled averages of the predictions of Y by each of the X-variables (Lorber et al., 1987). Also note that eq. 6.2.2.14 is exact, so the algorithm does not iterate if y is used in place of u in eq. 6.2.2.4.

Now, consider the general case where p is any number. Then $Y'X$ will be rank p, so the SVD becomes

$$X'Y = \sigma_1 wq' + \sigma_2 f_2 g_2' + \cdots + \sigma_p f_p g_p' \tag{6.2.2.15}$$

premultiplying by w' and noting that $w'w = 1$ and $w'f_i = 0$ for $i \neq 1$ gives:

$$w'X'Y = \sigma_1 q' \tag{6.2.2.16}$$

$$\therefore X'YY'Xw = \sigma_1 X'Yq$$

From eq. 6.2.2.13 w is an eigenvector of $X'Y$, so:

$$\therefore w \propto X'Yq \tag{6.2.2.17}$$

$$\therefore w \propto X'(q_1 y_1 + \cdots + q_p y_p)$$

which shows that, for any general Y-vector, w is the projection of the columns of X on a vector formed by a linear combination of the columns of Y.

This result can be used to contrast two approaches to the PLS algorithm. The first approach, called PLS1, always uses only one Y variable in the PLS model; i.e. $p = 1$. The second, often called PLS2, uses all the available information about the samples in the calibration set; i.e. $p > 1$. The first conclusion that can be drawn by comparing eq. 6.2.2.14 and eq. 6.2.2.17 is that PLS1 will give the most parsimonious model for any one Y-variable because it gives the maximum possible weight to the variable in question while ignoring all others (Manne (1987) arrived at a similar conclusion about the relative effectiveness of PLS1 and PLS2 using a different argument). Thus, if the columns of Y represent the quantities that we actually want to model PLS1 is the preferred modelling technique. PLS2 may be the preferred method when the Y-variables reflect various noisy measurements made on some latent effect that is difficult to measure.

6.2.3 Number of Components by Cross-validation

The discussion of principal component analysis (PCA) and partial least-squares (PLS) to this point has concentrated on concepts, calculation algorithms, and properties of the solutions without addressing one of the key questions of these data compression and modelling techniques: how many dimensions are required to adequately model the sensor-property model calculated from these techniques? One might be tempted to calculate dimensions until the model residual is a constant or some very low value (say, equivalent to the experimental error of the measurements); but that would not differentiate between the incorporation of relevant structural information or noise in the model. Since the ultimate aim of the estimated models is to predict properties in an unknown sample from sensor measurements, some technique that estimates the relative predictive power of models generated at subsequent dimensions is necessary. Cross-validation is such a method (S. Wold, 1978).

The principal of cross-validation is to calculate a prediction residual error sum of squares (PRESS) as a function of the number of dimensions incorporated into the model. In principle, as significant dimensions are incorporated into the model the model's predictive ability will improve and the PRESS will decrease. As the true number of significant dimensions is passed, however, noise will be incorporated into the model. The predictive ability of random noise being what it is, the PRESS will increase. This yields the criterion used by some authors (Sharaf, Illman and Kowalski, 1986) that the optimum number of components, a, is found when

$$\frac{\text{PRESS}(a+1)}{\text{PRESS}(a)} > 1 \qquad (6.2.3.1)$$

In very nonlinear situations, however, the PRESS may not reach a sharp minimum, but enters a "valley" where a number of consecutive dimensions give comparable PRESS. In this case, it is sometimes appropriate to use a criterion that choose a when

$$\text{PRESS}(a+1) - \text{PRESS}(a) < \varepsilon \qquad (6.2.3.2)$$

where ε is some measure of the level of noise in the data, perhaps the variance of the sensors or property measurements, whichever is larger. ε is sometimes taken as the variance of the Y-matrix residual left after the predictions of the first a dimensions have been subtracted.

The PRESS is calculated by an iterative method for each dimension. Starting with the first dimension, some of the samples are deleted from the calibration set. These samples become a prediction set which is not used to estimate the model. The model is calculated from the remaining calibration samples, then used to predict the properties of the samples (Y) in the prediction set from their sensor data (X). A prediction error can be calculated for each property

$$e_{ij} = \hat{y}_{ij} - y_{ij} \qquad (6.2.3.3)$$

where i is the sample (row) and j the property (column) index. The PRESS can be calculated for each property

$$\text{PRESS}_j = \sum_i e_i^2 \qquad (6.2.3.4)$$

At every dimension, this process is repeated until all the samples in the calibration set have been used once in the prediction set. The dimension counter is then incremented, and the whole process is repeated for the next dimension.

The best estimate of PRESS is made when the prediction set has only one sample at every iteration. This method, called Leave-one-out, makes the calculations very time consuming. A more practical solution is to use from 10 to 50% of the samples in the prediction set. This can give a reasonable estimate of PRESS if the data set is sufficiently large. After the optimum number of components is calculated using cross-validation, the model of the sensor-property relation is calculated using all the available data.

6.3 Nomenclature for Chapter 6

Letters in lower case italics (x) are scalars. Lower case bold italics ($\boldsymbol{x}$) is used for vectors. All vectors are column vectors, row vectors being denoted by the vector transpose. Upper case bold italics ($\boldsymbol{X}$) is used for matrices.

Superscripts and Subscripts

$(n \times m)$	Matrix dimensions, n rows by m columns
$\boldsymbol{X}'$	$\boldsymbol{X}$ Transpose

7

DESIGN OF CALIBRATION SET

7.1 Criteria for Experimental Design

Critical to any model building exercise is the selection of the data that will be used to estimate and validate the model. In multivariate sensor calibration, a set of samples representative of the range of properties that the analyzer will encounter must be collected and characterized. This is the calibration set. There are two basic types of calibration set design methodologies. If the experimenter has access to a large population of possible samples, say in a process plant environment, he can collect random samples. Random sampling has the advantage of providing information about the statistical distribution of properties in the operating space of the process (Helland, 1988). The second methodology is called controlled calibration. Here, the experimenter constructs samples with carefully controlled variation in properties, usually by employing a factorial (Box, Hunter, Hunter, 1978) or mixture (Cornell, 1990) design. The advantage of carefully designed experiments is that the properties in the calibration set can be varied independently. In choosing the proper approach, the context in which the calibration is to be used must be carefully considered.

To better understand the experimental design used in this work, consider first the concept of the latex property space. If we are studying a process that makes a product that has 5 properties of interest, then we can envision the product being produced at any given time as a point in a 5-dimensional property space. Each axis (basis vector) of this space represents one property. Most processes are incapable of moving to any arbitrary point in this space: they tend to vary along some lower dimensional plane in property space. Thus, in a random calibration set collected from an actual process, the properties of interest are often correlated. This is not a problem if the calibration set spans the entire space of normal process operation. A controlled, designed factorial

experiment, on the other hand, has the appealing property of allowing the effect of each property on the sensor response to be studied independently with a minimum number of samples or experiments. This is useful for initial screening, evaluation or isolating underlying physical phenomena that affect the sensors.

The approach to calibration set design taken here is a hybrid of the two discussed above. It reflects the requirements of a sensor the a realistic latex production environment of a semi-batch copolymerization reaction.

7.2 Experimentally Modeling a Semi-batch Reactor

The semi-batch reactor is an important process in industrial latex production. The process is conceptually simple: some water, initiator, emulsifier and monomers are charged to the reactor. The reaction starts, then more of the above are slowly fed into the reactor until the reactor is full. This process has great flexibility in the control of particle size distribution, particle concentration and morphology, and provides the opportunity to control the progress of the reaction as it occurs. As a result, it is responsible for many of the very high value added polymers produced today.

It is not too difficult to imagine the usual progression of latex properties throughout a semi-batch reaction. The initial charge is often designed to make a seed latex: low solids homopolymer with a very narrow particle size distribution. Other monomers and more water are then added to grow the particles. A usual strategy would be to keep the concentration of the polymer produced constant throughout the batch. Another might be to vary the concentration in some systematic way with the diameter of the particle. If sufficient extra emulsifier is added, a secondary nucleation of particles can occur, yielding bimodal particle size distributions. The batch is run at relatively high conversion to maintain control of the reaction.

This progression of the latex properties during the batch can be visualized as a trajectory through the multidimensional latex property space (Fig.7.2.1). The latex starts in a region of low solids, small particles, and some arbitrary co-polymer composition, and moves to a region of high solids, large particles, and perhaps some other co-polymer composition. The monomer conversion is roughly constant throughout.

As a result of this kind of operation, the analyzer system has two distinct roles to fulfil. First, it should be able to follow the entire course of the batch to distinguish where on the latex property trajectory a given sample belongs. It should screen out gross errors in the analyzer reading or detect major process upsets. Having done that, the analyzer must then make very accurate predictions of the properties of the latex based on the sensor responses. For most optical sensors, these criteria present some challenges. On the one hand, the sensor must respond to a large range of latex property variation, invariably resulting in a very nonlinear relationship between the sensor response and the property of interest. The accuracy of the calibration, on the other hand, is generally the highest in regions of linear sensor response (Geladi and Kowalski, 1986b; Geladi, MacDougall and Martens, 1985). The design of the calibration set must test the ability of an analyzer system to cope with these conflicting criteria.

The basic philosophy of the experimental design is to make latex batches with a wide range of properties representative of the property trajectory in a semi-batch reaction and, within this trajectory, to chose points about which small changes in latex properties are made to represent purturbations about the main trajectory. This can best be visualized by refering to Fig. 7.2.1. Latex

batches were made that could be classified as belonging in either Region A or Region B on that diagram. The difference in latex properties between these regions is quite large, as illustrated in Table 7.2.1. Within each of these regions properties were varied on a finer scale, using a combination of factorial and mixture experimental designs that attempted to vary each of the properties independently.

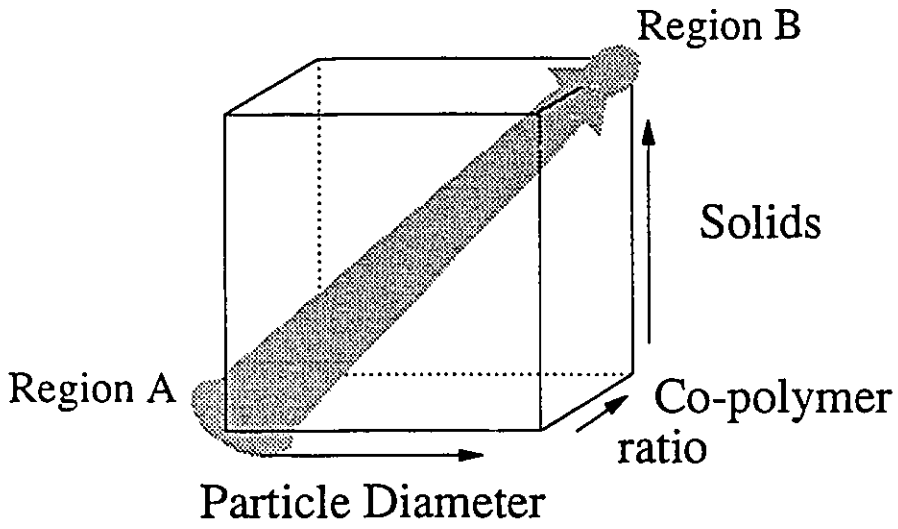

Fig. 7.2.1: Semibatch Reactor Property Trajectory

Property	Region A	Region B
Weight Average Particle Diameter [nm]	60-80	150-200
Beadth of PSD	narrow	broad
Poly(styrene)/Poly(MMA) Ratio	1.5-2.0	1.0-1.5
Solids Fraction	0.30	0.50

Table 7.2.1 : Properties of Calibration Samples

This calibration set could not be constructed by simply taking samples from our 4 litre pilot scale reactors run in semibatch mode because: (1) the volume of the reactor vessel is too small; and (2) small scale variation in the latex properties would be unpredictable and irreproducible because the progress of the semi-batch reaction could not be monitored. In this work, for experimental tractability and for finer control of latex properties, the following approach was used in make the latex that became the calibration set. The system chosen for study was a copolymerization of styrene and methyl methacrylate. Latex batches were designed to vary particle size, polymer fraction, and the copolymer ratio, and reacted to complete conversion. Attempts were made to vary the particle size and copolymer ratio between batches in a factorial design within small, local regions of the property space. This was only partly successful: particle nucleation is influenced by the ratios of monomers in the reactor, so these effects were often correlated; and later, when experience and careful formulation allowed for more precise specification of mean diameter, the breadth of the distribution could not be controlled enough to totally decouple changes in particle size distribution from composition. Once the batches were made, deviation in solids and monomer fractions on a smaller scale were modelled by adding water, styrene and methyl methacrylate to the latex in a classic mixture design.

7.3 Mixture Designs

For the purposes of this study, the composition of the 5 major constituents of the latex will be studied: water, styrene and methyl methacrylate (MMA) bound in polymer, and styrene and MMA monomer. The remaining constituents, though important in production and stability of the resulting latex, make up only a small fraction of the total latex mass (usually around 2%). Thus, only the composition of the 5 major constituents was considered in the experimental design and in the construction of the calibrations.

Compositions of these 5 components, when expressed as weight fractions, are subject to a unit sum constraint. Geometrically, then, the 5-dimensional latex composition space is constrained

to a 4-dimensional simplex that satisfies the unit sum constraint. A factorial design cannot be used to systematically vary all 5 of these components; instead, mixture designs are used to provide a framework for systematically varying the levels of the various constituents in the latex to maximize the amount of information provided by the minimum number of samples (Cornell, 1990; Aitchison, 1986).

While mixture designs provide a framework for dealing with the unit sum constraint of compositional systems, there are additional considerations that complicate the experimental design. Latex batches are, to a greater or lesser degree, unpredictable and irreproducible. This restricts one's ability to arbitrarily place the properties of a latex at any point in the constrained, 4-dimensional simplex. Furthermore, particle size, a property not subject to the unit sum constraint, must also be dealt with in this design. The following design, therefore, provides a framework for systematically varying the composition of the major 5 constituents and particle size.

First, consider a batch of latex, reacted to 100% conversion, as a point on the 2-dimensional simplex in the 3-dimensional space of water, poly(styrene) and poly(methyl methacrylate) (see Fig. 7.3.1a). The first step of the design is to make a factorial design based on particle size and copolymer ratio at constant water fraction and 100% conversion. In the ideal case, we would have, at each level of particle size, two batches with the same solids fraction, 100% conversion (no monomer), but different ratios of poly(styrene) to poly(MMA). These batches form the basis of subsequent samples formed by mixing latex, water, styrene, and MMA. The procedure follows.

Each batch is divided in half, and water is added to one half to give slightly lower solids. The amount of water added is determined by some arbitrary constraint on the maximum water fraction in the design. Each batch now has two samples associated with it: the original and the water-diluted one. Each of these samples is divided into 3 parts, one part being reserved as is. Two solutions of monomer are made up with different proportions of styrene to MMA. The monomer

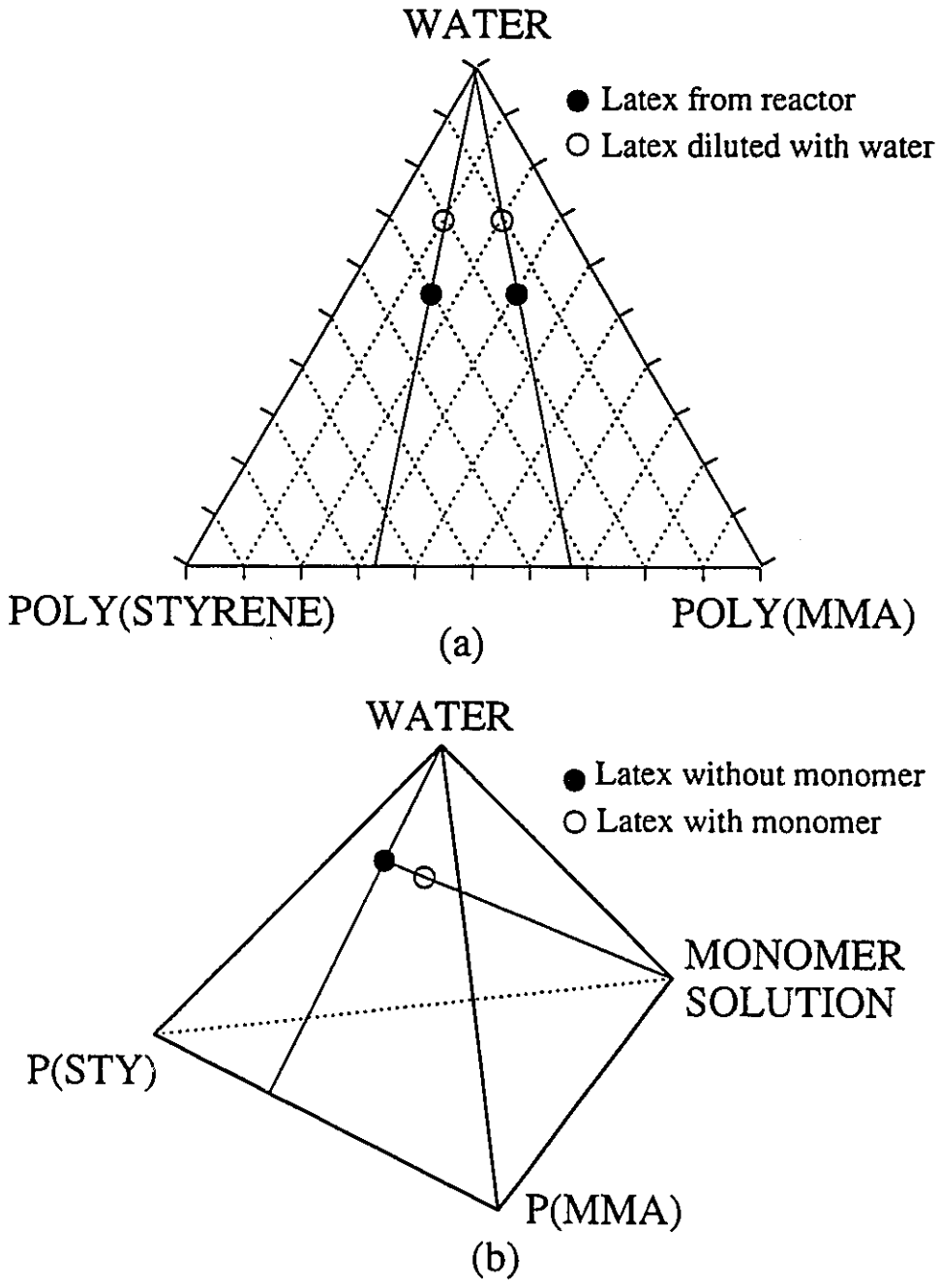

Fig. 7.3.1: Mixture Design for Calibration Set

solutions are mixed with the latex samples, one latex sample per monomer solution. The amount of monomer is determined by some arbitrary constraint on the total proportion of monomer in the sample.

These samples can be represented on the three-dimensional simplex of Fig. 7.3.1b. Three of the vertices are as before: water, poly(styrene), poly(methyl methacrylate). The fourth vertex is the monomer solution. Although this would be more accurately represented on a 4-dimensional simplex, with one vertex each for styrene and MMA monomers, this can not be drawn on paper. The design still can, however, be adequately visualized as a series of 3-dimensional simplexes.

This experimental design defines a concave polyhedron in the constrained 5-dimensional space of latex composition at each level of particle size. The polyhedron has 12 vertices; i.e. 6 samples are produced from each latex batch, 2 latex batches at each level of particle size. The weight fractions of the latex constituents at each of the vertices can be calculated by recognizing that the experimental polyhedron is bounded by the following constraints:

	Constraint	When active
1)	$C_1 \le x_{H2O} \le C_2$	no monomer present
2)	$x_{PS} + x_{PMMA} = C_7$	no monomer present
3)	$C_3 \le \frac{x_S}{x_{MMA}} \le C_4$	monomer present
4)	$C_4 \le \frac{x_{PS}}{x_{PMMA}} \le C_6$	always active
5)	$x_i \ge 0$	always active
6)	$\sum x_i = 1.0$	always active

where x_i are the weight fractions and C_i are constants selected by the experimenter. Five of these constraints are active at any one vertex. In this design, it is a simple matter to choose which five and calculate the compositions at each vertex.

7.4 Latex Characterization

An important part of building a calibration set for an empirical model is the accurate characterization of the properties of the latex. This task is greatly simplified in the experimental design outlined above because most of the sources of variation are under the control of the experimenter.

As mentioned above, each of the batches is run to complete conversion (which is close to, but never reaching, 100%). All reagents are precisely weighed at the beginning of the batch so that all the proportions are precisely known. Thus, at the end of a batch, the proportions of each monomer incorporated into the polymer particles is known from the recipe. The assumption of 100% conversion can be checked by gravimetric determinations done at the end of the batch.

Since all subsequent batches are made from the fully converted batches, the proportions of all constituents in them can be known by carefully weighing the latex, water, and monomers that are mixed to make the other samples.

Particle size is the only major property that cannot be predicted from the recipe. The NICOMP 370 dynamic light scattering photometer was used to measure the mean and breadth of the particle size distribution. This instrument is described in detail in Chapter 2. The weight average diameter was used as the measurement used for the calibration set because it is known to be a nearly linear function of turbidity for many latexes (Chapter 2).

7.5 Latex Recipes

7.5.1 Calibration Set A

This calibration set is made up of those samples from Region A in Fig. 7.2.1 (see Table 7.2.1), characteristic of latex made early in a batch or semi-batch process. The latex solids has around 30% solids, and a mean particle diameter of 60 to 80 nm. Table 7.5.1 gives the recipes for the batch reactions. The corresponding weight fractions are given in Table 7.5.4. The function of the water, styrene and methyl methacrylate in these recipes is obvious. Potassium persulphate is the initiator. Sodium dodecyl sulphate is the principal anionic emulsifier. The presence of anionic emulsifier increases viscosity at higher solids loadings due to the interaction of ionic double layers around the particle. This effect can be suppressed by adding counterions to the aqueous phase. Sodium bicarbonate serves this purpose. The stability of a latex is also affected by pH. A pH of 9 is optimal for poly(styrene) (Gordon and Dolgin, 1954). The sodium bicarbonate raises the pH of the latex from 2 to 6. The remaining difference was made up by adding ammonium hydroxide to the recipe.

The samples in this calibration set were made using batch reactor operation (mode B in Table 7.5.1). The recipe components were charged to the reactor, the reactor purged with high purity nitrogen for 15 minutes, and the temperature ramped to 70°C and reacted for several hours to complete conversion. The reactions were finished by ramping to 90°C for 15 to 30 minutes, then cooling.

Table 7.5.3 lists the recipes for latex samples synthesized using the batch samples as a base and adding water, styrene, and methyl methacrylate to various latexes in varying proportions, as determined by the mixture designs outlined above. Uptake times for monomer into latex particles can be long. Löhr (1980) reported the uptake times were dominantly controlled by the solubility of the diffusant, and the viscosity of the polymer. The longest

uptake time he reported was 5 hours for cyclohexane in poly(styrene) latex. For this reason, latex samples were gently shaken overnight after monomer was added. The presence of monomer droplets was tested for in a few samples by centrifugation after mixing. If any undissolved monomer droplets are present, a monomer layer will form above the aqueous supernatant (Keusch and Williams, 1973). No monomer layer was seen on centrifugation.

The results for solids fraction from gravimetry are presented in Table 7.5.5. The standard deviation of gravimetry measurements was calculated by pooling the standard deviations calculated from several repeat measurements, and was calculated to be 0.005 for a single gravimetry measurement. Of course, the standard deviation of averaged measurements is reduced by the standard $n^{-1/2}$ factor. A perfect match between solids calculated from the recipe and that calculated from gravimetry would indicate not only 100% monomer conversion, but also perfect measurement of all the recipe constituents and no coagulated polymer could be left behind in the reactor. The recipe solids fraction was calculated by assuming all the monomer had been converted to polymer, and that all the surfactants, the initiator, and the sodium bicarbonate remained as solids on drying. Nearly all the samples show some significant deviation from this ideal, recipe-based solids value. All samples in this calibration set are, however, over 97% conversion. For the purposes of this training set, these deviations from ideal conditions are acceptable: the deviation from the 100% conversion assumption are not significant enough to obscure the differences between polymer composition in each batch, so the copolymer ratio calculated from the recipe will be used in the calibration.

Characterization of the particle size distribution is not as straightforward. The particle size distribution is the property most likely to change on dilution and with age in the latex sample. As such, it was characterized several times throughout the life of a sample. Furthermore, many optical sensors, like UV spectrometers, take measurements on diluted latex samples. The benefits of dilution were made clear in earlier Chapters. Diluted latex samples are more stable than concentrated latex, so coating in the analyzer loop is either eliminated or minimized. Furthermore, the automated sampler-diluter discussed in Chapter 3 provides for

Sample Number	Mode	Water (g)	Styrene (g)	MMA (g)	SDS (g)	Rexol 15/25® (g)	Rexol 15/407® (g)	$K_2S_2O_8$ (g)	$NaHCO_3$ (g)	NH_3OH (g)
52	B	2500.0	645.5	430.6	43.00	0.00	0.00	1.50	2.50	28.50
53	B	2500.0	717.1	359.2	43.00	0.00	0.00	1.50	2.50	27.60
54	B	2502.8	644.9	430.7	43.50	0.00	0.00	1.50	2.50	27.80
55	B	2500.6	646.0	430.0	21.00	0.00	0.00	0.75	2.60	28.20
56	B	2501.0	717.1	359.3	21.00	0.00	0.00	0.65	2.70	28.80

Table 7.5.1: Latex Batch Recipes, Data Set A

Sample Number	Mode	Water (g)	Styrene (g)	MMA (g)	SDS (g)	Rexol 15/25® (g)	Rexol 15/407® (g)	$K_2S_2O_8$ (g)	$NaHCO_3$ (g)	NH_3OH (g)
28	SB	180.0	95.3	84.8	2.00	2.72	2.61	0.18	0.20	2.00
32	SB	1800.1	1080.0	720.0	20.00	40.00	0.00	2.20	2.00	20.00
35	SB	1800.4	953.6	848.6	20.10	27.20	30.70	2.20	2.00	20.60
38	SB	180.1	108.0	72.0	2.00	2.70	2.75	0.22	0.26	2.00
39	SB	180.1	108.0	72.0	2.17	2.36	3.75	0.25	0.20	2.06
40	SB	180.1	108.0	72.0	2.25	2.30	3.72	0.27	0.21	2.00
51	SB	1800.4	883.6	589.0	22.00	24.10	38.00	2.50	2.00	21.00

Table 7.5.2: Latex Batch Recipes, Data Set B

Sample Number	Original Latex Batch	Latex (g)	Water (g)	Styrene (g)	MMA (g)
57	53	232.96	38.04	0.00	0.00
58	53	244.03	38.99	0.00	0.00
59	53	239.04	38.16	4.61	3.06
60	53	222.37	36.34	3.61	3.61
61	53	232.62	37.63	2.98	4.44
62	53	237.31	0.00	4.74	3.15
63	53	237.34	0.00	3.92	3.90
64	53	221.22	0.00	2.90	4.34
65	53	213.14	35.29	3.53	3.52
66	53	217.45	0.00	3.56	3.56
67	54	304.25	46.68	0.00	0.00
68	54	314.57	48.07	0.00	0.00
69	54	293.58	45.50	5.78	3.85
70	54	290.04	45.01	4.74	4.72
71	54	296.79	45.57	3.86	5.77
72	54	280.56	0.00	5.52	3.67
73	54	305.34	0.00	5.03	5.01
74	54	273.77	0.00	3.61	5.38
75	54	278.32	43.60	4.54	4.52
76	54	268.43	0.00	4.40	4.38
77	55	291.45	39.97	0.00	0.00
78	55	292.21	39.82	0.00	0.00
79	55	296.05	40.21	5.83	3.88
80	55	268.10	37.42	4.39	4.38
81	55	287.53	39.40	3.82	5.70
82	55	258.03	0.00	5.14	3.41
83	55	296.06	0.00	4.90	4.89
84	55	305.69	0.00	4.09	6.10
85	55	280.05	38.77	4.60	4.58
86	55	292.41	0.00	4.90	4.88
87	56	262.35	36.72	0.00	0.00
88	56	279.37	38.64	0.00	0.00
89	56	259.55	36.21	5.12	3.41
90	56	256.00	35.90	4.20	4.19
91	56	287.62	39.72	3.78	5.65
92	56	282.03	0.00	5.63	3.75
93	56	275.65	0.00	4.53	4.51
94	56	240.42	0.00	3.16	4.72
95	56	257.01	36.02	4.27	4.26
96	56	258.43	0.00	4.24	4.23

Table 7.5.3 : Recipes for Synthesized Latex Samples, Data Set A

Sample	Water	P(sty)	P(MMA)	Styrene	MMA	Other
52	0.685	0.177	0.118	0.000	0.000	0.021
53	0.685	0.196	0.098	0.000	0.000	0.020
54	0.685	0.177	0.118	0.000	0.000	0.021
55	0.689	0.178	0.118	0.000	0.000	0.014
56	0.689	0.198	0.099	0.000	0.000	0.015
57	0.729	0.169	0.085	0.000	0.000	0.018
58	0.728	0.169	0.085	0.000	0.000	0.018
59	0.709	0.165	0.083	0.016	0.011	0.017
60	0.709	0.164	0.082	0.014	0.014	0.017
61	0.709	0.165	0.082	0.011	0.016	0.017
62	0.663	0.190	0.095	0.019	0.013	0.020
63	0.663	0.190	0.095	0.016	0.016	0.020
64	0.663	0.190	0.095	0.013	0.019	0.020
65	0.709	0.164	0.082	0.014	0.014	0.017
66	0.663	0.190	0.095	0.016	0.016	0.020
67	0.727	0.153	0.102	0.000	0.000	0.018
68	0.727	0.153	0.102	0.000	0.000	0.018
69	0.707	0.149	0.099	0.017	0.011	0.017
70	0.707	0.149	0.099	0.014	0.014	0.017
71	0.707	0.149	0.099	0.011	0.016	0.017
72	0.663	0.171	0.114	0.019	0.013	0.020
73	0.663	0.171	0.114	0.016	0.016	0.020
74	0.663	0.171	0.114	0.013	0.019	0.020
75	0.708	0.148	0.099	0.014	0.014	0.017
76	0.663	0.171	0.114	0.016	0.016	0.020
77	0.727	0.157	0.104	0.000	0.000	0.013
78	0.726	0.157	0.104	0.000	0.000	0.013
79	0.706	0.152	0.101	0.017	0.011	0.012
80	0.707	0.152	0.101	0.014	0.014	0.012
81	0.706	0.152	0.101	0.011	0.017	0.012
82	0.667	0.172	0.115	0.019	0.013	0.014
83	0.667	0.172	0.115	0.016	0.016	0.014
84	0.667	0.172	0.115	0.013	0.019	0.014
85	0.707	0.152	0.101	0.014	0.014	0.012
86	0.667	0.172	0.115	0.016	0.016	0.014
87	0.727	0.173	0.087	0.000	0.000	0.013
88	0.727	0.174	0.087	0.000	0.000	0.013
89	0.707	0.168	0.084	0.017	0.011	0.012
90	0.707	0.168	0.084	0.014	0.014	0.012
91	0.706	0.169	0.085	0.011	0.017	0.013
92	0.667	0.191	0.096	0.019	0.013	0.014
93	0.667	0.191	0.096	0.016	0.016	0.014
94	0.667	0.191	0.096	0.013	0.019	0.014
95	0.707	0.168	0.084	0.014	0.014	0.012
96	0.667	0.191	0.096	0.016	0.016	0.014

Table 7.5.4: Sample Component Weight Fractions, Data Set A

Sample	Solids Fraction				Conversion
	from Recipe	by Gravimetry	Difference	No. Of Samples	by Gravimetry
28	0.51115	0.47425	-0.0369	1	0.935
32	0.51141	0.50503	-0.0064	1	0.998
35	0.51163	0.48600	-0.0256	4	0.959
38	0.51113	0.46046	-0.0507	2	0.907
39	0.51132	0.47482	-0.0365	3	0.936
40	0.51151	0.46228	-0.0492	2	0.910
51	0.46438	0.423971	-0.0404	1	0.921
53	0.31524	0.299526	-0.0157	1	0.972
54	0.31500	0.303517	-0.0115	1	0.987
55	0.30320	0.297101	-0.0061	1	0.979
56	0.30319	0.293215	-0.0100	1	0.966

Table 7.5.5: Latex Batch Solids Fraction

periodic flushing of all the dilute latex lines for resetting of 100% transmittance on optical systems. One of the things that had to be checked was whether or not the dilution caused coagulation of the latex. This is possible if very pure water diluent is used, as it will strip some of the surfactant off the surface of the latex particles.

The effect of dilution on particle size distribution was checked using the narrowly distributed samples 53, 54, and 55. The latex was diluted by 1/2000 with a dilute SDS solution (4 g SDS / L deionized water), and the diluted latex left for 14 days. The particle size of the diluted latex was then measured by Dynamic Light Scattering and compared with measurements on the undiluted latex (Table 7.5.6). Both the mean and standard deviation of the latex were the same within the expected range of reproducibility of DLS.

The effect of monomer doping on particle size distribution was also checked. If the latex samples are assumed to be monodispersed, an approximate value for the monomer swollen mean diameter can be quickly calculated because the ratio of the old and new particle volumes is proportional to the cube of the diameter ratio. Taking Samples 53 and 62 as an example, the ratio of swollen to unswollen particle volume is approximately 1.13. This corresponds to a diameter increase of 4%, or 2.7 nm. Though small, this increase is within the range that could be resolved by the NICOMP 370 for narrow particle size distributions (see the values for standard deviation in Table 7.5.7). The measurement results in Table 7.5.7, however, show no statistically significant effect of adding monomer on the particle size distribution. The most likely reason for this is that, with the extreme dilution that the latex undergoes in the DLS instrument, most of the monomer is stripped from the particles. The DLS measurement, therefore, is done on unswollen polymer particles. Fortunately, the above calculations show that the difference in swollen and unswollen polymer particle diameters will be small; so, in Calibration Set A, the particle diameters for monomer swollen particles were taken to be those of the original latex.

7.5.2 Calibration Set B

This calibration set is made up of samples from Region B in Fig. 7.2.1 (see Table 7.2.1), characteristic of latex at the end of a batch or semi-batch process. The latex solids has around 50% solids, and a mean particle diameter of 150 to 200 nm. Table 7.5.2 gives the recipes for the batch reactions. The corresponding weight fractions are given in Table 7.5.8. These recipes

are more complex than those of Calibration Set A, owing mostly to the high solids content. High solids latex can be very viscous due to the interaction of ionic surfactant on the particle surfaces. Excessive use of counterions can, however, suppress the double layer so much that it can no longer stabilize the particles. Nonionic surfactants, therefore, are used to stabilize high solids latexes, as they produce no ionic double layer. The two used here are nonylphenyl PEO surfactants with 25 or 40 ethylene oxide units (Hart Chemicals, Rexol 15/25 and 15/407, respectively). The recipe modes are labelled semibatch (mode SB in Table 7.5.2), although most are rather simple extensions of the batch mode. For samples 28 through 40, all ingredients were charged to the reactor at the beginning except for about 10% of the water and the nonionic surfactant Rexol 25/407® (for sample 32, half of the Rexol 25/15® was used instead). The water and surfactant were mixed and added to the reaction when the reactor temperature was at about 50°C (on its way to 70°C), and just after polymer was detected by methanol precipitation. This was done to decouple particle nucleation from stability effects, and was only moderately successful. The resulting particle size distributions were very broad, indicating either secondary nucleation or coagulation in the reactor. Latex was, however, of high quality: little visible coagulum under a microscope, and good long term stability.

Gravimetric determinations of solids fraction are shown in Table 7.5.5. All latexes had over 90% conversion, with most over 95%. The particle size distribution was more difficult to characterize than with Data Set A. The distributions were very broad, meaning repeat measurements of the mean of the distributions were quite variable. Furthermore, over the course of a year, there was a consistent shift in the distribution of these samples. The

distributions tended to become narrower and the mean decreased. In these cases, the most recent particle size was used in the calibration. Nonetheless, the differences in particle size distribution between batches were always significantly larger than any drift in distribution properties over time. Table 7.5.10 gives values of the mean and standard deviation of the particle size distribution from DLS measurements for each sample.

Sample 51 was a more elaborate attempt at decoupling the particle size distribution from the particle composition. All ingredients were charged to the reactor with the exception of the monomer and, as always, the Rexol 25/407. Only 140. g of the styrene were charged initially and used to produce a seed latex in the reactor. Once the seed latex was produced, the additional nonionic surfactant was added. The remaining monomer was mixed in a feed tank and fed to the reactor after the seed was generated at a rate of 6.25 ml/min. The resulting latex coagulated very much in the reactor and had a very broad particle size distribution. It was kept in the calibration set to illustrate outlier detection capabilities of the calibration techniques.

	Concentrated Latex		Latex Diluted 1/2000 14 days after dilution	
Sample Number	Mean Diameter [nm]	Standard Deviation [nm]	Mean Diameter [nm]	Standard Deviation [nm]
53	58.6	12.3	56.9	13.3
54	66.3	11.7	-	-
55	75.5	11.6	76.8	10.0
56	76.5	13.4	75.0	12.5

Note: the values in the Concentrated Latex column are means of several measurements (see Table 7.5.7).

Table 7.5.6: Effect of Dilution on Particle Diameter (Volume Weighted) Data Set A

Sample Number	Number of Measurements	Mean Diameter [nm]	Standard Deviation [nm]	Comments
53	6	66.57 (0.596)	13.92 (2.35)	
62	1	67.4	12.7	Sample 53 swollen with monomer
65	1	66.8	10.4	Sample 53 swollen with monomer
54	3	72.53 (1.069)	12.7 (1.08)	
76	1	74.4	10.8	Sample 54 swollen with monomer
55	3	80.77 (0.379)	13.13 (3.35)	
86	1	81.8	15.8	Sample 55 swollen with monomer
56	4	84.28 (0.377)	15.7 (2.41)	
87	1	85.1	15.8	Sample 56 swollen with monomer
95	1	84.9	8.8	Sample 56 swollen with monomer
96	1	84.4	14.2	Sample 56 swollen with monomer

Note: when repeat measurements are involved, the numbers in brackets ( ) are standard deviations of measurements.

Table 7.5.7: Effect of Monomer on Particle Diameter (Intensity Weighted) Data Set A

Sample	water	P(sty)	P(mma)	styrene	mma	Other
28	0.489	0.258	0.229	0.000	0.000	0.024
32	0.489	0.293	0.195	0.000	0.000	0.023
35	0.488	0.257	0.229	0.000	0.000	0.025
38	0.489	0.292	0.195	0.000	0.000	0.025
39	0.489	0.291	0.194	0.000	0.000	0.026
40	0.488	0.291	0.194	0.000	0.000	0.026
36	0.595	0.232	0.155	0.000	0.000	0.018
37	0.581	0.211	0.187	0.000	0.000	0.021
41	0.569	0.245	0.164	0.000	0.000	0.022
42	0.558	0.252	0.168	0.000	0.000	0.022
43	0.440	0.264	0.176	0.053	0.047	0.021
44	0.440	0.264	0.176	0.060	0.040	0.021
45	0.440	0.232	0.206	0.053	0.047	0.023
46	0.440	0.232	0.206	0.060	0.040	0.023
47	0.535	0.209	0.139	0.053	0.047	0.016
48	0.536	0.209	0.139	0.060	0.040	0.016
49	0.523	0.190	0.169	0.053	0.047	0.019
50	0.523	0.190	0.169	0.060	0.040	0.019
51	0.536	0.261	0.174	0.000	0.000	0.029

Table 7.5.8: Sample Component Weight Fractions, Data Set B

Sample Number	Original Latex Batch	Latex (g)	Water (g)	Styrene (g)	MMA (g)
36	32	398.15	104.10	0.00	0.00
37	35	396.23	87.75	0.00	0.00
41	39	195.52	36.57	0.00	0.00
42	40	186.27	29.08	0.00	0.00
43	32	387.82	0.00	22.66	20.24
44	32	384.10	0.00	25.64	17.09
45	35	388.50	0.00	22.76	20.32
46	35	360.73	0.00	24.04	16.03
47	32	319.88	83.57	23.65	21.11
48	32	318.79	83.62	26.74	17.83
49	35	357.92	79.44	25.68	22.93
50	35	314.97	69.61	25.58	17.06

Table 7.5.9 : Recipes for Synthesized Latex Samples, Data Set B

Sample Number	Mean Diameter [nm]	Standard Deviation [nm]
28	217.5	67.1
32	152.0	44.1
35	187.6	47.8
36	152.0	44.1
37	187.6	47.8
38	172.7	60.5
39	165.9	52.1
40	145.1	51.2
41	165.9	52.1
42	142.4	37.4
43	152.7	43.9
44	158.3	71.2
45	176.3	60.5
46	176.4	61.0
47	166.2	70.5
48	156.3	41.4
49	167.3	28.1
50	184.1	56.9
51	73.9	42.1

Table 7.5.10: Particle Diameter (Volume Weighted), Data Set B

8

ULTRAVIOLET SPECTROSCOPY OF LATEX

This Chapter deals with the evaluating an ultraviolet spectrometer as a sensor for particle size and composition in a poly(styrene/methyl methacrylate) latex process. The equipment envisioned could be a simple extension of that designed in earlier Chapters for particle sizing of poly(vinyl acetate) latex by UV turbidity. This Chapter is also a tutorial on the application of multivariate statistical techniques to nonlinear spectral data. As such, it will give more detail on the calibration methodology than the subsequent Chapters on near-infrared spectroscopy and combined multivariate sensors.

8.1 Constituent and Latex Spectra

8.1.1 Instrument Description

All the UV spectra for this work were taken using a Hewlett-Packard 8451a scanning photodiode array spectrometer, which measures absorbances at 2 nm intervals from 190 to 820 nm. A rectangular cuvette with a 10.0 mm path length was used for all measurements. The cell was made from Hellma SUPRASIL I® quartz, chosen for its high transmittance over the entire wavelength range. Each spectrum was the averaged over 10 s.

8.1.2 constituent spectra

Figures 8.1.1 and 8.1.2 show the UV spectra of all the constituents of the latex except water, since water is used as the background for the UV spectra of the latex. Fig. 8.1.1 shows

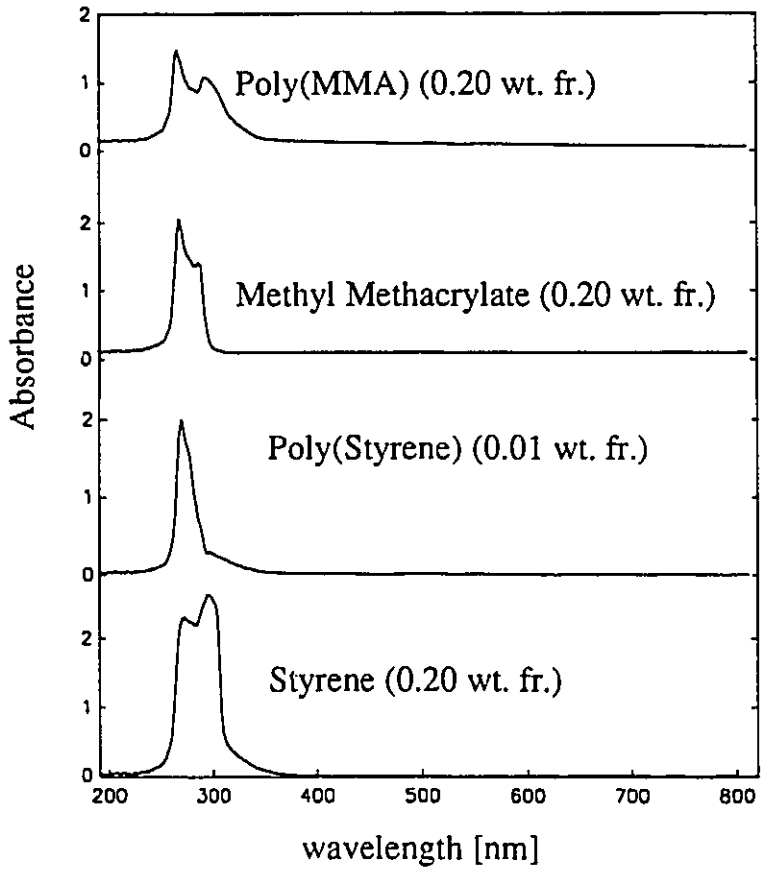

Fig. 8.1.1: UV Spectra of Latex Constituents; Dissolved in Tetrahydrofuran

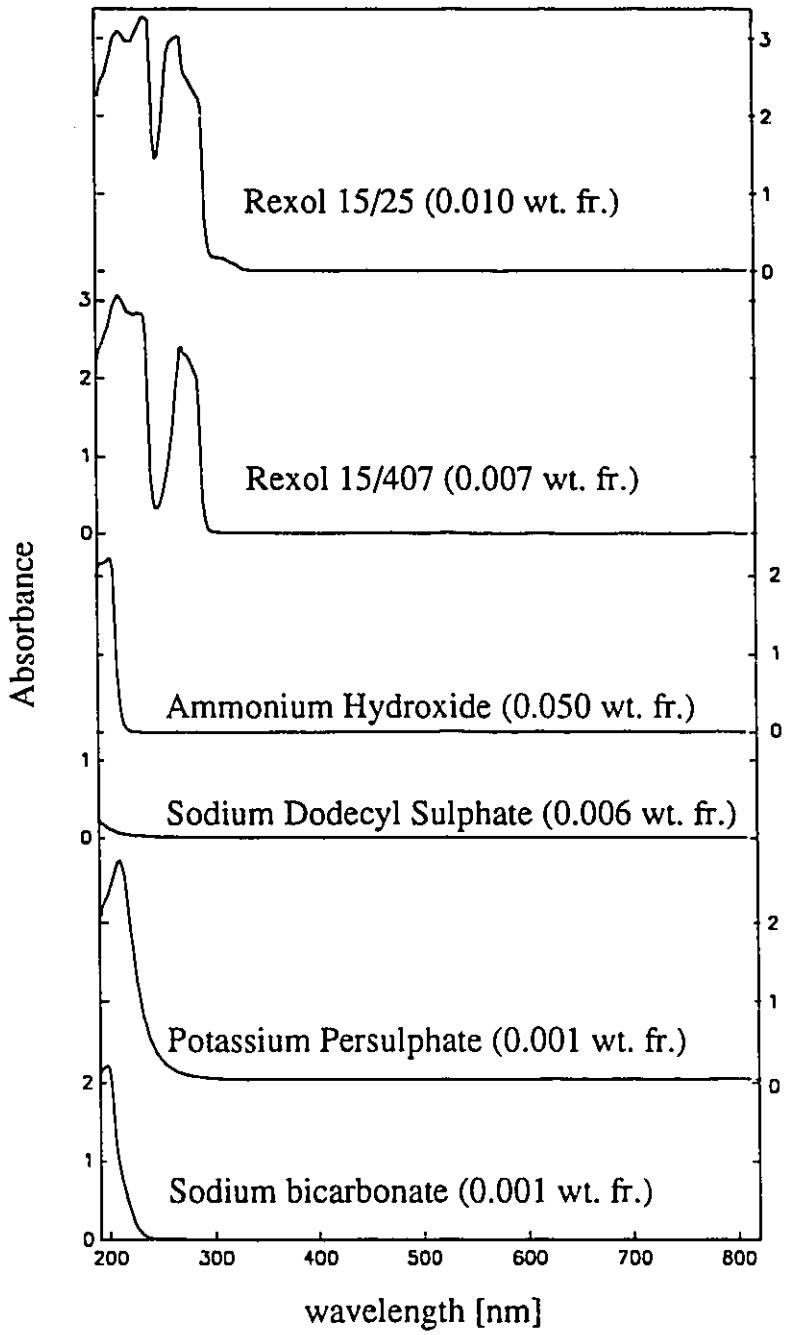

Fig. 8.1.2: UV Spectra of Latex Constituents; Dissolved in Water

the spectra of the principle, organic phase constituents referenced to a THF background. The compounds were dissolved in THF (tetrahydrofuran, HPLC grade) in approximately the weight fractions shown in the Figure. Fig. 8.1.2 show the spectra of the water soluble compounds referenced to water.

These spectra give the approximate location of the absorption peaks of interest in the UV spectra of the latex. Recall, however, that the absorption peak in the UV region are very sensitive to the molecular environment: the location and shape of the peaks change if different solvents are used, and there is a marked difference between the spectra of, say, a mechanical mixture of poly(styrene) and poly(MMA), and a copolymer of the same two monomers (Gallo and Russo, 1974). Two important points can nonetheless be made from studying these spectra. The first is that the spectra are highly overlapped: there is no single wavelength that will respond exclusively to the composition of one of the properties of the latex. The second point is related to the first: when drawing conclusions about the appropriateness of UV spectroscopy to measuring the composition of one or the other constituent in the latex, it is important to ascertain whether or not the models are actually causal. Two techniques help to determine this. First, the basis vectors of the reduced space of X should have high weights at wavelengths with high absorbance for the particular compound of interest. Second, it is important to ensure that the concentration of a compound with similar spectral features is not highly correlated to with the constituent of interest. Good experimental design ensures this to some degree.

8.1.3 latex spectra

The UV spectra are considerably more complex than simply a linear superposition of the constituent spectra. Light scattering by polymer particle accounts for much of the attenuation in latex, so the latex must be diluted considerably to be transparent to light in the 10 mm sample cell. The diluent was a solution of 4g/L Sodium Dodecyl Sulphate in deionized water. The dilution ratio was chosen to be in a region of linear relationship between polymer

concentration and absorbance in the non-absorbing part of the UV spectrum (above 350 nm). A plot of absorbance readings vs. dilution ratio for two of the more turbid batches (Fig. 8.1.3) shows that a dilution ratio of 1/2000 (5×10^{-4}) will guarantee this linear relationship.

Fig. 8.1.4a shows the UV spectra for some representative samples from both calibration sets A and B at the 1/2000 dilution ratio. Reference blanks of the diluent were scanned frequently (every 3 or 4 sample scans) to minimize baseline drift. Measurements of selected samples were repeated several times to test the reproducibility of the technique. The plot shows two distinct groups of spectra. The group with the higher absorbances is the latex from Calibration Set B (the high solids, high particle size group of samples). The lower absorbance belong to Calibration Set A, the ones with low solids fraction and low particle size.

One obvious feature of the UV spectra at 1/2000 dilution (Fig. 8.1.4a) is that the absorbance is saturated below about 300 nm for the latex in group B. This is the part of the spectrum where the organic constituents of the latex absorb, so important composition related information is contained in that region. For that reason, all the samples in Group B were diluted by another factor of 10, and the spectra scanned again. The results are shown in Fig. 8.1.2b. These spectra have much more spectral detail in the region below 350 nm.

8.2 Data Analysis and Calibration

8.2.1 Pattern Recognition using Principal Component Analysis

Before any calibration model can be estimated, the spectra must be analyzed to detect outliers and to find meaningful structure and clusters in the data. While the benefits of doing

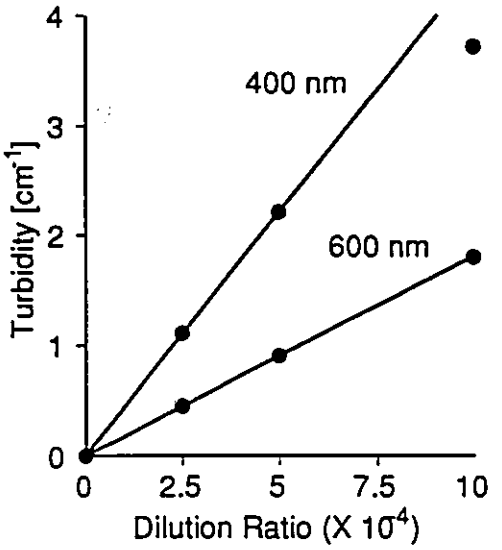

(a) Latex SM_B_32

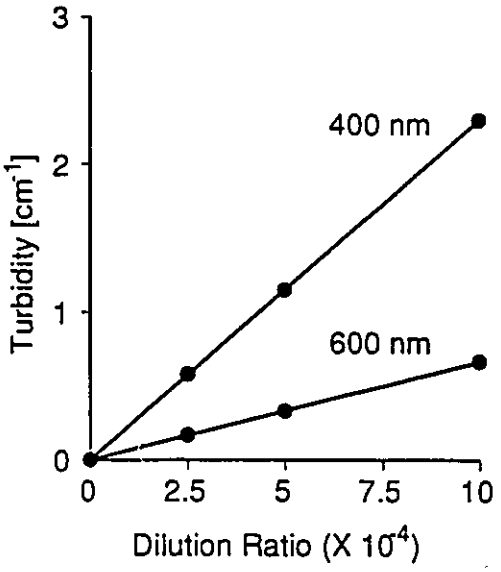

(b) Latex SM_B_35

Fig. 8.1.3: Linearity of Turbidity with Dilution Ratio for Styrene/MMA Latex

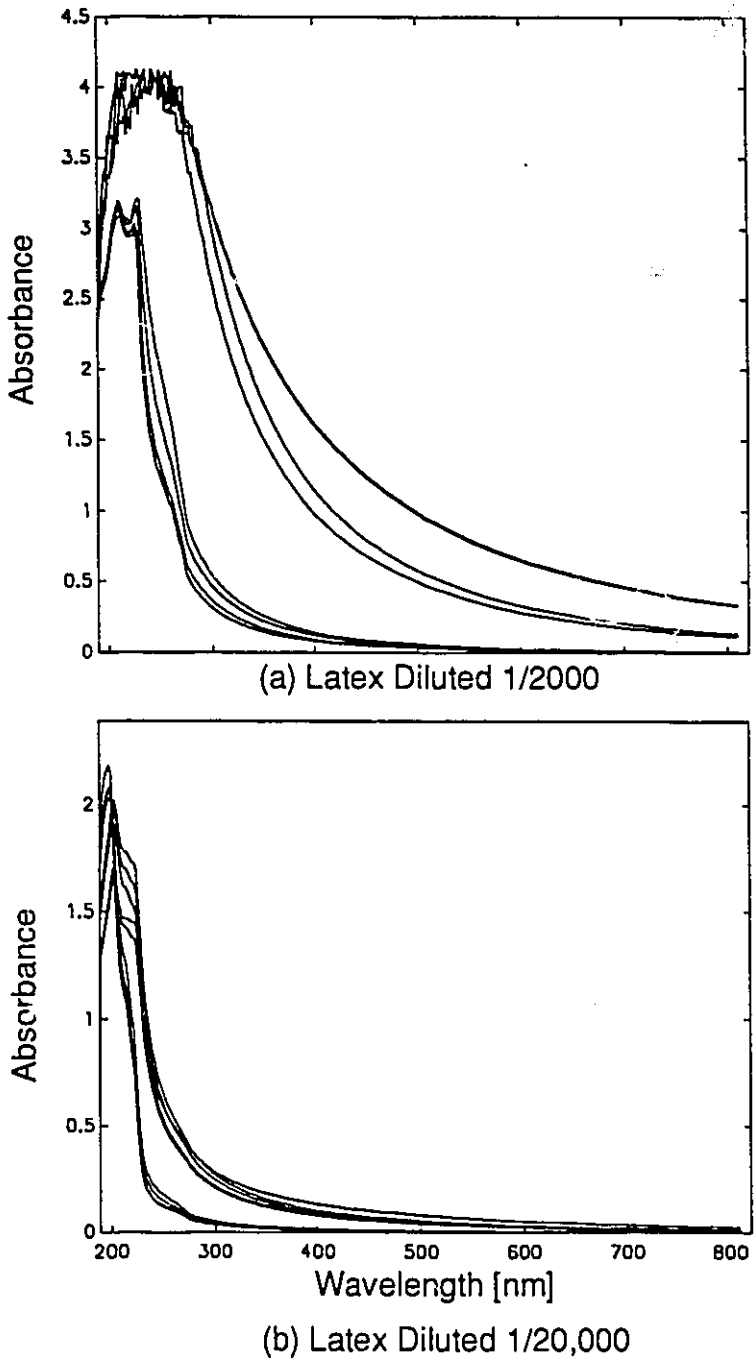

Fig. 8.1.4: UV Spectra of Poly(Styrene/MMA) Latex

this will become apparent as the discussion unfolds, it is obvious that the raw spectra (Fig. 8.1.1 & 2) are difficult to interpret: the only pattern that is easily seen is the distinction between the spectra of Calibration Set A and those of Calibration Set B.

Principal Component Analysis (PCA) is a useful tool for pattern recognition because most of the variation in a highly colinear data set can often be summarized in two or three dimensions. These dimensions are easily plotted and often yield important insights into the structure of the data. In the terminology of chemometrics, what will be covered in this section is called "supervised learning" (Sharaf, Illman and Kowalski, 1988): given many measurements of samples with known properties, the measurement space is collapsed and displayed in the reduced space. Any patterns that are seen there are explained by referring back to the known properties of the samples.

Figure 8.2.1 shows a plot of the *t*-scores from the first two PCA dimensions. The results are presented as a score plot: each axis represents the values in the *t* vectors, with points on the graph corresponding to the *t*-scores of each latex sample. Three samples have been marked. Samples 51 and 52 are known outliers: the latex coagulated significantly in the reactor. Note that these points are detached from the other clusters of data associated with Calibration Sets A and B. This is one kind of outlier: the kind that can detect abnormal process conditions. There is another outlier in this picture associated with sample 32 that is equally important. Three spectra were taken of sample 32. They are all labelled. Two of the spectra are close together, and also close to all the other samples that were synthesized from sample 32. The other is an obvious outlier that must be deleted from the sample set before calibration can proceed.

The other remarkable feature of this plot is the ability of PCA to detect structure in the data. The two obvious, large clusters correspond to the two calibration sets. Some finer structure can be seen with each of these larger clusters. These clusters mostly correspond to the

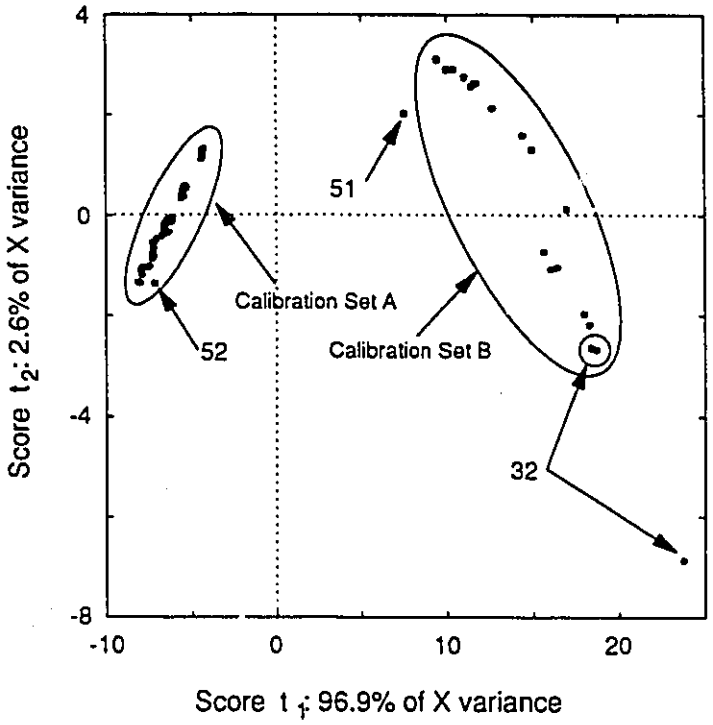

Fig. 8.2.1: PCA Scores of all UV Spectra with 1/2000 Dilution Ratio.

various latex batches and the samples synthesized from them. This structure will be examined in more detail in subsequent sections, where each of the larger clusters are examined separately.

Widely separated clusters must often be analyzed separately when building PLS calibration models because PLS is a linear model. Although the same property of the latex must be predicted in each cluster, the effects distinguishing the clusters are highly nonlinear, meaning that no linear relationship can map one of the clusters onto the other. Thus, no linear relationship will exist to model an equivalent range of properties within the clusters; so, each of the calibration sets will have to be modelled separately to get adequate calibration models.

8.2.2 Calibration Models for Calibration Set A

Outlier Detection by PCA

Fig. 8.2.2 shows the results of Principal Component Analysis on all the UV spectra of Calibration Set A; i.e. all the samples with $t_1 < 0$ in Fig. 8.2.1. The sample numbers correspond to those in Table 7.5.5. The first thing to notice is that, in Fig. 8.2.2(a), sample 52 is easily detected as an outlier. This reinforces the ability of PCA of multivariate spectra to note abnormal operation.

Cluster Detection by PCA

Figure 8.2.2(b) shows the PCA score plot (t_1 vs. t_2) of the same spectra, but with sample 52 removed. In this plot, all latex samples that were synthesized in the same batch are shown with the same style of marker. Examination of this plot shows that samples synthesized from the same batch tend to appear in the same area of the plot, but that the spectra do not cluster into easily separated, mutually exclusive clusters. This means that the property that most distinguishes between the batches (the particle size distribution, in this case) does not dominate

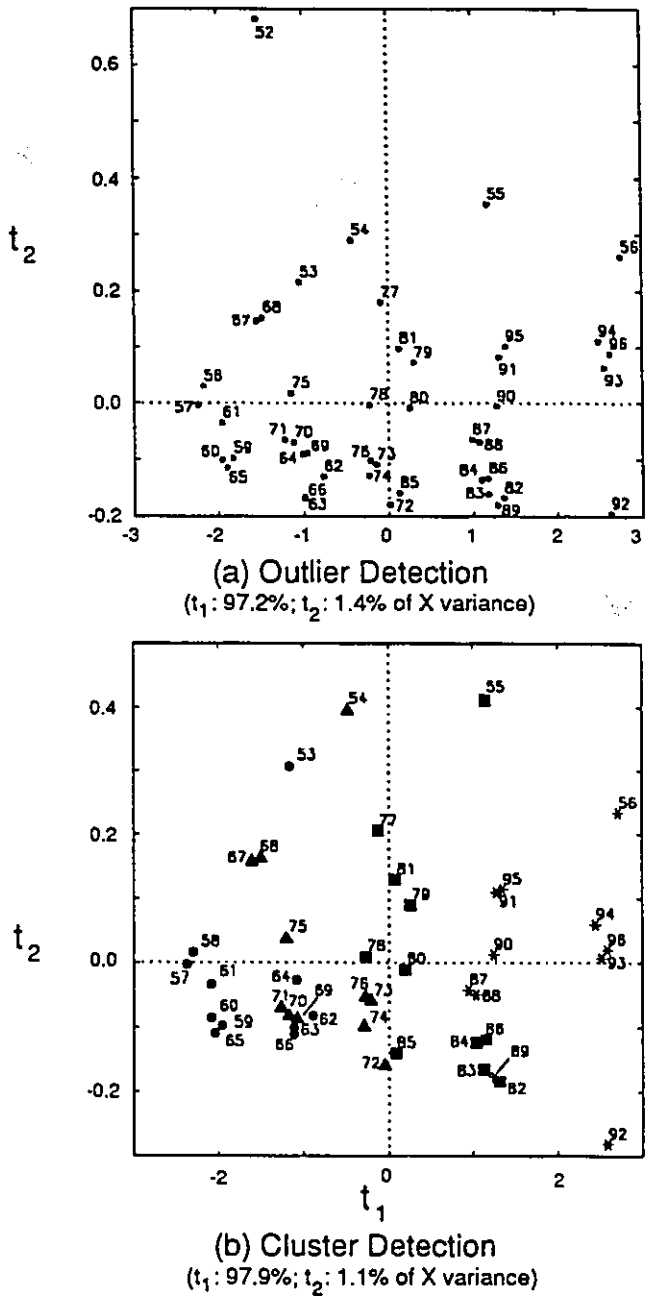

Fig. 8.2.2: PCA Scores of UV Spectra of Calibration Set A, 1/2000 Dilution Ratio

the variance of the *X* block. This is an advantage in PLS modeling.

A second point to notice in this plot is that the scores of replicate spectra are, in most cases, close to each other. There are three sets of replicates associated with each latex batch. Sample numbers in the same decade ending in -7 and -8 (e.g. 57 and 58) are replicates, as are those ending with -1 and -5, and with -2 and -6. This is an early indication that the signal-to-noise ratio may be adequate for building the PLS calibration model.

PLS Calibration Models

This section discusses the estimation of multivariate calibration models for each of the properties of the latex. The models in this section were calculated from all the 44 spectra shown in the score plot of Fig 8.2.2(b). Models for each *Y*-variable were predicted separately using PLS1, and the number of components were estimated by cross-validation in a leave-one-out algorithm. In Section 6.2.3, two criteria for choosing the number of components from cross-validation were discussed. The simplest is to choose the number that gives the minimum PRESS. An example of this criterion is shown in Fig. 8.2.3(b) for the prediction of methyl methacrylate monomer from the UV spectra. In many cases, there is no sharply defined minimum PRESS. In these cases, the number of components kept for the model is taken at the point where the slope of the PRESS curve goes to some small value that is on the order of the sum-of-squares of the *y*-residual. An example of this criterion is shown in Fig. 8.2.3(a) for the prediction of poly(styrene) composition.

Each of the columns of the property matrix *Y* were scaled to unit variance before calculating the PLS model. This has the advantage of making the PRESS easy to compare between models for different components of models built from different data sets. A value of PRESS/(n-1) around 1.0 means that the prediction error is the same magnitude as the variance of the property of interest, and that the PLS model is no better than a random model. Lower values of PRESS/(n-1) indicate progressively better model. In most cases, a PRESS/(n-1) less

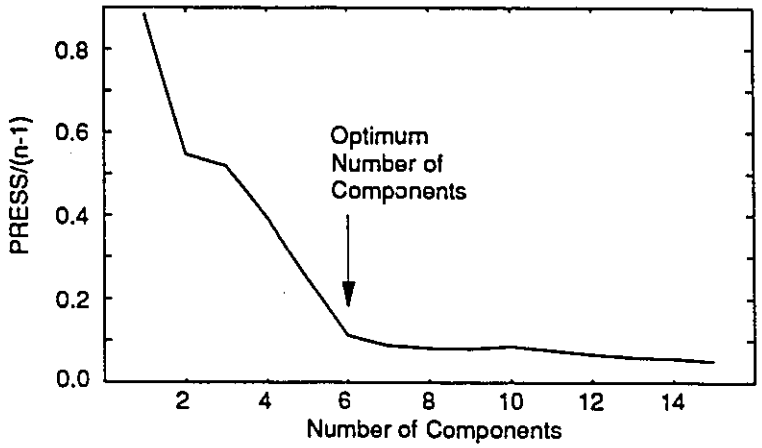

(a) Poly(Styrene)

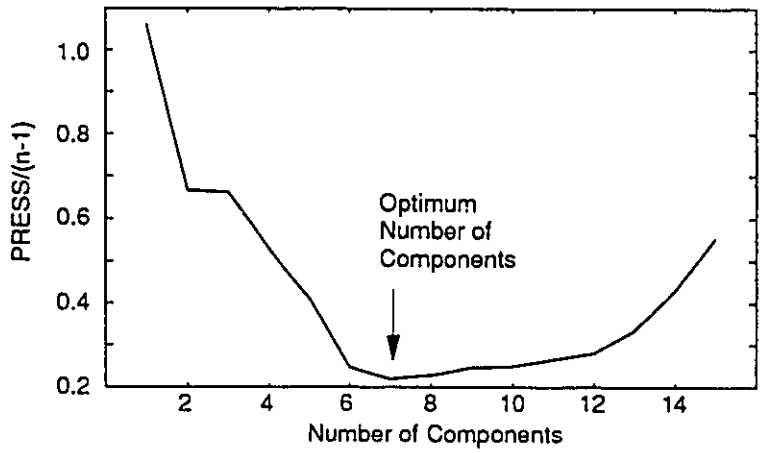

(b) Methyl Methacrylate

Fig. 8.2.3: Prediction Error vs. No. of PLS Components

than 0.2 indicated that the model predicted the latex property quite well. Generally, the PRESS/(n-1) was found to be one of the most useful tools in evaluating the relative ability of the PLS calibration models to predict the latex properties.

The standard error of prediction (SEP) of the calibration model can be calculated directly from the PRESS. If the data in the latex property matrix is mean centered and scaled to unit variance, then

$$y_i = (c_i - y_{av})/\sigma_c^2 \tag{8.2.1}$$

where c is the original data, y_{av}, the mean of the data, and σ_c^2 the variance of c. The SEP is calculated from the PRESS by

$$SEP^2 = \frac{PRESS}{(n-1)}\sigma_c^2 \tag{8.2.2}$$

Fig 8.2.4 show the resulting calibration models. Each plot show the values of the y prediction from the leave-one-out procedure at the optimum number of PLS components. The prediction error (SEP) for each property is also shown in this diagram. The 45° line on each plot indicates where perfectly predicted points will lie. These plots show that the PLS models for mean diameter, poly(styrene), and styrene monomer give excellent predictions. The models for water, methyl methacrylate monomer and poly(MMA) do not perform well. Note that, although the MMA Monomer model has a low SEP and a relatively low PRESS, there is no correlation between the predicted and actual weight fraction values within the two clusters of the property values.

One problem with evaluating the models for organic phase compositions is the lack of precision in knowing the ratio of polymer to monomer of a given species. This arises because of the way polymer fraction was calculated by assuming that each batch reaction went to 100% conversion. One way to evaluate the models without using this assumption is to develop

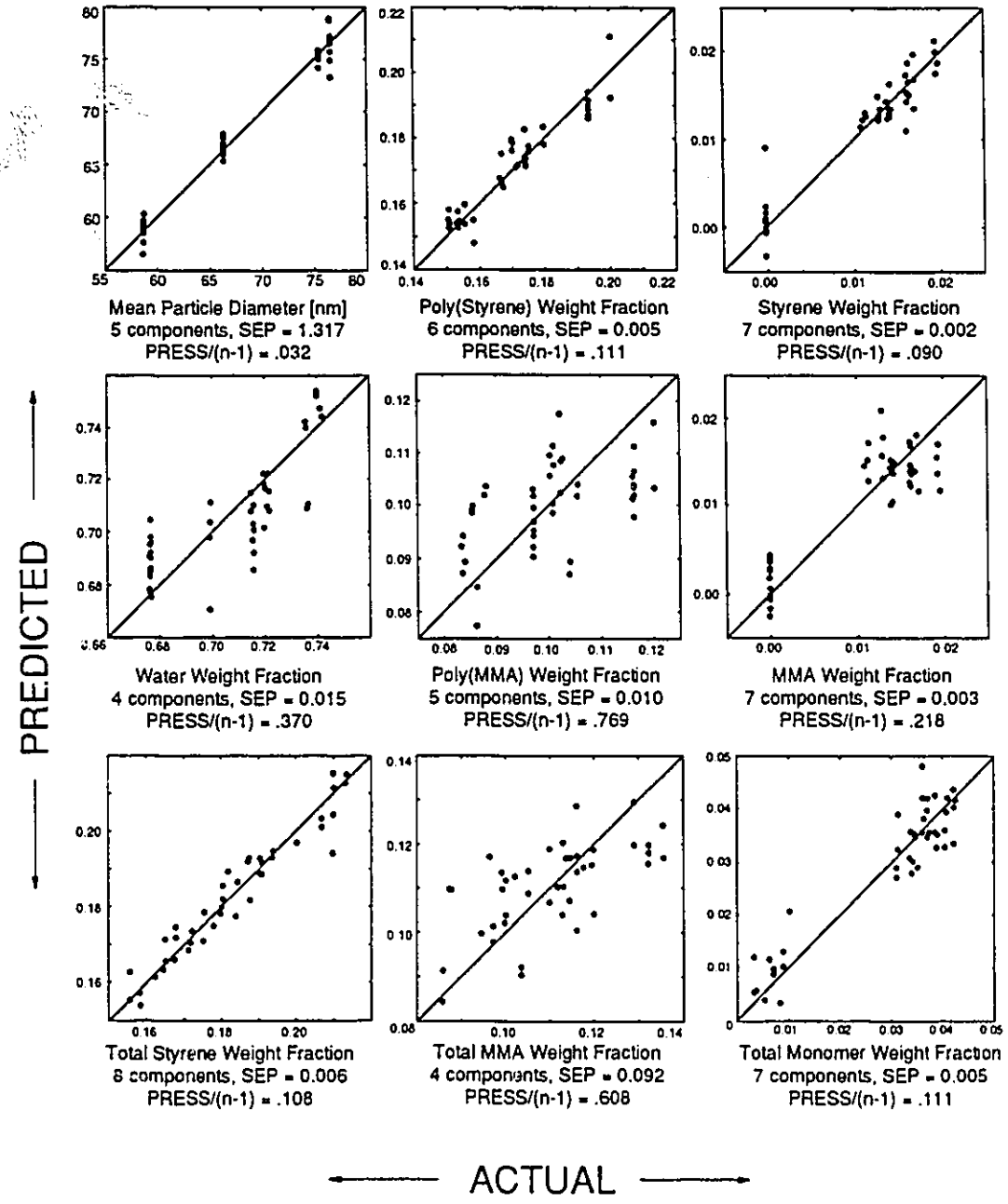

Fig. 8.2.4: Latex Properties vs. PLS Predictions from UV Spectra, Calibration Set A

calibrations for the total fraction of each organic species. This is done and reported in the last line of plots in Fig. 8.2.4. These plots confirm the conclusion that the weight fraction of styrenic compounds are well predicted by the model, but the methyl methacrylate ones are not.

There are several diagnostic tools available for calibrating optical spectra that help in determining whether the calibration models are indeed causal, or whether they are just the result of some spurious correlation with another effect that has a strong influence on the UV spectrum. The first thing to check is that there is no high correlation between the properties that have good models; i.e. between diameter, poly(styrene), and styrene. The correlations between these properties are: -0.082 for poly(styrene) and diameter; 0.050 for poly(styrene) and styrene; 0.009 for diameter and styrene. These are all very low.

A second, very powerful, qualitative diagnostic tool is to examine the X matrix loadings, w. These vectors weight each X variable by its ability to predict y. For the prediction of styrene concentration, therefore, we would expect high w weights in regions of high styrene absorption. Particle size, on the other hand, affects attenuation at all frequencies, so the w vectors should reflect that. The relative contribution of X to the y prediction along each PLS component is easily calculated. Recall that the prediction of y is given by

$$\hat{y} = tq' = \sum_{i=1}^{a} t_i q_i \tag{8.2.3}$$

The total variance of the y prediction is, therefore,

$$\mathrm{var}(\hat{y}) = \sum_{i=1}^{a} q_i^2 \mathrm{var}(t_i) \tag{8.2.4}$$

and the relative contribution of each PLS dimension to the variance of $\hat{y}$ is given by the relation

$$\left\{\begin{array}{c}\text{fraction contribution}\\ \text{of the}\\ i\text{th dimension}\\ \text{to } \hat{y}\end{array}\right\} = \frac{q_i^2 \mathrm{var}(t_i)}{\mathrm{var}(\hat{y})} \tag{8.2.5}$$

The variance of t_i is calculated from the data used for the calibration. Note that the contribution of the ith dimension to the prediction $\hat{y}$ does not provide any information about whether $\hat{y}$ models the original y data well or not. That inference can only be made using the PRESS discussed in Section 6.2.3. The contribution of each dimension serves only to rank dimensions by their relative importance in the prediction of y.

Finally, it is a good check on the number of PLS components chosen to ensure that the X loading vector of the last component chosen has some apparent, interpretable spectral features, and does not resemble white noise. This is some assurance that the final components are still finding relevant structural features in the X matrix residuals.

Figures 8.2.5, 8.2.6 and 8.2.7 are plots of selected loading vectors from the PLS models for styrene, poly(styrene), and diameter, respectively, ranked by their contribution to the prediction of their respective property. The percent y prediction variance values are calculated from eq. 8.2.5. These vectors were calculated using all the 44 data points of Calibration Set A with no cross-validation, but the number of components calculated was that determined from cross-validation previously. The expectations stated above are confirmed. The loading vectors for diameter strongly weight loading vectors with weightings across all wavelengths. The loading vectors for styrene and poly(styrene) are more closely focussed on the region of styrene absorption. Thus, it is reasonably certain that the PLS models are indeed responding to predominantly causal links between composition and UV spectrum responses.

8.2.3 Calibration Models for Calibration Set B

Outlier and Cluster Detection by PCA

Figure 8.2.8 shows the score plots from Principal Component Analysis (PCA) of the matrix of the mean centered UV spectra of Calibration Set B. The spectra used for this

Calibration Set were

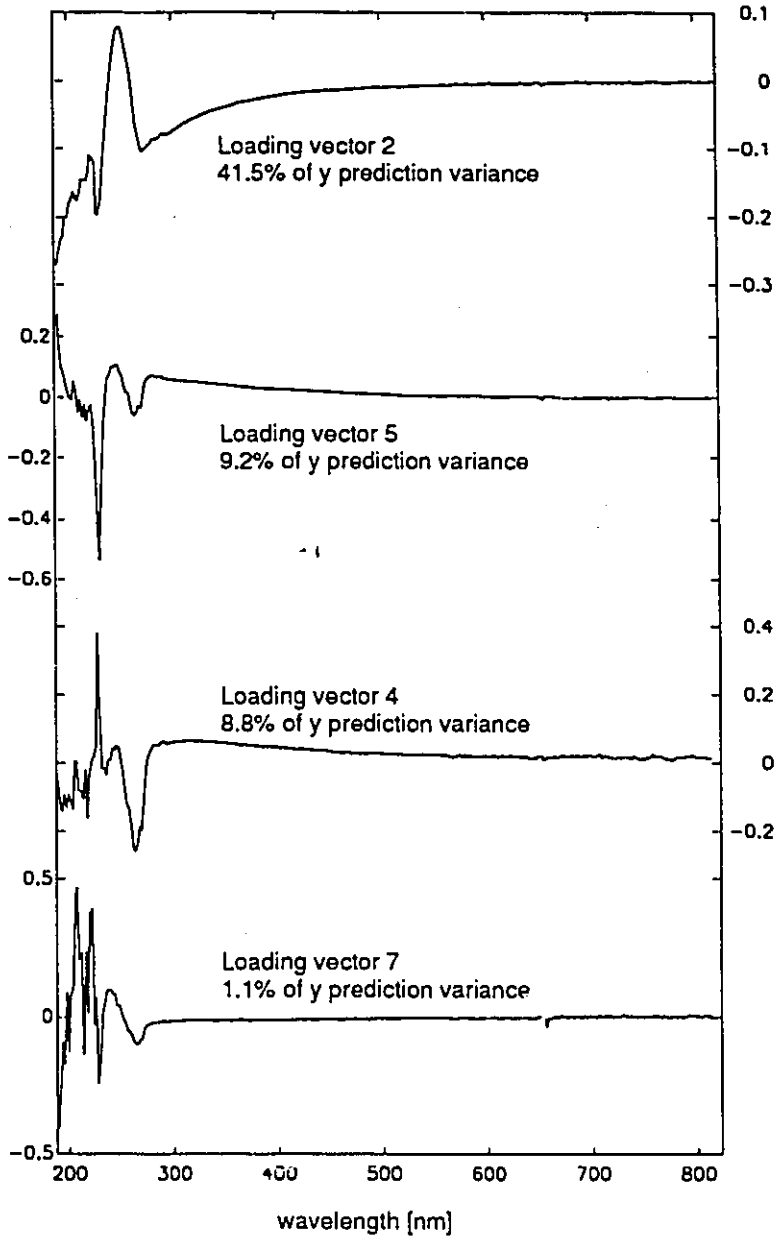

Fig. 8.2.5: PLS Loading Vectors for Styrene, Calibration Set A

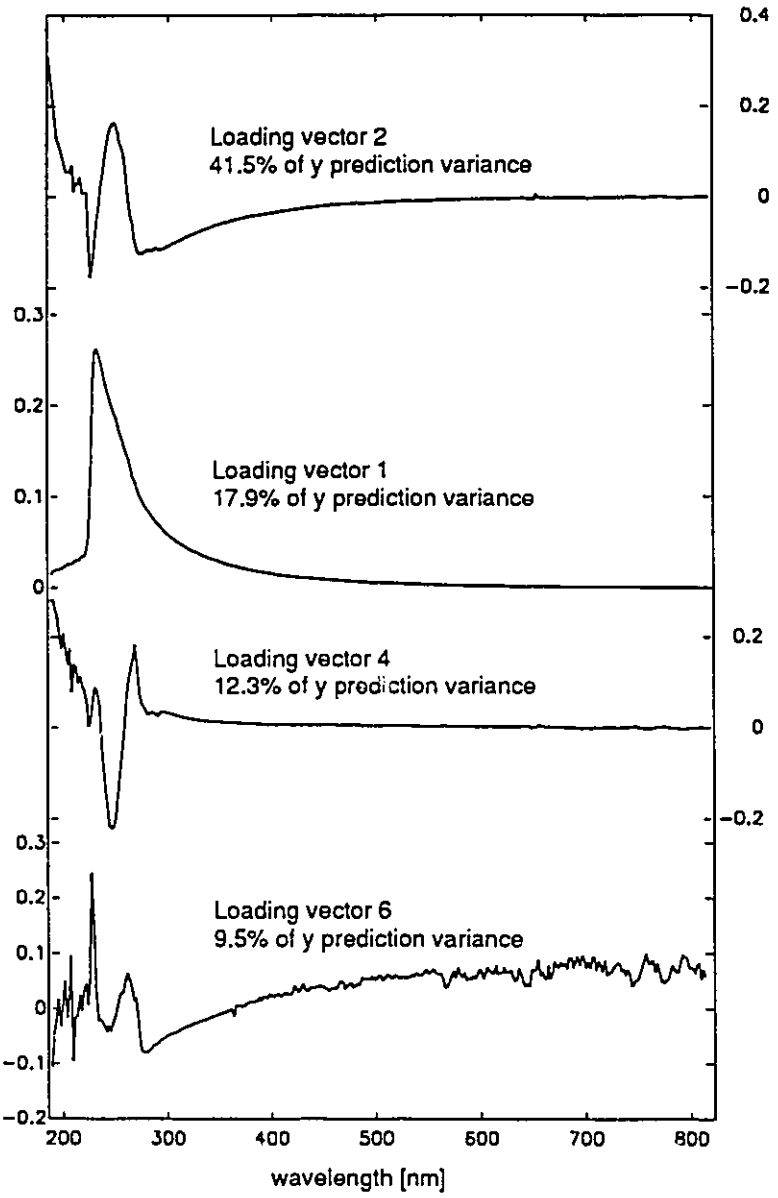

Fig. 8.2.6: PLS Loading Vectors for Poly(Styrene), Calibration Set A

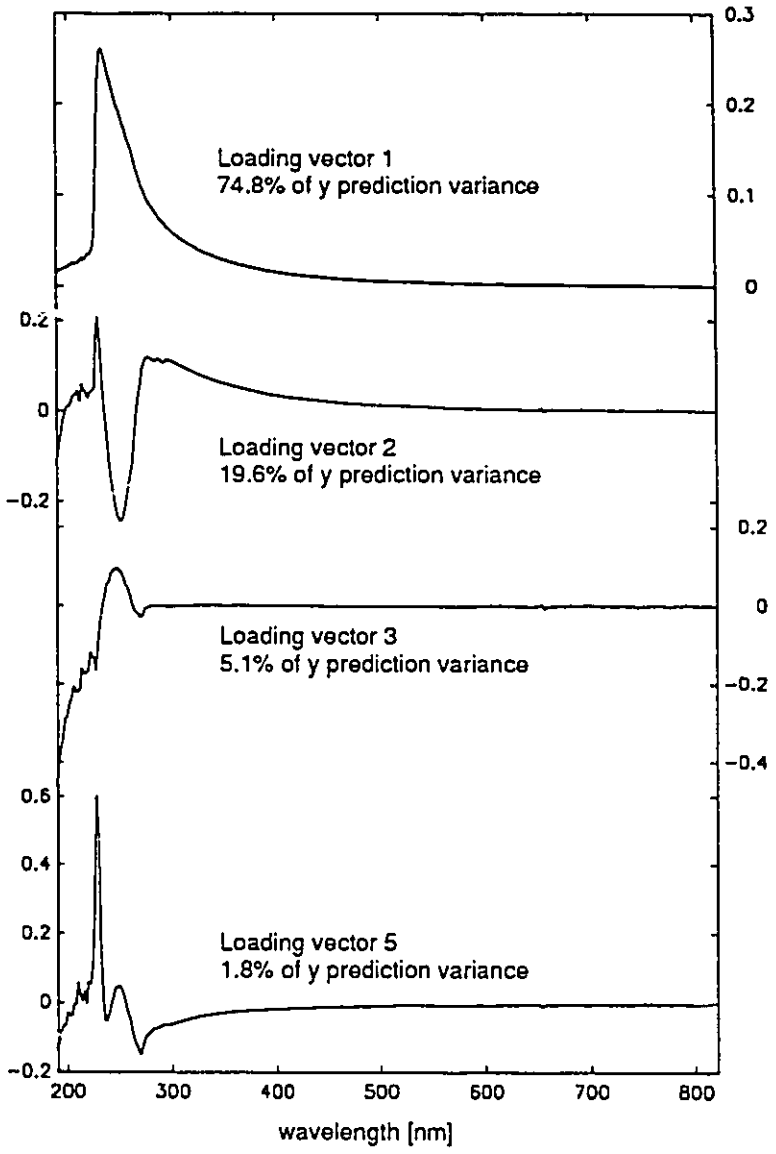

Fig. 8.2.7: PLS Loading Vectors for Mean Diameter, Calibration Set A

taken from latex diluted 1/20,000 so that the absorbance was not saturated below 350 nm. The plot shows the first three PCA dimensions. The first dimension accounts for little of the structural variation in the UV spectra, although it accounts for 80.9% of the X matrix variance. Components 2 and 3 show much of the structure of the UV data. Sample 28 is shown to be an outlier. Referring to Chapter 7, this sample has a particle size distribution that is significantly different from the others: it has both a significantly higher mean and a larger standard deviation than the rest of the samples. It will be removed from the Calibration Set for all subsequent analysis.

Two clusters are easily identified in Fig. 8.2.8. They are easily identified by the second component, and correspond to positive and negative t_2. All points with $t_2<0$ are from spectra of latex batch 32 or samples synthesized from it. The points with $t_2>0$ are batch 35 and all its associated samples, along with batches 38, 41, and 42, which have the same polymer composition as 32, but were produced in a smaller reactor. The discussion of the previous section suggests that each of these clusters should be analyzed separately so that small scale variation within each cluster can be adequately modelled. That approach, unfortunately leaves too few degrees of freedom for adequate model evaluation: each cluster has about the same number of points as there are sources of variation in the experimental design.

PLS Calibration Models

The PLS calibration models for Calibration Set B were calculated in the same way as those for Set A discussed above. The results of the calibration, including cross-validation predictions, PRESS, and SEP, are shown in Fig 8.2.9. These results generally support those from Calibration Set A: poly(styrene), styrene and methyl methacrylate monomers are well predicted, and the other components are not. Styrene and methyl methacrylate monomer compositions are very highly correlated in this data set (0.98), so the good MMA weight fraction predictions may result from that. As a final check, the two non-ionic surfactants are also strong absorbers in the UV region. Their composition does not, however, correlate strongly with any of the other compositions: the highest correlation coefficient is 0.51 between

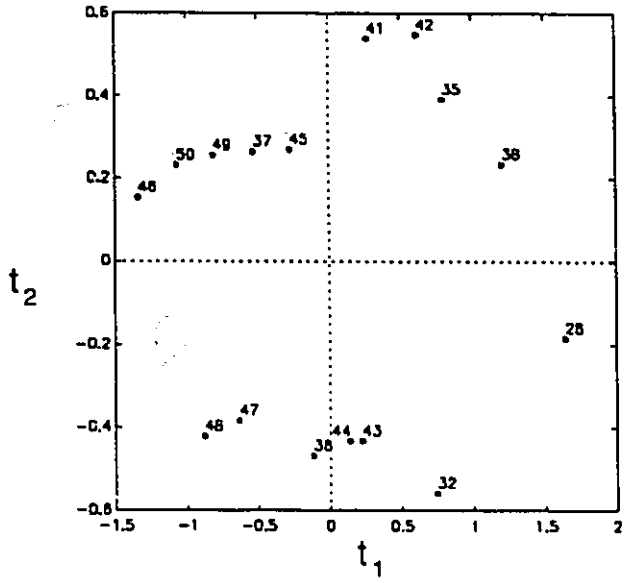

(t_1: 80.9%; t_2:17.3% of X variance)

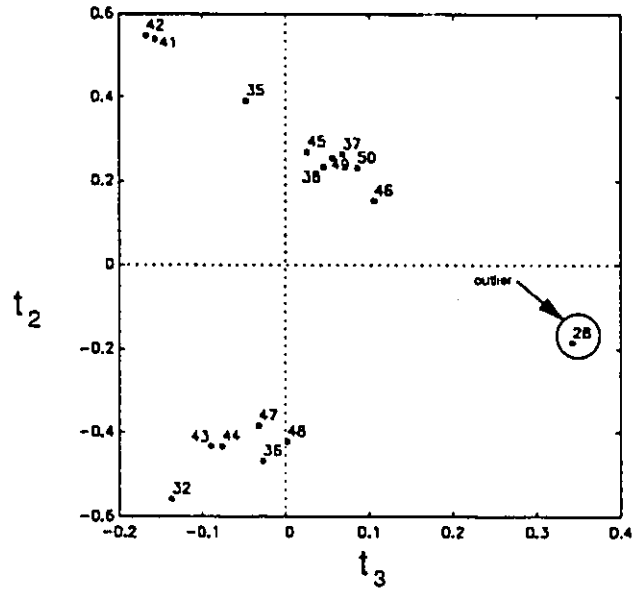

(t_3: 1.7%; t_2:17.3% of X variance)

Fig. 8.2.8: PCA Scores of UV Spectra of Calibration Set B, 1/20,000 Dilution Ratio

Rexol 15/407 and poly(MMA). The correlation between poly(MMA) and the total nonionic surfactant concentration is 0.88. None of the other have correlation coefficients over 0.5. Thus, it is unlikely that any hidden effect is responsible for the good correlations that are seen for poly(styrene).

The poor modeling of mean particle diameter may arise from two facts: first, the variation in particle size distribution between samples arises not only from differences in the means, but there is also a large difference in the breadth of the distributions between samples; second, the Dynamic Light Scattering values for weight average mean diameter of a broad distribution are not as accurate as those of the narrower distributions of Set A.

8.3 Summary

In this chapter, the ultraviolet/visible light spectrum from 190 to 820 nm was evaluated as a technique for measuring composition and particle diameter in a styrene/methyl methacrylate latex. In this region of the optical spectrum, the latex constituents absorb only below 350 nm. The absorption peaks are highly overlapped and their maxima tend to shift, depending on the molecular environment of the consituent. The polymer particles in the latex have a mean diameter on the order of the wavelength of the UV/Vis light, so light scattering is an important and very nonlinear mechanism for the attenuation of the spectrometer's incident beam.

The latex was diluted 1/2000 and 1/20,000 to make the 10 mm thick samples transparent to the spectrometer beam, and to ensure a linear relationship between the turbidity ($\ln(1/T)$) and the polymer concentration in the non-absorbing region (>350 nm) of the spectrum.

Principal Component Analysis (PCA) was used to reduce the high dimensional, colinear space of UV absorbances to a smaller dimensional, more easily interpreted set of variables. Over 98% of the variance in the original data could usually be explained by the first 2 or 3 principal

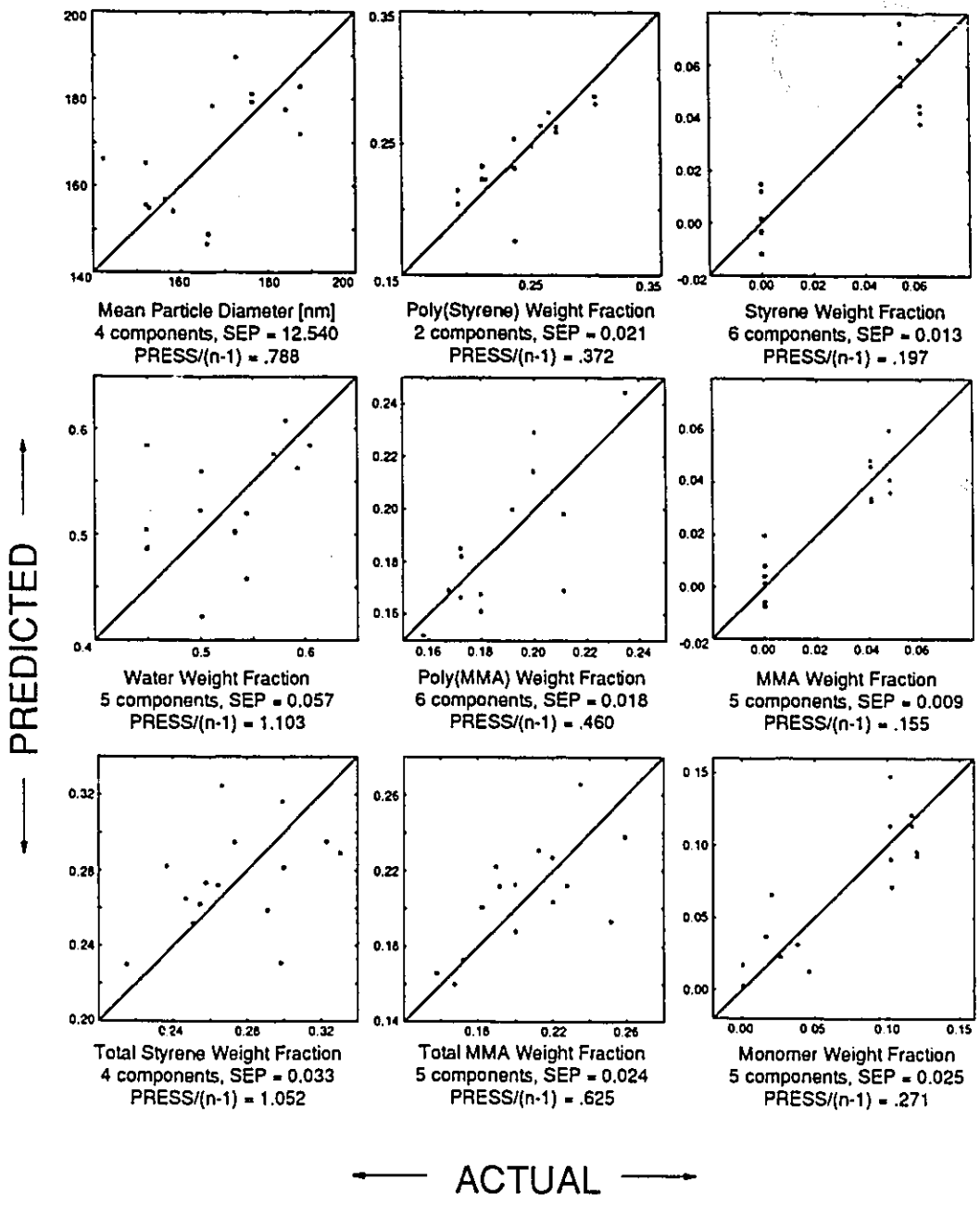

Fig. 8.2.9: Latex Properties vs. PLS Predictions from UV Spectra, Calibration Set B

components. PCA of the UV spectra was able to detect outliers among the calibration samples, whether they were anomolous latex samples or poor spectra of good latex. PCA could also detect structure in the data, clustering similar samples together on plots of the data plotted in the reduced space of the principal components.

The UV spectra were used to predict the compositions of major latex constituents and the mean particle diameter using multivariate calibrations calculated by Partial Least Squares. The models were evaluated based on their prediction error, calculated by crossvalidation. The weight fractions of styrene monomer, poly(styrene), total styrene, and total monomer were predicted very well. The models for mean diameter were very good for a group of samples with narrow particle size distributions of similar breadth. Latex with broad size distributions were not modelled well at all. Water and methyl methacrylate compositions were also not well predicted by the UV spectra.

9

NEAR INFRARED SPECTROSCOPY OF LATEX

9.1 Constituent and Latex Spectra

9.1.1 Instrument Description

Near-infrared spectra were taken with an L.T. Industries (Rockville, Maryland) Quantum 1200 NIR analyzer (Landa, 1979). The spectrometer scans wavelengths using a moving, holographic grating. The wavelength range used for this work was from 900 to 1800 nm. The spectra are digitized at 0.75 nm intervals, yielding absorbances at 1201 wavelengths per spectrum. The spectrometer transmits light to the sample and receives light from the sample through a 20 ft. bidirectional fibre optic cable, with 18 fibres transmitting light to the sample and 18 returning light to the detector in the spectrometer.

In NIR spectroscopy, measurements are taken of either the transmitted or reflected light, depending on the type of sample. In all samples, the incident light reaching the sample is either absorbed, transmitted, or reflected. In classical absorption spectroscopy, no light is reflected, so the absorbance A is defined in terms of the transmittance T:

$$A = \log\left(\frac{1}{T}\right) = \log\left(\frac{I_0}{I_t}\right) \qquad (9.1.1.1)$$

where I_0 is the intensity of the incident light and I_t, that of the transmitted light. According to Beer's law, the concentration c of an absorber in the sample is directly proportional to the absorbance

$$A \propto cl \qquad (9.1.1.2)$$

where l is the path length of the light through the sample. In this expression, the logarithm can be either base 10 or base e. Although base 10 logarithms are standard in definitions of absorbance, base e will be used in this Chapter to be consistent with the preceding work on turbidity. In transmittance spectroscopy, the path length is kept constant by the design of the sample cell, so absorbance is proportional to the concentration of the absorber.

In turbid samples, there is always some reflected or scattered radiation. Completely opaque samples transmit no light, so an apparatus must be constructed to collect the reflected radiation (Birth and Hecht, 1987). In that case, many authors (Williams and Norris, 1987) relate reflectance R to the concentration of an absorber in the sample using the same Beer's law relation as for transmittance

$$A = \log\left(\frac{1}{R}\right) \propto cl \tag{9.1.1.3}$$

This expression lacks rigor because the path length in a scattering sample is variable. Kubleka-Munk linearization (Birth and Hecht, 1987) was developed for this case to provide a more fundamental relation to concentration; but, the $\log(1/R)$ transformation has proven satisfactory for many applications.

Figure 9.1.1 illustrates how a fibre optic probe would be set up in a process environment for either reflectance or transmittance measurements. It also shows a nontraditional probe configuration that is very popular in NIR spectroscopy, one called transflectance. For transflectance, the fibre optic probe carries light both to and from the spectrometer, as in reflectance measurements. A mirror is attached to the end of the probe to reflect the light that is transmitted across the gap back into the probe. This configuration has several attractive

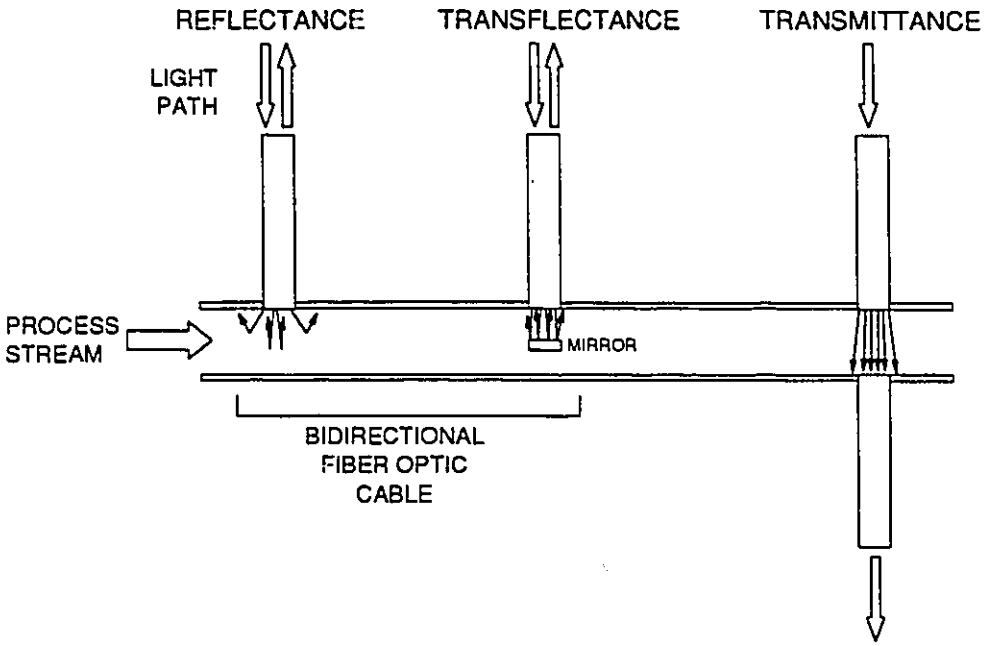

Fig. 9.1.1: NIR Fiber Optic Probe Configurations

features. For samples that do not scatter light, this probe can give a transmittance reading without the need to align the sending and receiving fibre bundles. For opaque or translucent samples, this probe can greatly increase the signal at the detector by collecting both reflected and transmitted light. This probe configuration is also very practical for in-plant quality control laboratories because it can be quickly dipped into several samples without the need to transfer the sample to a special cell, and the probe is easily cleaned. This is the mode of operation used for taking most of the spectra in this Chapter. The transflectance probe used has a 3 mm gap, which gives a 6 mm path length for transmittance measurements.

For latex production, the transflectance probe would not be appropriate for an in-line application like the one pictured in Fig. 9.1.1. Polymer would quickly build up on the probe, necessitating frequent cleaning. Other options would be a reflectance configuration on the process stream, or a transmittance measurement on a diluted sample, like the UV turbidity and transmittance measurements of earlier Chapters. Some aspects of these options will be discussed below.

9.1.2 Constituent Spectra

Figures 9.1.2 and 9.1.3 show the NIR transflectance spectra of all the constituents in the latex except for water. Fig. 9.1.1 show the spectra of the organic phase constituents referenced to a THF background. The compounds were dissolved in THF in approximately the weight fractions shown in the Figure. An important feature of these plots is that the spectral features corresponding to various structural features of the molecules do not overlap nearly as much as they do in the UV region (Fig. 8.1.2). The aromatic peaks for styrene (=CH aromatic) at around 1145 and 1680 nm overlap with adjacent MMA peaks, but have distinct peak locations. The peak for the monomers at 1640 nm is quite distinct from the other major peaks and corresponds to $=CH_2$.

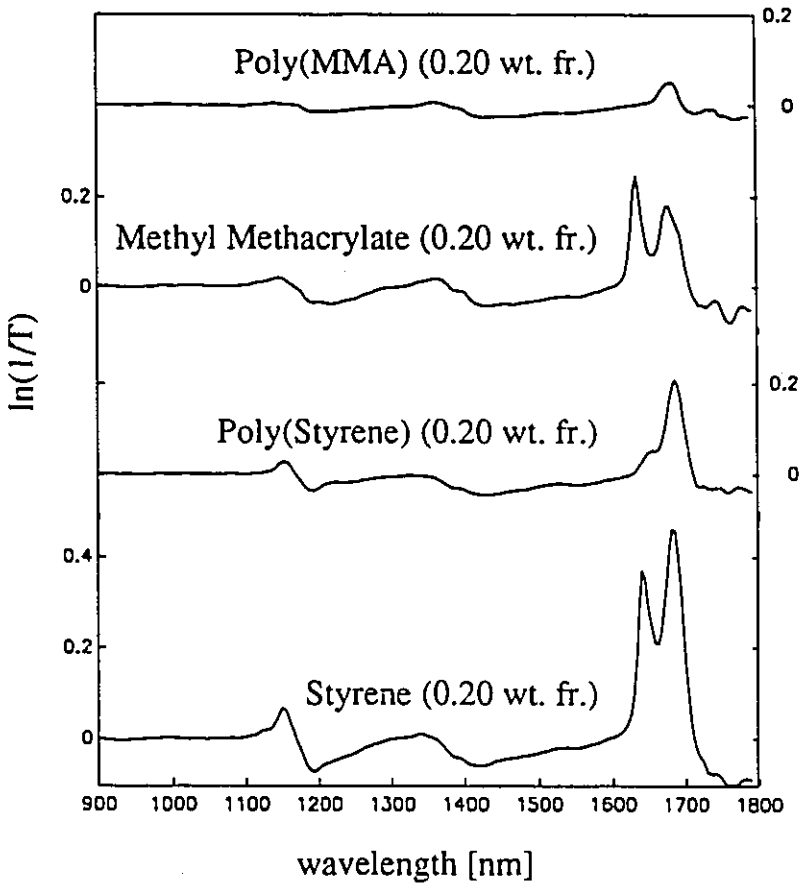

Fig. 9.1.2: NIR Spectra of Latex Constituents; Dissolved in Tetrahydrofuran

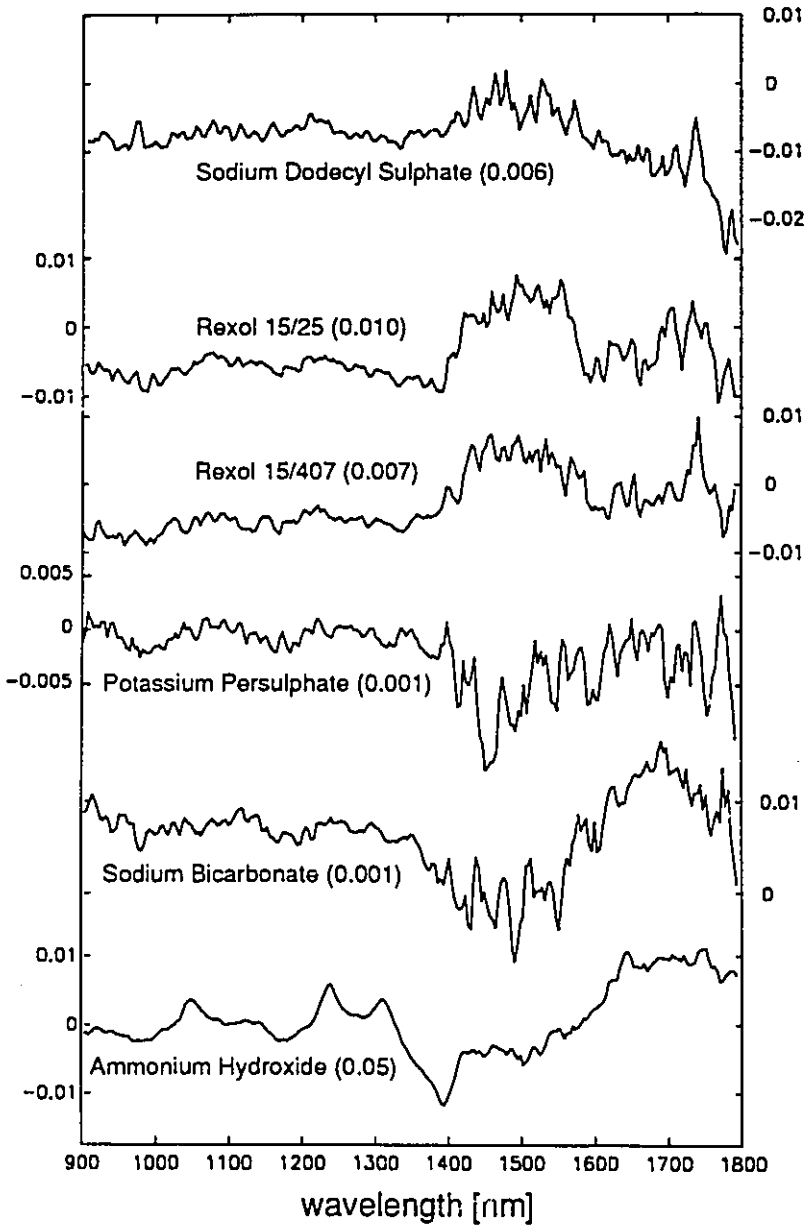

Fig. 9.1.3: NIR Spectra of Latex Constituents; Dissolved in Water

Figure 9.1.3 shows the spectra of all the water soluable constituents referenced to water. The concentrations of the constituents in the samples is around the maximum encountered in the concentrated latex samples. The main conclusion to be drawn from this plot is that none of these components have any significant absorption in the NIR region in the concentrations encountered, so they should not present any interferences to the multivariate calibration models.

9.1.3 Latex Spectra

Figure 9.1.4 shows NIR transflectance spectra of some representative latex samples from both Calibration Sets A and B (Chapter 7 explains the calibration sets). The latex was scanned as is without dilution, using the transflectance probe. The spectra are referenced to pure water. Each spectrum is the average of 300 successive scans of the entire wavelength range. Spectra were screened before being added to the data set. Gross errors due to the presence of a large air bubble in the probe gap, or a significant change in the background are easily seen by comparing the scans to some representative ones. The background was rescanned every 2 to 4 scans to minimize the effects of instrument drift. The native units of the instrument are transmittance ($T = I/I_0$). These were transformed by the standard $\log(1/T)$ before plotting or any subsequent data analysis.

The first thing immediately obvious from Fig. 9.1.4 is that, not only are the two calibration sets easily differentiated by the NIR spectra, but that the effects distinguishing them are highly nonlinear. The spectra of Calibration Set A look more like standard turbidity spectra: there is attenuation at all wavelengths due to particle scattering, with the absoption peaks due to the organics clearly present. The region between 1440 and 1500 nm, where the spectra change very little, is the primary absorption peak for water in this region. The negative absorbances at 1400 nm occur because 30% of the water (which is the reference spectrum) has been replaced by polymer and monomer.

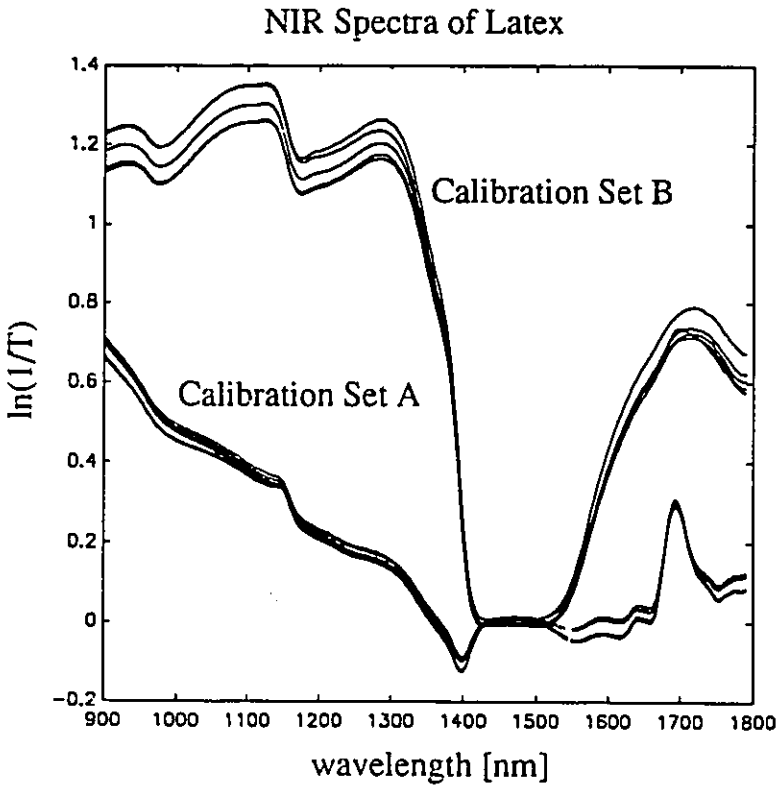

Fig. 9.1.4: NIR Spectra of Poly(Styrene/MMA) Latex

The spectra for Calibration Set B are less easy to interpret. They look, in fact, like the inverse of the spectrum for water (referenced to air, a relative nonabsorber). Few of the spectra have any recognizable organic phase absorption peaks. Fig. 9.1.5 explains the anomolous behaviour of these spectra. This figure shows the transflectance spectra of two concentrated latex samples plotted with the reflectance spectra of the same samples. The reflectance spectra were taken by simply removing the mirror from the transflectance probe tip, but they were still referenced to the same water background as the transflectance spectra. Fig. 9.1.5(b) shows that for sample 32 the transflectance and reflectance spectra are virtually identical, meaning the 3 mm thickness of latex in the gap is effectively opaque. For sample 35 (Fig. 9.1.5(a)), some of the light reflects off the mirror and back to the detector. The trend of lower absorbance for transflectance spectra at higher wavelengths is consistent with scattering in the Rayleigh regime, where the intensity of scattering is inversely proportional to the fourth power of the wavelength.

9.1.4 Effects of Dilution on Transflectance Spectra

Fig. 9.1.6 shows the NIR transflectance spectra of a latex from Calibration Set B at several dilutions. The latex was diluted in the hope of increasing the signal-to-noise ratio by getting more of the incident light reflected from the mirror. While dilution does make the latex less opaque, there is no dramatic increase in the amount of spectral detail in the diluted latex spectrum. Quantitative analysis of the effects of dilution will be covered in Section 9.2.3 below.

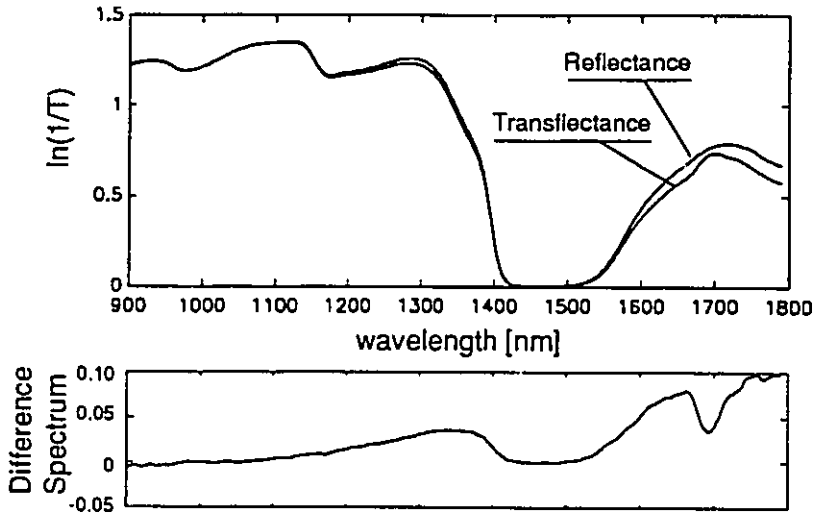

(a) Sample 35

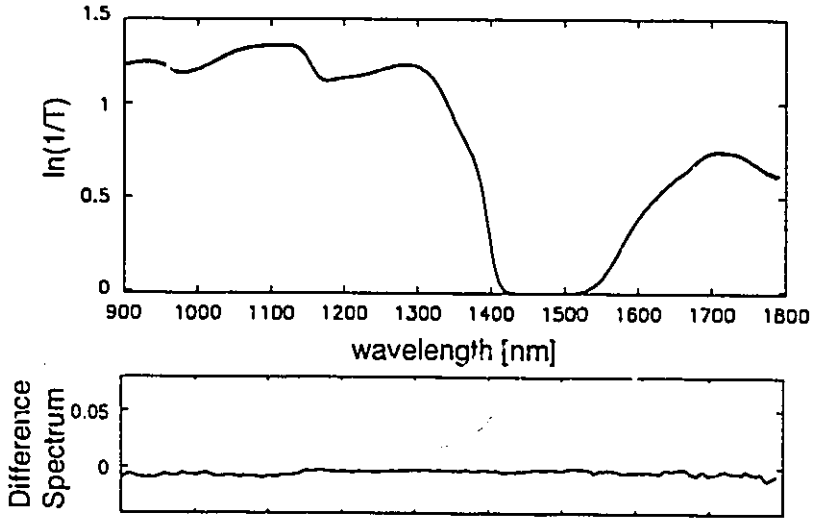

(b) Sample 32

Fig. 9.1.5: NIR Transflectance vs. Reflectance Spectra for Latex from Calibration Set B

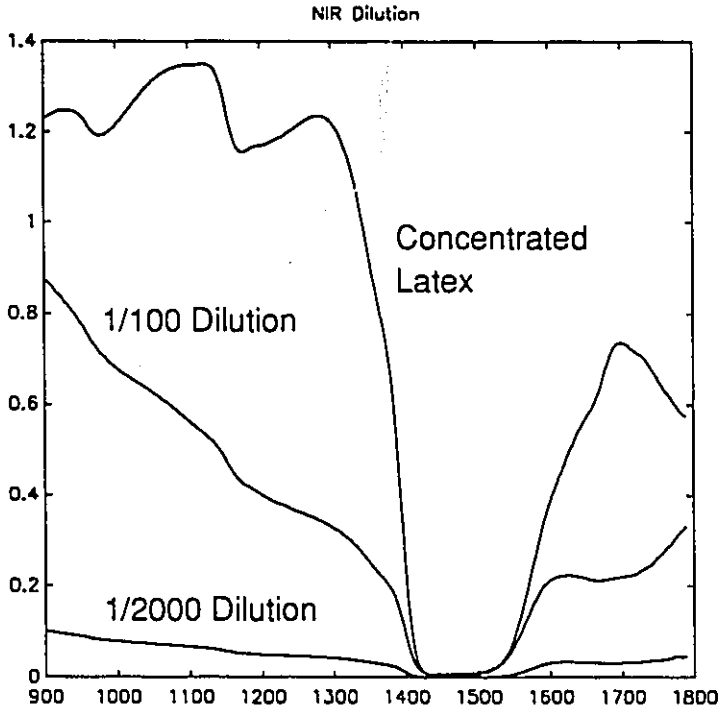

Fig. 9.1.6: Effect of Dilution on NIR Spectra of Poly(Styrene/MMA) Latex

9.2 Data Analysis and Calibration

9.2.1 Pattern Recognition using Principal Component Analysis

As in Chapter 8, Principal Component Analysis (PCA) can be used on the whole data set to detect outliers and look for structure in the data. The plot of scores from the first two dimensions is in Fig. 9.2.1. The conclusions are similar to those of PCA of the UV spectra: the samples from calibration sets A and B are easily differentiated. There are no outliers because of the careful screening process done with every scan, and because the two samples representing bad latex (51, 52) were not included in this data set. As with the UV spectra, the multivariate calibration models for each cluster will be calculated separately.

9.2.2 Calibration Models for Calibration Set A

Cluster Detection by PCA

Figure 9.2.2 show the PCA score plot of the first two dimensions for Calibration Set A. All the samples that come from the same latex batch are given the same style marker on the plot. There is a tendency for latexes from the same batch to cluster in the same region of the plot, although from a purely qualitative comparison to Figure 8.2.2, the clusters boundaries are less well defined than those from the UV spectra. An understanding of the phenomena involved suggests two reasons for this. First, the signal-to-noise ratio of the NIR spectra is likely lower than that for UV spectroscopy. This conclusion is supported by the fact that spectra of repeat samples are not as close to each other in the NIR score plot as are those in the UV score plot (Fig. 8.2.2). Secondly, the main property that differentiates latexes associated with different batches is the particle size distribution. In the NIR region, the particle scattering is mostly in the Rayleigh regime (see Chapter 2), so scattering is not only less, it is also not as strong a function of particle size as in the UV/Vis region of the optical spectrum.

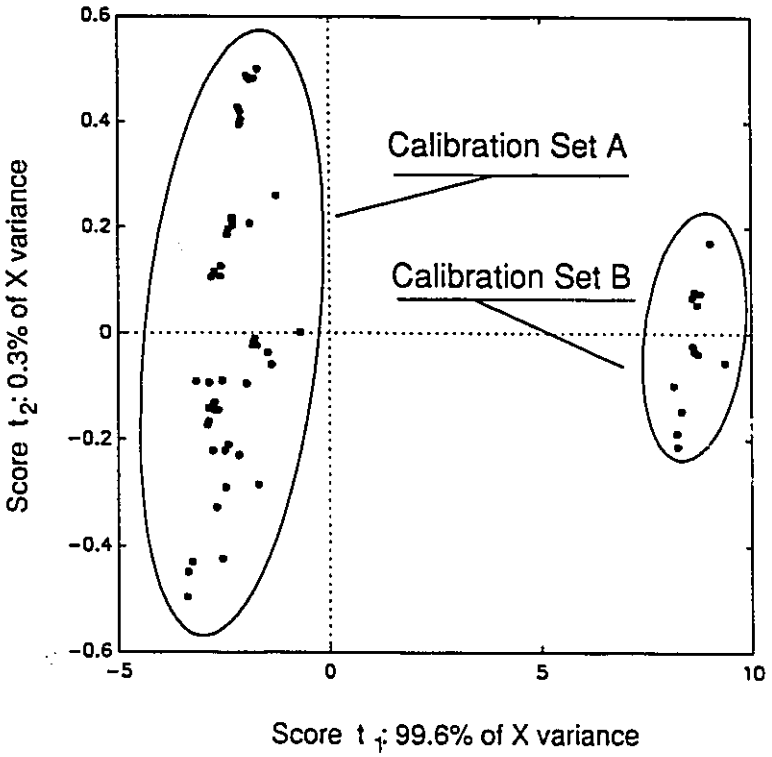

Fig. 9.2.1: PCA Scores of all NIR Transflectance Spectra of Concentrated Latex

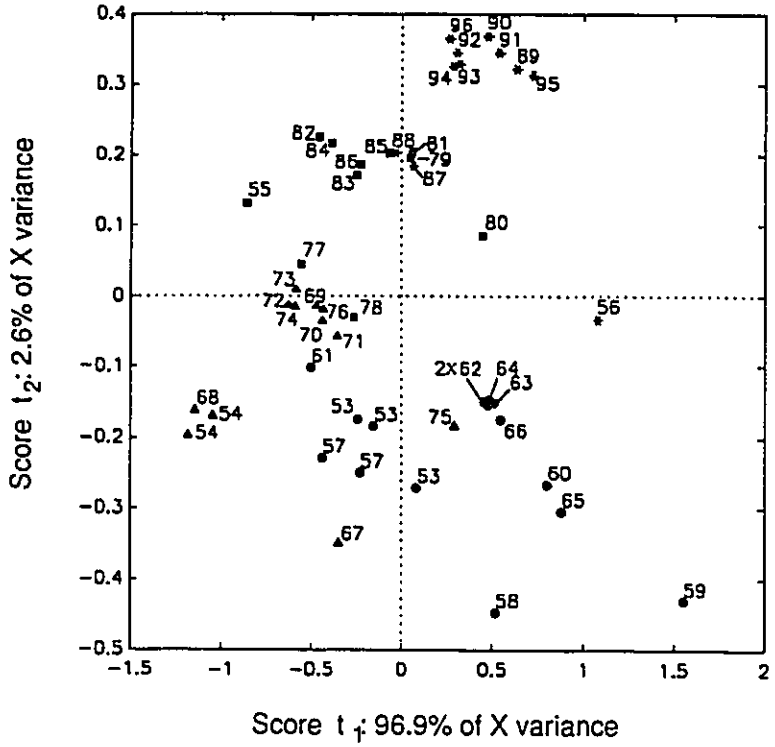

Fig. 9.2.2: PCA Scores of NIR Transflectance Spectra of Calibration Set A

PLS Calibration Models

Calibration models were calculated for each of the *Y* variables the same way as they were in Section 8.2.2 for UV spectra. To speed up the calibration calculations, the number of wavelengths included in the calibration was decreased by a factor of 5, from 1200 to 240. This was done by taking the absorbance at every fifth wavelength as the average of that absorbance and the two to either side. Not only did this speed up calculations and decrease data storage requirements, in some cases it even slightly improved the prediction error of the models, probably because of the noise filtering introduced by the averaging.

All the spectra represented in Fig. 9.2.2 were included in the calibration and the prediction error was calculated using a leave-one-out crossvalidation procedure. As before, each of the *Y* variables was scaled to unit variance to make comparison of the PRESS/(n-1) meaningful. The plots of the latex properties predicted by the PLS1 model vs. the actual values is in Fig. 9.2.3. The extraordinary feature of these calibration models is that all the weight fractions are predicted with a standard error (SEP) of less than 0.5 wt. %, and the mean diameter, with an SEP of 0.8 nm. The plots of total styrene and total MMA concentration predictions show predictions of compositions independent of the assumption that all batch reactions went to 100% conversion. The total monomer plot in Fig. 9.2.3 is also shown for the same reason: the monomer fraction in the batch reactions can be calculated from the monomer conversion measured by gravimetry (Table 7.5.6).

The way in which PLS selectively weights wavelengths relevant to predicting the property in question is demonstrated in the series of Figures 9.2.4 to 9.2.6. Fig. 9.2.4 shows the loading (*w*) vectors for the first three dimensions of the PLS model for total styrene concentration, ranked by their contribution to the *y* prediction (see Section 8.2.2). The eighth loading vector is also shown to illustrate that there is still some relevant spectral information in

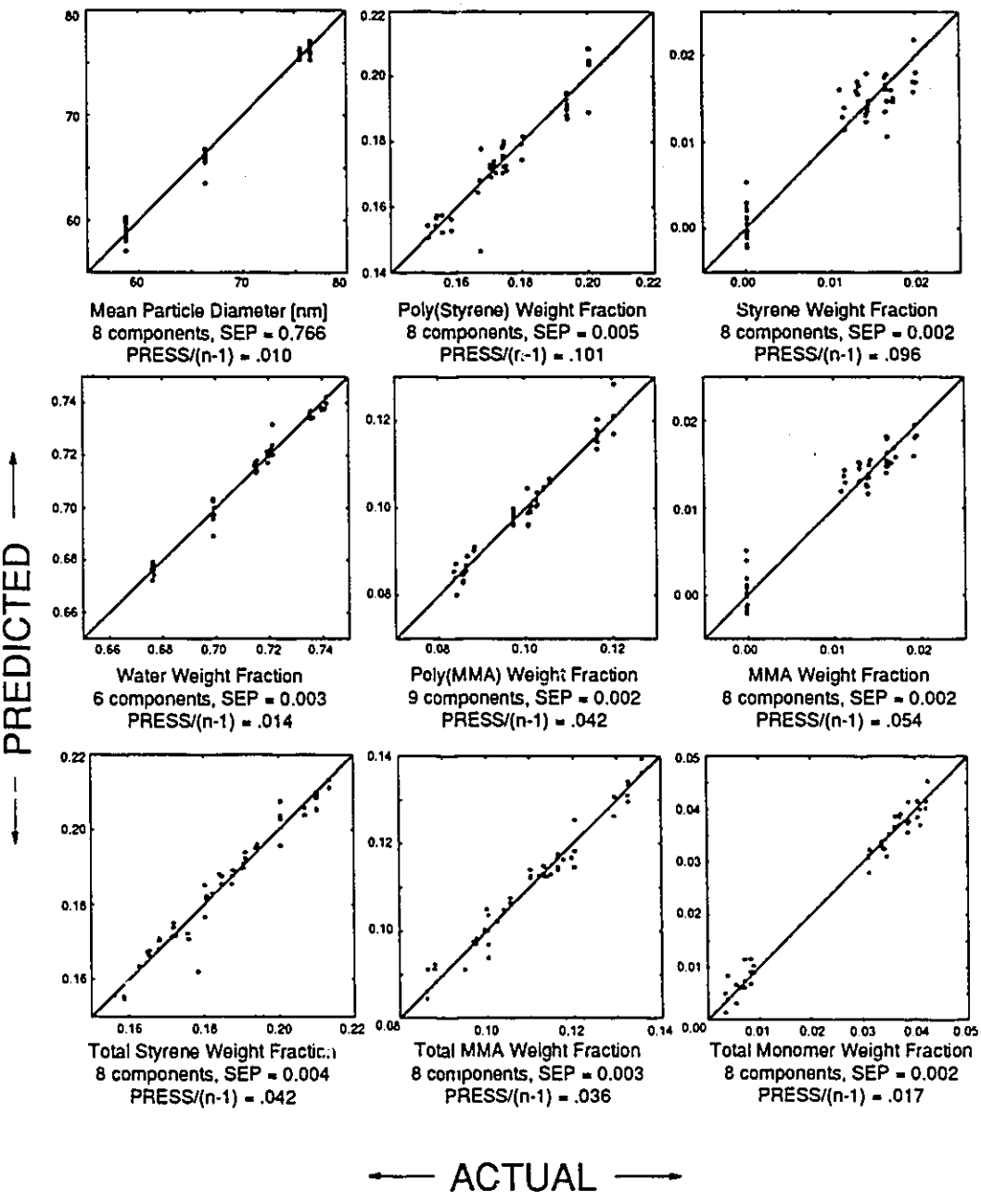

Fig. 9.2.3: Latex Properties vs. PLS Predictions from NIR Spectra, Calibration Set A

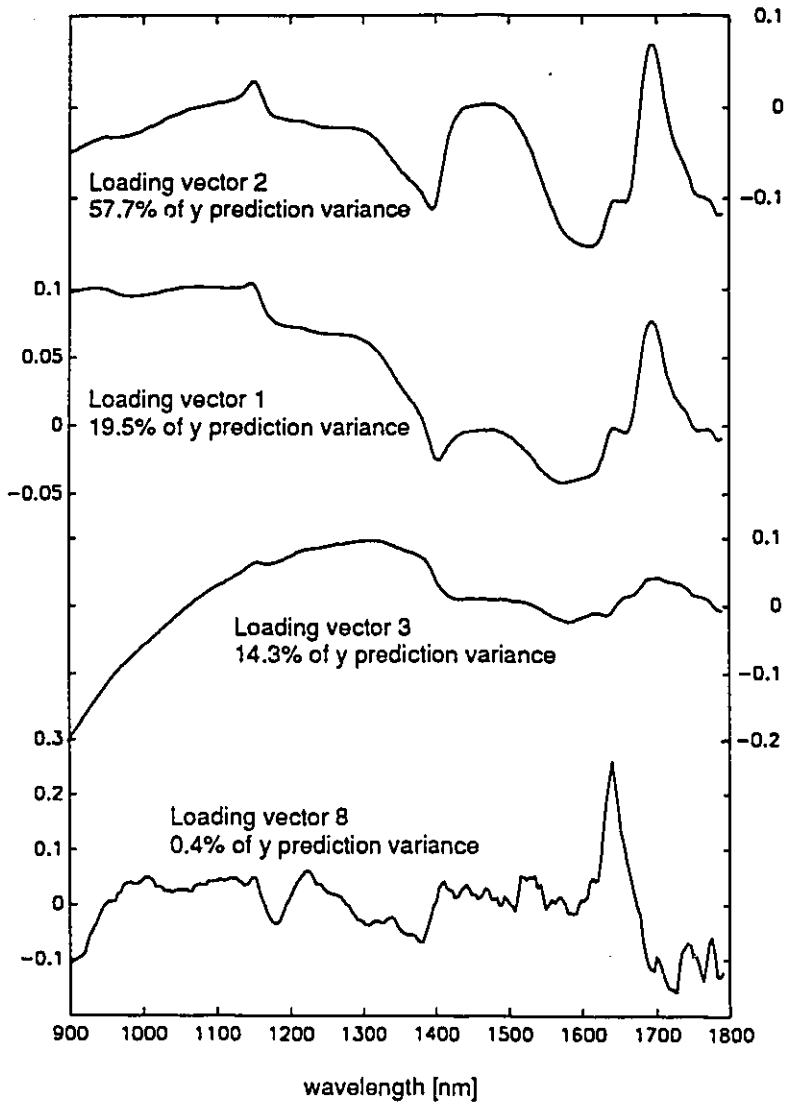

Fig. 9.2.4: PLS Loading Vectors for Styrene, Calibration Set A

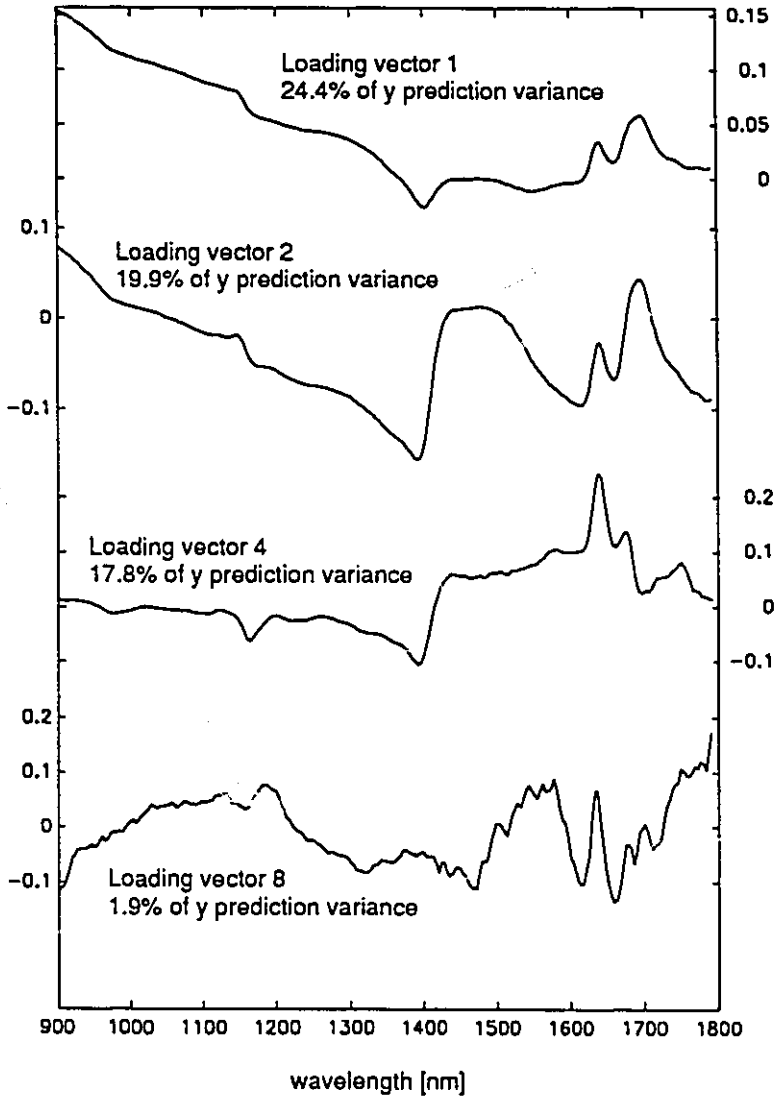

Fig. 9.2.5: PLS Loading Vectors for Monomer, Calibration Set A

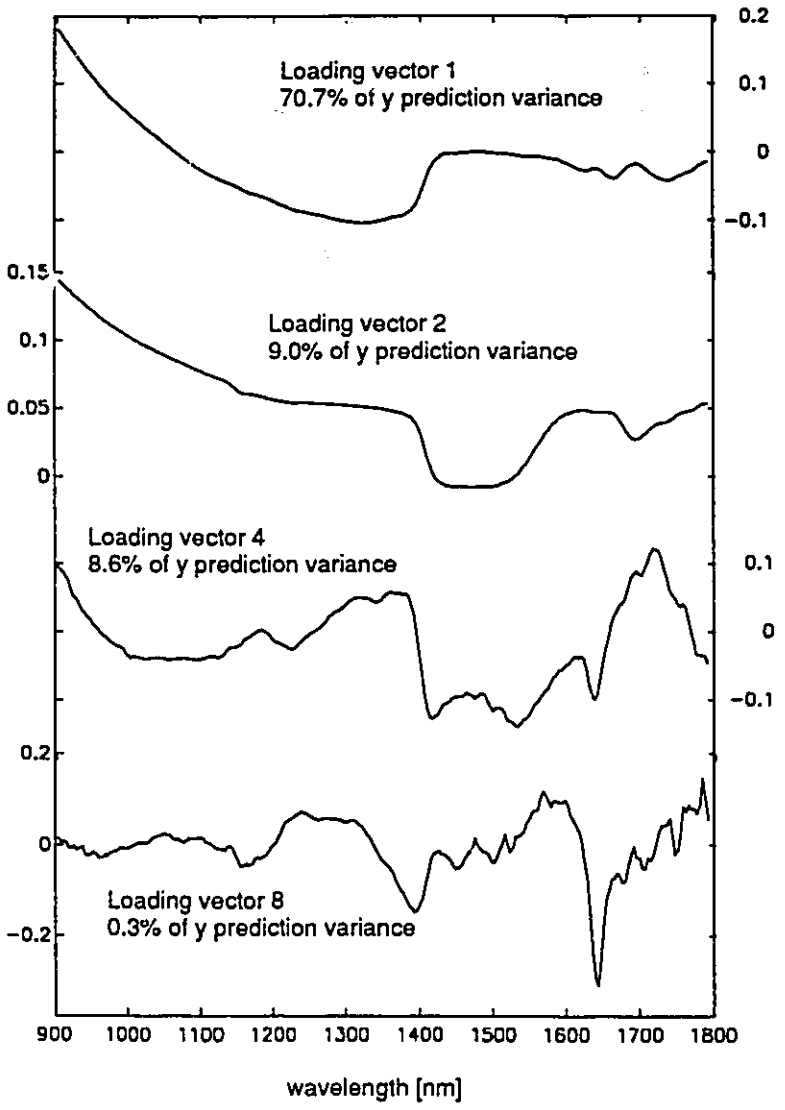

Fig. 9.2.6: PLS Loading Vectors for Mean Particle Diameter, Calibration Set A

the last PLS dimension. In the first two loading vectors, both the aromatic ring peaks at 1440 and 1680 nm are given significant weight. These two vectors account for 77.2% of the styrene concentration prediction. Contrast these to Fig. 9.2.5, which shows the loading vectors for the total monomer prediction equation. Here, the peak for the unsaturated $=CH_2$ at 1640 nm is prominent in the weightings, and the aromatics peak is suppressed. In this case, the first three vectors account for 62.1% of the monomer concentration prediction, and they all show significant weighting around 1640 nm. Finally, since particle scattering affects absorption at all wavelengths, Fig. 9.2.6 shows the loading vectors for the mean particle diameter prediction. Here, the first two vectors explain 79.7% of the prediction variance. Their primary characteristic is the suppression of most spectral features in favour of a smooth weighting of all spectral features, especially below 1400 nm.

9.2.3 Calibration Models for Calibration Set B

Both the NIR transflectance spectra of the concentrated latex and of the latex diluted 1/100 were evaluated for prediction in PLS1 calibration models. The calibration procedure is the same as that for all the above models: gross outliers were detected by PCA of the spectra and removed from the calibration set. The prediction error was calculated by a leave-one-out procedure.

The results are listed in Table 9.2.1. Consider first the concentrated latex. The columns for the number of components and the PRESS/(n-1) show that the models are very poor. For most models, the minimum PRESS/(n-1) was achieved in the first PLS component. A minimum PRESS/(n-1) greater than 1 indicates that the models are no better than a random model for prediction. The fact that the minimum PRESS is found after only one PLS component indicates that no significant correlation structure between X and y exists. The three models for monomer (styrene, MMA, and total monomer) explain some correlation using

	Concentrated Latex			Latex Diluted 1/100		
Latex Property	# PLS components	PRESS (n-1) (n=12)	Prediction Error (SEP)	# PLS components	PRESS (n-1) (n=16)	Prediction Error (SEP)
Water	1	1.769	0.064	7	0.213	0.019
Poly(Styrene)	1	1.316	0.046	1	0.783	0.029
Poly(MMA)	1	1.542	0.034	1	1.126	0.034
Styrene Monomer	6	0.393	0.019	1	0.486	0.034
MMA Monomer	6	0.431	0.015	1	1.488	0.027
Mean Particle Diameter	1	0.873	13.9	1	0.930	18.6
Total Styrene	1	1.390	0.036	5	0.181	0.012
Total MMA	1	1.012	0.025	3	0.699	0.019
Total Unsaturation	6	0.521	0.039	1	1.597	0.053

Table 9.2.1 : Prediction Error for PLS of NIR Spectra for Calibration Set B

six PLS dimensions, but these models are also inadequate for prediction. This result implies that, although there is some correlation between the spectra and the latex properties, the signal-to-noise ratio of the transflectance spectra with a 3 mm gap is inadequate.

Refering again to Table 9.2.1, two models give very good predictions for the latex that has been diluted 1/100: those for water and total styrene. Apparently, while dilution allows more light to be transmitted through the latex, the resulting drop in concentration of the absorbing species is so large that only those species with high molar absorptivities yielded a sufficiently high signal to give good prediction models.

9.3 NIR Spectroscopy of a Poly(Styrene-Butadiene) Latex

The results so far have shown that NIR spectroscopy is successful in the case where the latex is translucent for a path length of 6 mm (3 mm transflectance probe gap). In that case, the composition of all the major constituents in the latex could be measured, as could the particle size distribution. For a latex that is opaque (or nearly so) over the 6 mm path length, not enough reflected light is gathered by the transflectance probe used in this work to measure latex compositions. As most commercial latexes are opaque, it is important to show that the failure of the technique is due to elements of the spectrometer configuration that are under the control of the designer, and not a fundamental flaw in the concepts of multivariate calibration of NIR spectra.

The work so far has shown that the transflectance probe gives sufficient signal-to-noise ratio if light reflected off the mirror reaches the detector. The most obvious way of accomplishing this with the more opaque latexes is to decrease the gap width of the probe. In this section, a 1 mm gap width is evaluated with some commercial poly(styrene-butadiene) (SBR) latex. The 1 mm gap was not used with the poly(styrene-MMA) latex because that latex had coagulated by the time the 1 mm gap was available.

Table 9.3.1 gives the properties of the latex samples used for this SBR Calibration Set. The latex has been steam stripped, so no monomer is present. Furthermore, the compositions of minor constituents has been ignored, so the mass fractions of styrene, butadiene, and acrylic acid polymers plus water sum to unity. The mean particle diameters are similar to those of calibration set B for the poly(styrene-MMA) latex (see Table 7.5.10).

Some features of this sample set should be noted. The acrylic acid is present in only very small amounts, and there is not sufficient variation in the its concentration to allow any inferences to be made about the ability of NIR to detect changes in it. The standard deviation of the acrylic acid concentration is on the order of the best prediction errors for composition in Fig. 9.2.3. The polymer weight fraction, while comparable to that of Calibration Set B, has a much smaller range of solids fraction variation (36 to 51% solids for Set B compared to 51% to 55% for the SBR latex). As a result, styrene and butadiene weight fractions are almost perfectly correlated (correlation coefficient = -0.99), so this data set cannot be used to investigate the ability of NIR to determine their compositions independently. Finally, the data set is small (10 samples), and therefore not ideally suited for modelling very complex, nonlinear phenomena.

Some representative spectra of the SBR latex are shown in Fig. 9.3.1. Compare these spectra to those in Fig. 9.1.4. These spectra are more like the transflectance spectra of Calibration Set A. The pronounced absorption peaks for styrene and butadiene around 1700 nm indicate that light reflected off the mirror is reaching the detector.

Table 9.3.2 shows the results of PLS1 calibrations performed in the same way as all the previous ones. First, the styrene composition in the polymer latex is very well modelled. This reinforces the conclusions of the previous section that multivariate calibration of NIR spectra can be used to measure composition in latex if the signal-to-noise ratio is sufficiently high. The standard error of prediction (SEP) is about 4 times that of the calibrations for Set A, but that can be attributed to a large part to the small sample size.

Sample Number	Weight Fraction				Mean Diameter [nm]
	Styrene	Butadiene	Acrylic Acid	Water	
1017	0.290	0.237	0.018	0.455	231.0
1163	0.128	0.369	0.016	0.487	171.9
1376	0.402	0.108	0.012	0.478	147.7
1377	0.372	0.160	0.018	0.450	151.4
1380	0.328	0.198	0.012	0.462	173.7
1382	0.229	0.306	0.012	0.453	156.0
1406	0.268	0.260	0.008	0.464	209.3
1006	0.220	0.295	0.012	0.473	184.8

Table 9.3.1 : Properties of Styrene-Butadiene Latex

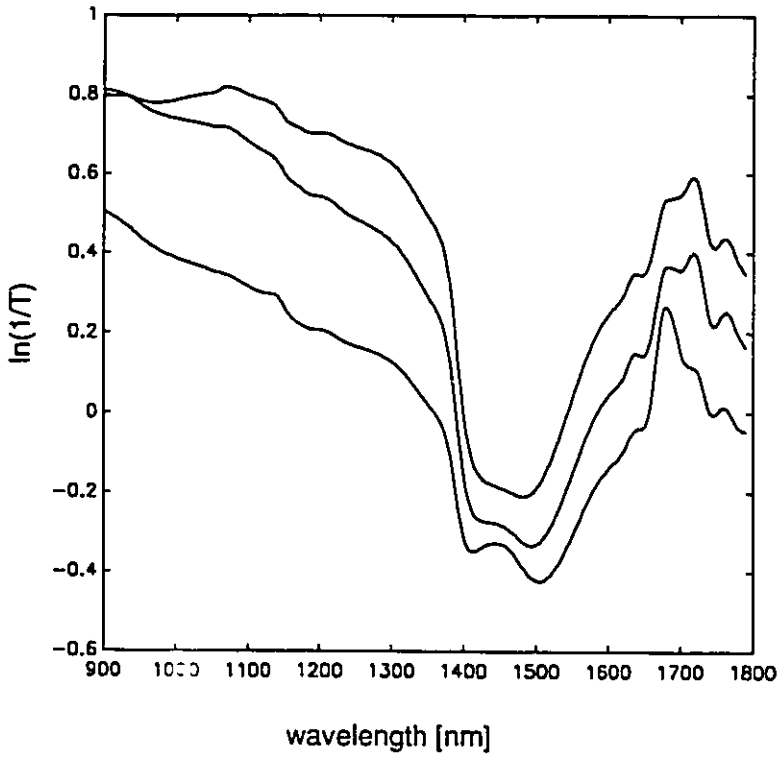

Fig. 9.3.1: NIR Spectra for Poly(Styrene-Butadiene) Latex with 1 mm Transflectance Probe Gap

Latex Property	# PLS components	PRESS (n-1) (n=10)	Prediction Error (SEP)
Poly(Styrene)	5	0.021	0.012
Water	1	1.572	0.015
Mean Particle Diameter	2	1.109	28.3

Table 9.3.2 : Prediction Error for PLS of NIR Spectra for SBR Latex

The water concentration is very poorly predicted. The standard deviation of the water concentration in this calibration set is the same as the SEP of the styrene concentration prediction. A calibration set with more variation in the water concentration is, therefore, needed to evaluate the ability of NIR to predict water concentration with this probe configuration and signal-to-noise ratio.

The PRESS/(n-1) value greater than 1 shows that mean particle diameter is also very poorly predicted. This is consistent with the result using Calibration Set B, and suggests that there may be some fundamental reason that mean diameter cannot be modelled from the optical spectrum. This would be consistent with the mechanistic understanding of scattering phenomena (Chapter 2). For a general particle size distribution, the turbidity is a very complex function of the shape and location of the distribution, and only in the special case of low polymer refractive index at UV wavelengths is the turbidity easily related to a mean of the distribution. The very good results for predicting the mean of the distribution from Calibration Set A are most likely valid only for very small particles and very narrow particle size distributions with constant breadth.

9.4 Summary

This Chapter reported on results of multivariate calibration of NIR latex. Spectra were taken with a transflectance fiber optic probe with a 3 mm gap in the range 900 to 1800 nm. Two calibration sets were analyzed. Set A had small particles, around 30% solids, and was translucent. Set B had larger particle with a broader distribution, was around 50% solids, and was opaque to the NIR spectrometer.

PLS calibration models of the NIR spectra of Set A yielded excellent predictions of mean particle diameter, and of the concentrations of all the major components (water, poly(styrene), poly(MMA), styrene, MMA).

PLS calibration models of the NIR spectra of Set B were generally very poor. None of the predictions from spectra of concentrated latex were any good. The latex was diluted by a factor of 100 to make it more transparent light and the spectra were taken again. The result was that calibration models for water and total styrene are good, but none of the other models gave better prediction.

A third, small calibration set made up of commercial poly(styrene-butadiene) latex was evaluated using the NIR spectrometer with the transflectance fiber optic probe with a 1 mm gap. This latex was similar to Calibration Set B above. Light could be transmitted through the 1 mm gap, increasing the amount of light received at the detector. The PLS calibration models gave good results for poly(styrene) prediction, but poor results for particle diameter. These results imply that NIR spectrometer can be used for measuring concentration of bulk constituents in latex provided that the signal-to-noise ratio is adequate. For industrial applications, the solutions that should be pursued include increasing the light transmitted to the sample and the reflected light collected from the sample by using more fibres in the fibre bundle between the spectrometer and the probe. Detector configurations that maximize the reflected light collected from the sample (Birth and Hecht, 1987) should also be investigated.

10

COMBINING MULTIVARIATE SENSOR DATA

The previous two chapters have considered multivariate calibration of UV/Vis and NIR spectra separately. There is no reason why these spectra could not be combined in a single, large spectral data matrix and PLS performed so that all the available information is used in the calibrations. Other sensors that are more sensitive to some properties than optical spectra could also be included in the sensor matrix, as could any other on-line process measurements. The more data included in the calibration, the more complete a picture can be constructed of the operation of the process and the type of product being produced.

This chapter deals with the methodology of combining information from several sensors either to obtain better predictions of product properties, or to draw inferences about which sensor is the best in a given situation. The sensors considered are the UV and NIR spectrometers of Chapters 8 and 9, respectively, the density meter described in Chapter 3, and ultrasound attenuation (Wasmund, 1991).

10.1 PLS for Combining Sensor Data

The most obvious method of combining multiple analyzers is to simply apply the PLS1 algorithm (Chapter 6) with all the sensor data lumped into one data matrix. One problem that can be anticipated is that the different analyzers will have a widely disparate number of variables (columns in the data matrix): from 316 for the UV to only 1 for density. Recalling that PLS1 weights each variable by its covariance with the product property, y, an analyzer with 300 variables will get a much higher overall weighting than one with only one variable. This is not

desirable if the informaton from each is thought to be of roughly equal value. The effect of differing numbers of variables in each data block can be compensated for by scaling the variables so that the total sum of squares in each block is identical. If the data associated analyzer i is in X_i, and if the columns in X_i have been mean centered, then the sum of squared deviations of each variable from its respective column mean is calculated by

$$ssq(X_i) = \sum_i \sum_j x_{ij}^2 \tag{10.1.1}$$

To make all blocks have the same sum of squares, all the variables in each block can be scaled by:

$$x_{ij}^{scaled} = x_{ij} \left\{ \frac{\text{ssq(total)}}{b^2\, \text{ssq}(X_i)} \right\}^{\frac{1}{2}} \tag{10.1.2}$$

where $$\text{ssq(total)} = \sum_i \text{ssq}(X_i)$$

and b is the number of blocks of data.

Aside from scaling, another problem is how to deal with repeat measurements on the same sample. Samples may be measured several times on one analyzer, but only once on another. For the purposes of this chapter, repeated measurements on a single sample were simply averaged and this average considered a single measurement. This is obviously not the optimal approach: generally, repeat measurements have important information about the variance of the measurements. The repeats could be included in separate data rows, with the other sensors' contributions treated as missing data. PLS can then proceed with the calculation techniques that deal with missing data (Chapter 6). Alternatively, the variables could be weighted by their standard deviations, noting that the variance of an average decreases with the square root of the number of samples incorporated into it. Nonetheless, the procedure used here is simple enough to be useful while not detracting from the main emphasis of this chapter, which is to discuss the methodology of sensor calibration of multiple blocks of sensors.

10.2 Multiblock PLS

Herman Wold's (1982) early conception of PLS was as a technique to model very complex correlation structures between many blocks of dependent and independent data. This concept might have an application in combining data from several multivariate sensors (like NIR, UV, and density) to predict one set of latex properties. Wold and coworkers (1987) published an algorithm to calculate the PLS models for the case of multiple X (dependent) blocks used to predict multiple Y (independent) blocks. Wangen and Kowalski (1988) modified the X matrix deflation (residual calculation) of that algorithm to make it more in keeping with the standard PLS model of the X matrix. They have also included the more general path models of Wold (1982) in their formulation.

The following algorithm is a special case of the algorithm of Wangen and Kowalski (1988). It treats the case where multiple X blocks are used to predict one y variable. This will facilitate comparison with the PLS1 algorithm used in Chapters 8 and 9. The extension to multiple variables in the Y block is an obvious analog to the PLS algorithm of Chapter 6. The notation used below is different from that of Wangen and Kowalski (1988), but is consistent with that of the preceeding chapters. The basic premise of this MBPLS1 (for MultiBlock PLS1) model is similar to that of PLS1: there are b data matrices $X_{i,(n \times m_i)}; i = 1..b$. Each matrix is a function of a_i orthogonal latent vectors $t_{ij}; j = 1..a_i$

$$X_i = t_{i1}p'_{i1} + \cdots t_{ia_i}p'_{ia_i} \tag{10.2.1}$$

The y variable is predicted as a linear combination of the same latent factors:

$$y = \sum_i \sum_j b_{ij}t_{ij} + f_a \tag{10.2.2}$$

The algorithm for estimating the latent vectors is given below.

1) Mean center X and y
2) For $a = 1..A, E_0 = X, f_0 = y$
   2.1) For $i = 1..b$

2.1.1)	$w'_{ia} = f_{a-1}'E_{a-1}$	(10.2.3)
2.1.2)	$w_{ia} = w_{ia}/\|w_{ia}\|$	(10.2.4)
2.1.3)	$t_{ia} = E_{a-1}w_{ia}$	(10.2.5)

2.2) $$T = \{t_{1a}, \cdots, t_{ba}\} \quad (10.2.6)$$

2.3) $$w'_{Ta} = y'T \quad (10.2.7)$$

2.4) $$w_{Ta} = w_{Ta} / \| w_{Ta} \| \quad (10.2.8)$$

2.5) $$t_{Ta} = T w_{Ta} \quad (10.2.9)$$

2.6) $$q_a = t'_{Ta} y / (t'_{Ta} t_{Ta}) \quad (10.2.10)$$

2.7) For $i = 1..b$

2.7.1) $$p_{ia} = E'_{a-1} t_{ia} / (t'_{ia} t_{ia}) \quad (10.2.11)$$

2.7.2) $$E_a = E_{a-1} - t_{ia} p'_{ia} \quad (10.2.12)$$

2.8) $$f_a = f_{a-1} - q_a t_{Ta} \quad (10.2.13)$$

When data on unknown samples becomes available, the y-variable can be estimated from the MBPLS1 model:

1) Subtract the mean values of the relevant X_i blocks of the calibration step (from Step (1) above).

2) For $i = 1..b$

2.1) For $a = 1..A$, $e_0 = x$

2.1.1) $$t_{ia} = e'_{ia} w_{ia} \quad (10.2.14)$$

2.1.2) $$e_a = e_{a-1} - t_{ia} p'_{ia} \quad (10.2.15)$$

3) Estimate the sample property $$y = \sum_{a=1}^{A} q_a w'_{Ta} \{t_{1a} \cdots t_{ba}\}' \quad (10.2.16)$$

Note that at each dimension a the regression coefficient of the ith block on y (eq. 10.2.2) can be calculated from

$$b_{ai} = q_a w_{Ta}(i) \quad (10.2.17)$$

where $w_{Ta}(i)$ is the element of the w_{Ta} vector associated with block i.

10.3 Methods for Comparing PLS Models

Before considering how the different sensors will be combined, the method for evaluating which is the best of several alternative models will be considered. In light of what has been discussed in previous chapters, the most obvious solution would be to calculate the PRESS/(n-1) for all the competing models by crossvalidation, and then chose as best the one with the lowest minimum PRESS/(n-1). Unfortunately, several problems lie in the way of a straightforward application of this idea.

The first problem is the definition of the "best" model. First, differences in the value of PRESS should be evaluated for statistical significance: there is no reason to prefer a model with a lower PRESS if the difference is not outside the bounds that can be explained by random error. Given a base case model with some minimum PRESS, a simple F-test would be enough to determine the bound below which another model's PRESS would be deemed significant. There is, however, another aspect to chosing the "best" model that is more complex, and that is the issue of whether a competing model achieves a lower PRESS in more or fewer PLS dimensions than the base case model. A more parsimonious (lower dimensional) model may be preferred, even if it has a higher PRESS than a high dimensional model. Having fewer dimensions in a model means that the relationship between X and y is more nearly linear. In light of this complication, a model will be called "better" than some base case model if it achieves the same or a significantly lower PRESS than the base case in fewer or the same number of PLS dimensions.

The second problem with evaluating competing models based on their PRESS is the fact that the procedure is very computationally intensive; a more efficient way of coming to the same conclusion as this procedure would be preferable. When two models are being compared, a method based on crossvalidation PRESS is really the only statistically sound method for determining if one is better than the other. When several competing models are being tested, however, it would be useful to have a method for quickly screening them to determine which is the best among them.

One common way of comparing models is to compare the *y* residual variance as a function of the PLS dimension. Successive PLS dimensions could be calculated for all the models and their *y* residual variances compared. A model will be deemed better than all the others in a group, and potentially better than the base case model, if its *y* residual variance is the first to drop below the crossvalidated PRESS of the base case model, provided it does so in fewer or the same number of dimensions than was used in the base case. The crossvalidation PRESS need only be calculated for that one alternative model that is the best among all the alternatives.

Two examples will be used to illustrate this method. In NIR spectroscopy, various transformations of the original transmittance or reflectance spectra are often tried to get the best sensitivity and linearity in a model. A Multiplicative Scatter Correction (MSC) is sometimes used to reduce the effects of different amounts of scattering due to particle size variation (Geladi, MacDougall and Martens, 1985; Isaksson and Næs, 1988; Miller, 1989). In reflectance measurements, Kubelka-Munk linearization is often preferred to the ln(1/R) transformation (Birth and Hecht, 1987). Taking derivatives of spectra is also frequently used to resolve overlapping spectral features or to accentuate small absorption peaks. Four different transformation of the NIR spectra will be compared below in an attempt to improve the models for total styrene composition and for mean diameter. Only the data from Calibration Set A will be considered.

The first two transformations will be the first and second derivatives of the ln(1/T) NIR spectra. The derivatives of the spectra with respect to wavelength are calculated using a boxcar algorithm. The derivative at a given wavelength is calculated by taking the average absorbance of the absorbances at the next 10 wavelengths, and subtracting them from those at the previous 10 wavelenghts. The third transformation applies the Multiplicative Scatter Correction (MSC) to the raw transmittance spectra before the $\ln(1/T_{msc})$ linearization. The final transformation is the first derivative of the third transformation.

Recall that for all the models calculated previously, the *y* vector was scaled to have unit variance to facilitate comparisons between the many models. This practise is continued in this chapter. In Chapter 9, the PRESS/(n-1) for the prediction of the total styrene concentration was 0.042 after 8 PLS1 dimensions (Fig. 9.2.3). Table 10.3.1 shows the *y* residual variance as a function of the PLS1 dimension for the four competing models. The variance of both the first and second derivative of the ln(1/T) spectra drops below 0.042 at the fourth PLS1 dimension. The residual variance of the second derivative model is the lowest at this stage, so it will be chosen as the "best" candidate for comparison to the original.

Table 10.3.2 shows the PLS1 PRESS/(n-1) calculated by leave-one-out crossvalidation for each of the NIR transformation models. The F ratio necessary for a significantly lower standard PRESS/(n-1) at a 95% confidence is

$$\frac{\sigma^2_{best}}{\sigma^2_{new}} \propto F_{0.05}(48,48) = 2.00$$

meaning the new PRESS/(n-1) must be less than 0.021 to be statistically significant. The minimum PRESS/(n-1) for the second derivative is 0.023 at 8 dimensions. Though lower, the difference is not statistically significant, and the number of dimensions is the same as the original model. Note, however, that the second derivative model does give virtually the same prediction error as the original model in as few as 4 PLS1 dimensions. It would be reasonable, therefore, to replace the 8 dimensional model based on the ln(1/T) transform of the NIR spectra with the 4 dimensional model based on the second derivative. Also note from Table 10.3.2 that the *y* residual variance comparison did pick the model which ultimately results in the lowest prediction error.

The second example to illustrate this technique will be the prediction of the mean diameter of the latex particles from Calibration Set A. The same transformations of the same spectra as the previous example will be used. Recall that, in Chapter 9, the PRESS/(n-1) for the prediction of the total styrene concentration was 0.010 after 8 PLS dimensions (Fig. 9.2.3). Table 10.3.3 shows the *y* residual variance as a function of the PLS1 dimension for the four competing models.

	PLS1 Dimension							
	1	2	3	4	5	6	7	8
$\frac{d}{d\lambda}\{\ln(1/T)\}$	0.189	0.102	0.050	0.035	0.016	0.012	0.006	0.004
$\frac{d^2}{d\lambda^2}\{\ln(1/T)\}$	0.281	0.067	0.050	0.024	0.014	0.006	0.004	0.003
$\ln(1/T_{msc}$	0.773	0.609	0.253	0.168	0.089	0.047	0.021	0.140
$\frac{d}{d\lambda}\{\ln(1/T_{msc})\}$	0.555	0.305	0.232	0.125	0.036	0.018	0.014	0.008

Table 10.3.1: Total Styrene Residual Variance vs. PLS1 dimension for Various Tranformations of the NIR Spectra

	PLS1 Dimension							
	1	2	3	4	5	6	7	8
$\ln(1/T)$	0.879	0.307	0.122	0.066	0.064	0.058	0.047	0.043
$\frac{d}{d\lambda}\{\ln(1/T)\}$	0.216	0.122	0.065	0.047	0.029	0.032	0.038	0.035
$\frac{d^2}{d\lambda^2}\{\ln(1/T)\}$	0.313	0.080	0.061	0.046	0.034	0.027	0.024	0.023
$\ln(1/T_{msc}$	0.844	0.687	0.310	0.219	0.139	0.080	0.039	0.038
$\frac{d}{d\lambda}\{\ln(1/T_{msc})\}$	0.690	0.383	0.308	0.173	0.078	0.039	0.044	0.039

Table 10.3.2: Total Styrene PRESS/(n-1) vs. PLS1 dimension for Various Tranformations of the NIR Spectra

	PLS1 Dimension							
	1	2	3	4	5	6	7	8
$\frac{d}{d\lambda}\{\ln(1/T)\}$	0.426	0.187	0.164	0.042	0.017	0.010	0.005	0.003
$\frac{d^2}{d\lambda^2}\{\ln(1/T)\}$	0.801	0.624	0.329	0.242	0.118	0.061	0.044	0.030
$\ln(1/T_{msc})$	0.436	0.311	0.149	0.088	0.059	0.013	0.010	0.007
$\frac{d}{d\lambda}\{\ln(1/T_{msc})\}$	0.480	0.324	0.212	0.067	0.042	0.021	0.011	0.006

Table 10.3.3: Mean Diameter Residual Variance vs. PLS1 dimension for Various Tranformations of the NIR Spectra

	PLS1 Dimension							
	1	2	3	4	5	6	7	8
$\ln(1/T)$	0.365	0.239	0.199	0.190	0.129	0.069	0.043	0.010
$\frac{d}{d\lambda}\{\ln(1/T)\}$	0.507	0.250	0.231	0.068	0.029	0.020	0.015	0.013
$\frac{d^2}{d\lambda^2}\{\ln(1/T)\}$	0.887	0.793	0.550	0.495	0.257	0.222	0.212	0.234
$\ln(1/T_{msc})$	0.485	0.353	0.223	0.138	0.087	0.039	0.029	0.025
$\frac{d}{d\lambda}\{\ln(1/T_{msc})\}$	0.564	0.381	0.303	0.131	0.080	0.054	0.047	0.041

Table 10.3.4: Mean Diameter PRESS/(n-1) vs. PLS1 dimension for Various Tranformations of the NIR Spectra

Here the first derivative of ln(1/T) goes to 0.010 first, at the 6th PLS1 dimension. Table 10.3.4 shows that this model does not attain a lower PRESS in 8 dimensions that the base case ln(1/T) model. The first derivative does, however, give a prediction error that is not significantly different from the base case in 6, instead of 8, dimensions, and is, therefore, still a good candidate for the "best" model. Also note that comparing the *y* residual variances of the four alternate models did yield the model with the lowest crossvalidation prediction error of those models.

A second technique for comparing competing PLS1 models could be developed based on the MBPLS1 algorithm of the previous section. Recall that for a group of *b* data matrices are decomposed using the orthogonal expansion

$$X_i = t_{i1}p'_{i1} + \cdots t_{ia_i}p'_{ia_i} \tag{10.2.1}$$

and the *y* variable is predicted using the relation:

$$y = \sum_i \sum_j b_{ij}t_{ij} + f_a \tag{10.2.2}$$

Using this model, the contribution of each block *i* to the variation in the *y* prediction could be estimated by

$$\begin{matrix}\text{contribution} \\ \text{of block } i \\ \text{to } \hat{y}\end{matrix} = \sum_j b_{ij}^2 \text{var}(t_{ij}) \tag{10.3.1}$$

These contributions could be compared, and the block with the highest sum after some specified number of dimensions would be chosen as the "best" from among the competing models. This method is attractive because it does not require some *a priori* prediction error estimate from a base case model: all the competing models are included in the MBPLS1 calibration, and the best is chosen from that calibration model. A further advantage is that the *y* residual variance need not be calculated at all, saving some computation time. One disadvantage of this technique is that there is no straightforward stopping criterion for the number of dimensions, especially if the *y* residual variance is not being calculated. Note, however, that the sum in eq. 10.3.1 could be expected to asymptotically approach some constant value as the X_i matrix residuals steadily decrease and var(t_{ij}) approaches 0. The stopping criterion could therefore be based on the change of that sum from dimension to dimension being less than some tolerance value. Another stopping criterion that

better addresses the application at hand is to chose as "best" that model that maintains the highest prediction contribution sum for at least 2 or 3 successive MBPLS1 dimensions. That model would probably ultimately be the best because the contributions of subsequent dimensions are always being deflated by the var(t_{ij}) term of the sum.

An important point about this method for model comparison is that it is only valid if the total variance of each X_i block is the same. Thus, all blocks must be scaled to have equal total variance using the scaling of eq. 10.1.1 before the MBPLS1 calculations proceed.

This technique will be demonstrated on the same two examples as above, namely the prediction of total styrene and of mean diameter from a collection of different transformations of NIR spectra. All transformations, including the base case, are used in the calibration. Table 10.3.5 shows the cumulative sum of the contribution of each block to the prediction of the total styrene concentration. Recall that the previous work demonstrated that the second derivative of the ln(1/T) spectra gave the best prediction. MBPLS1 already signals the correct result in the first model dimension. There is no change in the rank of the correct solution in subsequent dimensions, and after 5 dimensions there is little change in the magnitudes of the sums.

Table 10.3.6 shows the cumulative sum of the contribution of each block to the prediction of the diameter. Recall that the previous work demonstrated that the first derivative of the ln(1/T) spectra gave the best prediction. In this case, the MBPLS1 algorithm does not signal the correct result, but instead picks the MSC corrected absorbance spectrum ($\ln(1/T_{msc})$ as "best", and ranks the first derivative spectrum second. This is a puzzling result, since from the results in Table 10.3.3 it is clear that $d/d\lambda\{\ln(1/T)\}$ has a lower y residual from the first PLS1 dimension on. Since the MBPLS1 solution is equivalent to the PLS1 solution for the first dimension, MBPLS1 could be expected to weight the $d/d\lambda\{\ln(1/T)\}$ transformation as the highest in the first dimension. The only reasonable answer to the incorrect weighting is that the variance scaling of the blocks is not the optimal one for comparing these models, as scaling effects would enter in the var(t) term.

	PLS1 Dimension							
	1	2	3	4	5	6	7	8
$\ln(1/T)$	0.076	0.076	0.076	0.076	0.076	0.076	0.076	0.076
$\frac{d}{d\lambda}\{\ln(1/T)\}$	0.075	0.078	0.080	0.083	0.084	0.084	0.084	0.084
$\frac{d^2}{d\lambda^2}\{\ln(1/T)\}$	0.162	0.163	0.178	0.179	0.180	0.182	0.183	0.184
$\ln(1/T_{msc})$	0.057	0.058	0.059	0.059	0.059	0.059	0.059	0.059
$\frac{d}{d\lambda}\{\ln(1/T_{msc})\}$	0.007	0.017	0.018	0.018	0.019	0.020	0.020	0.020

Table 10.3.5: Cumulative Contribution of Various Tranformations of NIR Spectra to the Prediction of Total Styrene by MBPLS1

	PLS1 Dimension							
	1	2	3	4	5	6	7	8
$\ln(1/T)$	0.006	0.044	0.044	0.045	0.045	0.045	0.045	0.045
$\frac{d}{d\lambda}\{\ln(1/T)\}$	0.028	0.032	0.048	0.062	0.064	0.067	0.068	0.068
$\frac{d^2}{d\lambda^2}\{\ln(1/T)\}$	0.017	0.018	0.038	0.046	0.053	0.055	0.058	0.058
$\ln(1/T_{msc})$	0.112	0.116	0.117	0.118	0.118	0.118	0.118	0.118
$\frac{d}{d\lambda}\{\ln(1/T_{msc})\}$	0.012	0.033	0.040	0.044	0.045	0.046	0.046	0.046

Table 10.3.6: Cumulative Contribution of Various Tranformations of the NIR Spectra to the Prediction of Diameter by MBPLS1

Since the computational advantages of the MBPLS1 algorithm are not necessarily superiour to PLS1 (especially if PLS1 is programmed using the algorithm of Manne, 1987), and since the interpretation is MBPLS1 is ambiguous at this stage, the y residual variance will be used to compare treatments when studying the effects of combining multivariate sensors below.

10.4 Combining Multivariate Sensors

In Chapters 8 and 9, absorbances at many wavelengths in the UV and NIR regions of the optical spectrum were used to predict compositions and particle diameter in a latex. By simple extension of the ideas in that section, it would be interesting to study the effect of combining both the UV and NIR spectra to see if it improves the predictive power of the PLS models. In Chapters 2 to 5, density measurements were used to decouple concentration from particle diameter effects in the UV turbidity of a latex. It would be interesting to try and use the density in conjunction with NIR and UV spectra to help improve the prediction of particle size and composition effects. This section addresses both these ideas.

When combining spectra, both PLS1 and MBPLS1 models will be considered as methods of combining the data. The y residual variance will be used to compare the various algorithms. The same two example models will be considered in this section as in the previous one: total styrene and mean diameter. X block scaling, when mentioned, is that of eq. 10.1.2.

Table 10.4.1 shows the y residual variance for various methods of combining UV and NIR spectra to predict the total styrene concentration. For each calibration method, the spectra were used both as is, and scaled to give equal block variance.

Table 10.4.1 shows that if the spectra are used separately to predict the concentration, the NIR spectrum gives lower y residual variance than UV for all but the second PLS1 dimension. For

	PLS1 Dimension							
	1	2	3	4	5	6	7	8
NIR Spectra	0.798	0.328	0.091	0.047	0.044	0.025	0.017	0.012
UV+NIR by PLS1 no *X* scaling	0.763	0.607	0.126	0.094	0.073	0.038	0.019	0.017
UV+NIR by PLS1 *X* scaling	0.677	0.498	0.134	0.084	0.058	0.030	0.026	0.020
UV+NIR by MBPLS1 no *X* scaling	0.763	0.177	0.127	0.063	0.056	0.042	0.034	0.024
UV+NIR by MBPLS1 *X* scaling	0.677	0.176	0.109	0.052	0.041	0.027	0.018	0.015

Table 10.4.1 : Total Styrene Residual Variance from Combined UV and NIR Spectra

	PLS1 Dimension							
	1	2	3	4	5	6	7	8
NIR Spectra	0.400	0.216	0.170	0.060	0.034	0.012	0.003	0.002
UV Spectra	0.264	0.071	0.066	0.033	0.016	0.011	0.007	0.006
UV+NIR by PLS1 no *X* scaling	0.253	0.199	0.039	0.033	0.024	0.014	0.011	0.006
UV+NIR by PLS1 *X* scaling	0.220	0.192	0.049	0.033	0.025	0.013	0.010	0.004
UV+NIR by MBPLS1 no *X* scaling	0.253	0.170	0.062	0.052	0.035	0.028	0.027	0.025
UV+NIR by MBPLS1 *X* scaling	0.220	0.140	0.052	0.031	0.022	0.017	0.014	0.010

Table 10.4.2 : Mean Diameter Residual Variance from Combined UV and NIR Spectra

the combined spectra, the MBPLS1 calibration using scaled spectra gave the lowest *y* residual variance at all dimensions. Recall that, for NIR spectra, the crossvalidation PRESS/(n-1)=0.043 in 8 dimensions, and for UV spectra, it is 0.108 in 8 dimensions. Based on the *y* residual variance, the combined UV+NIR spectra do better than either of the spectra separately for the first 5 dimensions. In dimensions 6 to 8, however, where the crossvalidation calculations say the minimum PRESS will exist, the combined lie between the UV and NIR spectra, doing just a bit worse than the NIR spectra calibrations alone. Thus, it appears that the combined UV+NIR spectra will do no better than NIR can do alone.

Table 10.4.2 shows the *y* residual variance for combined UV and NIR spectra used to predict the mean particle diameter. In this case, the UV spectra give lower *y* residual variance than the NIR spectra if used separately in all but dimensions 7 and 8, where the differences are negligible. Recall that, for NIR spectra, the crossvalidation PRESS/(n-1)=0.010 in 8 dimensions, and for UV spectra, it is 0.032 in 5 dimensions. For the combined models, both PLS1 and MBPLS1 give comparable residual variances. As in the above example, the combined spectra do better in the first 4 dimensions, but do worse than the better of the two separate spectra (UV in this case) in the higher dimensions.

In interpreting these results, emphasis should be put on the fact that UV and NIR spectroscopy are not complementary analysis techniques, but instead both respond to the same, underlying physical phenomena of composition and particle size. It appears, therefore, that in a situation like this, the better of the two analyzers for a given situation should be used, since poorer information from analogous sensors does not improve the ability to model *y*.

A more interesting case study would be to add a sensor that is more specific to one of the properties that confound the optical spectra. Table 10.4.3 lists the density, measured by the Anton-Paar densitometer (Chapter 2), for each of the latex samples in Calibration Set A. Density changes with the solids fraction, the composition of the polymer, and the monomer conversion. It

Sample Number	Density [g/ml]
28	1.05465
32	1.04870
35	1.05432
36	1.03880
37	1.04445
38	1.04948
41	1.04227
42	1.04287
43	1.04644
44	1.04637
45	1.04927
46	1.04877
47	1.03531
48	1.03660
49	1.03809
50	1.03917

Table 10.4.3 : Density of Calibration Set A

does not respond to the particle size distribution of the latex. Density might help to deconvolve particle size effects from UV and NIR spectra, just as it did in the earlier chapters on particle sizing by turbidity.

Density was combined with the optical spectra in two ways. First, the density measurement vector was simply added as an extra column in the optical spectra X matrix. Both unscaled and block scaling models were evaluated. Note that MBPLS1 cannot be used in this case because the density measurement block is only rank 1, so only one MBPLS1 dimension could be extracted in the calibration. The second method of combining optical spectra and density recalls that Mie theory predicts that the specific turbidity (τ/C) varies linearly with mean diameter for polymers with refractive indeces close to that of water (Chapter 2). Since density is highly correlated with the polymer fraction in this data set (correlation coefficient = 0.769), dividing each of the absorbances by density may yield better estimates of the mean particle diameter. These ideas were tested on the UV and NIR spectra separately, using the same two examples: total styrene and mean particle diameter.

Table 10.4.4 and 10.4.5 show the y residual variance for PLS1 models that use UV spectra and density to predict total styrene and diameter, respectively. Interestingly, in both cases, when the UV matrix is augmented with density without further scaling, the results is exactly the same as that of UV alone. This is understandable, since the relative variance of the one column of densities is miniscule when compared to the 316 columns of UV absorbances. For total styrene, scaling the UV and density blocks to have equal variance yielded better explanatory power of X on y for the first dimension, but not for any of the subsequent dimensions. UV spectra divided by density also did not improve modelling ability for total styrene. The results are similar for mean diameter. There, UV divided by density gave a better model than simple UV only in the first PLS1 dimension, and comparable or worse models in subsequent dimensions.

	PLS1 Dimension							
	1	2	3	4	5	6	7	8
UV Spectra	0.802	0.256	0.218	0.181	0.083	0.051	0.031	0.025
[UV|ρ] by PLS1 no *X* scaling	0.802	0.256	0.218	0.181	0.083	0.051	0.030	0.025
[UV|ρ] by PLS1 *X* scaling	0.632	0.308	0.241	0.211	0.166	0.067	0.046	0.029
[UV]/ρ by PLS1	0.807	0.287	0.218	0.179	0.067	0.045	0.030	0.024

Table 10.4.4 : Total Styrene Residual Variance from Combined UV Spectra and Density

	PLS1 Dimension							
	1	2	3	4	5	6	7	8
NIR Spectra	0.264	0.071	0.066	0.033	0.016	0.011	0.007	0.006
[UV|ρ] by PLS1 no *X* scaling	0.264	0.071	0.066	0.033	0.016	0.011	0.007	0.006
[UV|ρ] by PLS1 *X* scaling	0.276	0.221	0.067	0.055	0.041	0.012	0.009	0.006
[UV]/ρ by PLS1	0.258	0.077	0.066	0.040	0.023	0.009	0.007	0.005

Table 10.4.5 : Mean Diameter Residual Variance from Combined UV Spectra and Density

Some of the properties for which density would be expected to give important information are the polymer fraction and the water fraction. The correlation coefficient between density and these two compositions is 0.77 and 0.89, respectively. Since NIR spectra also give good predictions of these properties, density and NIR together might improve prediction.

Table 10.4.6 shows the *y* residual variance for PLS1 models using both NIR and NIR augmented with density and scaled to equal block variance. For total polymer, the density gives a large improvement in the modeling power of the first dimension, owing to the high covariance of density with the total polymer concentration. In subsequent dimensions, however, the model including density is worse that just the NIR spectra. For the water calibration, on the other hand, incorporating density is advantageous in all except the fourth dimension. It is interesting to note that the *y* residual variance for a simple, one-parameter linear model between density and water weight fraction is 0.200; so, the first PLS1 dimension of the combined sensors improves on both the NIR and density calibrations. Recalling that the water PRESS/(n-1) was 0.014 after 6 PLS1 components for the NIR calibration (Fig. 9.2.3), the combined sensors reach that level in 5. Table 10.4.7 shows the PRESS/(n-1) as a function of PLS1 dimension for the water calibration for both models. None of the prediction errors is significantly different at PLS dimensions 3 through 8 and, although the combined sensor model gives a minimum PRESS at fewer dimensions, these improvements are not significant and probably do not warrant the purchase of a densitometer to augment the NIR spectrometer.

		PLS1 Dimension							
Constituent	*X*	1	2	3	4	5	6	7	8
Total Polymer	NIR	0.883	0.345	0.211	0.042	0.037	0.026	0.017	0.008
Total Polymer	[NIRρ]	0.432	0.387	0.204	0.200	0.050	0.031	0.022	0.014
Water	NIR	0.459	0.361	0.073	0.013	0.007	0.006	0.004	0.003
Water	[NIRρ]	0.184	0.080	0.062	0.021	0.006	0.004	0.004	0.003

Table 10.4.6 : Residual Variance from Combined NIR Spectra and Density

	PLS1 Dimension							
X	1	2	3	4	5	6	7	8
NIR	0.762	0.436	0.091	0.018	0.015	0.012	0.011	0.012
[NIRρ]	0.210	0.092	0.073	0.028	0.008	0.008	0.009	0.010

Table 10.4.7 : Water PRESS/(n-1) from Combined NIR Spectra and Density

REFERENCES

Abbey, K.J. (1981) "Polymerization Kinetics by Precision Densimetry", in Bassett and Hamielec, 345-356.

Barth, H.G., Ed. (1984) *Modern Methods of Particle Size Analysis*, J. Wiley and Sons, New York.

Bassett, D.R., A.E. Hamielec, Eds. (1981) *Emulsion Polymers and Emulsion Polymerization*, ACS Symposium Series, no. 165, Washington, D.C.

Birth, G.S., H.G. Hecht (1987) "The physics of Near-Infrared Reflectance", in Williams and Norris.

Beyer, G.L. (1987) "Particle Counter for rapid Determination of Size Distributions", *J. Colloid Interface Sci.*, **118**, 1, 137-147.

Brandrup, J., E.H. Immergut, Eds. (1975) *Polymer Handbook*, 2nd Edition, John Wiley & Sons, New York.

Brandolin, A., L.H. Garcia-Rubio (1990) "On-Line Particle Size Distribution Measurement for Latex Reactors", ACS Polymeric Materials Science and Engineering Preprints, **62**, Boston Meeting, Spring 1990.

Brown, R.D., J.E. Glass (1988) "Spectroscopic Determination of Copolymer Composition in High Isocyanate Content Polymers", *J. Appl. Polymer Sci*, **36**, 1909-1923.

Buchanan, B.R., D.E. Honigs (1987) "Detection of Methanol in Gasoline Using Near-Infrared Spectroscopy and an Optical Fiber", *Appl. Spectrosc.* ,**41**, 8, 1388-1392.

Buchanan, B.R., D.E. Honigs, C.J. Lee, W. Roth (1988) "Detection Of Ethanol in Wines Using Optical-Fiber Measurements and Near-Infrared Analysis", *Appl. Spectrosc.* ,**42**, 6, 1106-1111.

Bunville, L.G. (1984) "Commercial Instrumentation for Particle Size Analysis", in Barth.

Burns, N. (1986) *The Statistical Analysis of Light Scattering Data for Polymer Characterization*, M.Eng. Thesis, McMaster University, Hamilton, Ontario.

Cahn, F., S. Compton (1988) Multivariate Calibration of Infrared Spectra for Quantitative Analysis Using Designed Experiments", *Appl. Spectrosc.* ,**42**, 5, 865-872.

Cambell, J.D. (1985) *Emulsion Polymerization of Styrene*, M. Eng. Thesis, McMaster University, Hamilton, Ontario.

Ciurczak, E.W. (1987) "Uses of Near-Infrared Spectroscopy in Pharmaceutical Analysis", *Appl. Spectrosc. Reviews*, **23**, 1&2, 147-163.

Davis, D.M., R.T. Kroutil (1990) "Application of digital filters to process data for ion mobility spectrometry", *Anal. Chimica Acta*, **232**, 261-266.

DeBold, D., D. van Hare (1987) "Analysis of Radioactive Solutions Using a Modified Diode-array Spectrophotometer", Hewlett-Packard UV/VIS Technical Note 87-1.

Depireux, T., F. Dumont, A. Watillon (1987) "Measurement of the Complex Refractive Index of Polyvinyltoluene in the UV, Visible, and Near-IR: Application to the Size Determination of PVT Latices", *J. Colloid Interface Sci.*, **118**, 2, 314-325.

Devaux, M.F., D. Bertrand, P. Robert, M. Quannari (1988a) "Application of Multidimensional Analyses to the Extraction of Discriminant Spectral Patterns from NIR Spectra", *Appl. Spectrosc.*, 42, 6, 1015-1019.

Devaux, M.F., D. Bertrand, P. Robert, M. Quannari (1988b) "Application of Principal Component Analysis on NIR Spectral Collection after Elimination of Interferences by a Least-Squares Procedure", *Appl. Spectrosc.*, **42**, 6, 1020-1023.

Draper, N.R., H. Smith, (1981) *Applied Regression Analysis*, 2nd Ed., John Wiley & Sons, New York.

Donahue, S.M., C.W. Brown, R.J. Obrimski (1988) "Multicompoment Analysis Using Fourier Transform Infrared and UV Spectra", *Appl. Spectrosc.*, **42**, 2, 353-358.

Fitch, R.M (1980) *Polymer Colloids II*, Plenum Press, New York.

Ford, J.R., A.A. Morfesis, R.L. Rowell (1985) "Sedimentation and Light Scattering Studies of Copolymer Latexes", *J. Colloid Interface Sci.*, **105**, 2, 516-520.

Foster, G.N., S.B. Row, R.G. Griskley (1964) "Infrared Sepctrometry of Polymers in the Overtone and Combination Regions", *J. Appl. Polymer Sci.*, **8**, 1357-1361.

Frank, I.E., J.H. Kalivas, B.R. Kowalski (1983) "Partial Least Squares Solutio ıs for Multicomponent Analysis", *Anal. Chem.*, **55**, 11, 1800-1804.

Fuller, M.P, G.L. Ritter, C.S. Draper (1988) "Partial Least-Squares Quantitative Analysis of Infrared Spectroscopic Data, I & II", *Appl. Spectrosc.*, **42**, 2, 217-236.

Gallo, B.M., S. Russo (1974) "Ultraviolet Absorption Spectra of Styrene Copolymers. I.Solvent Effects on the Hypochromism of Poly(strene-co-methyl methacrylate) at 2695 Å", *J. Macromol. Sci. - Chem.*, **A8**, 3, 521-531.

Garcia-Rubio, L.H., N. Ro (1985) "Detailed Copolymer Characterization Using Ultraviolet Spectroscopy", *Can. J. Chem.*, **63**, 253-263.

Garcia-Rubio, L.H. (1987) "Averages from Turbidity Measurements" in Provder.

Garcia-Rubio, L.H. (1989) "Latex Particle Size Distribution from Turbidimetry Using Inversion Techniques", *J. Colloid Interface Sci.*, **129**, 1, 192-200.

Geladi, P., D. MacDougall, H. Martens (1985), "Linearization and Scatter-Correction for Near-Infrared Reflectance Spectra of Meat", *Appl. Spectrosc.*, **39**, 3, 491-500.

Geladi, P., B.R. Kowalski (1986a) "Partial Least Squares Regression: A Tutorial", *Anal. Chim. Acta*, **185**, 1-17.

Geladi, P., B.R. Kowalski (1986b) "An Example of 2-Block Predictive Partial Least Squares Regression with Simulated Data", *Anal. Chim. Acta*, **185**, 19-32.

Greene, C.F., R.A. Conzalez, G.W. Poehlein (1976) in I. Piirma and J.L. Gardon, Ed., ACS Symposium Series 24, Washington, D.C. 341.

Heller, W., W.J. Pangonis (1957a) "Theoretical Investigation on the Light Scattering of Colloid Spheres. I. The Specific Turbidity." *J. Chem. Phys.*, **26**, 498-506.

Heller, W., R.M. Tabiban (1957b) "Experimental Investigation on the Light Scattering of Colloidal Spheres; II: Sources of Error in Turbidity Measurements", *J. Colloid Interface Sci.*, **12**, 25-39.

Hoffman, E.J. (1984) *Kinetic Modelling of Emulsion Copolymerization of Styrene and Acrylonitrile*, M. Eng. Thesis, McMaster University, Hamilton, Ontario.

Höskuldsson, A. (1988) "PLS Regression Methods", *J. of Chemometrics*, **2**, 211-228.

Hruschka, W.R. (1987) "Data Analysis: Wavelength Selection Methods" in Williams and Norris.

Ilari, J.L., H. Martens, T. Isaksson (1988) "Determination of Particle Size in Powders by Scatter Correction in Diffuse Near-Infrared Reflectance", *Appl. Spectrosc.*, **42**, 5, 722-728.

Isaksson, T., T. Næs (1988) "Effect of Multiplicative Scatter Correction (MSC) and Linearity Improvement in NIR Spectroscopy", *Appl. Spectrosc.*, **42**, 7, 1273-1284.

Jones, K.M. (1986) *Copolymerization Kinetics of Methyl Methacrylate/P-Methyl Styrene to High Conversion*, M. Eng. Thesis, McMaster University, Hamilton, Ontario.

Jöreskog K.G., H. Wold, Eds. (1982) *Systems under Indirect Observation; Causality, Structure, Prediction*, North-Holland Publ. Co., Amsterdam.

Kaye, W. (1954) "Near-infrared spectroscopy; I. Spectral identification and analytical applications", *Spectrochimica Acta*, **6**, 257-287.

Kerker, M. (1969) *The Scattering of Light and Other Electromagnetic Radiation*, Acedemic Press, New York.

Kiparissides, C. (1978) *Modelling and Experimental Studies of Continuous Emulsion Polymerization Reactors*, Ph.D. Thesis, McMaster University, Hamilton, Ontario.

Koppel, D.E. (1972) "Analysis of Macromolecular Polydispersity in Intensity Correlation Spectroscopy: The Method of Cumulants", *J. Chem. Phys.*, **57**, 11, 4814-20.

Kourti, T., J.F. Macgregor, A.E. Hamielec (1987) "Minimum Number of Turbidity Measurements Required for the Determination of Particle Size Distributions", *J. Colloid Interface Sci.*, **120**, 1, 292-295.

Kourti, T., J.F. Macgregor, A.E. Hamielec (1987a) "Particle Size Determination using Turbidity Spectra: 1. Estimation of Particle Size Distribution", submitted to *J. Colloid Interface Sci.*

Kourti, T., J.F. Macgregor, A.E. Hamielec (1987b) "Particle Size Determination using Turbidity Spectra: 2. Effect of Errors on the Estimated Particle Size Destribution and the Apparent Diameter Approach", submitted to *J. Colloid Interface Sci.*

Kourti, T., J.F. Macgregor, A.E. Hamielec (1987c) "Particle Size Determination using Turbidity Spectra: 3. Resolution of some Conflicts in the Literature", submitted to *J. Colloid Interface Sci.*

Kourti, T (1989) *Polymer Latexes: Production by Homogeneous Nucleation and Methods for Particle Size Determination*, Ph.D. Thesis, McMaster University, Hamilton, Ontario.

Kvalheim, O.M. (1988) "Interpretation of Direct Latent-Variable Projection Methods and Their Aims and Use in Analysis of Multicomponent Spectroscopic and Chromatographic Data", *Chemometrics and Intell. Lab. Systems*, **4**, 11-25.

Landa, I. (1979) High-Energy Spectrophotometer for Rapid Constituent Analysis in the Range of 0.25-2.4 μm", Rev. Sci. Instrum., **50**, 1, 34-40.

Lee, C.H., R.G. Mallinson (1990) "Surfactant Effects in the Emulsion Polymerization of Vinyl Acetate", *J. App. Polymer Sci.*, 39, 2205-2218.

Levenspiel, O (1972) *Chemical Reaction Engineering*, 2nd. Ed., John Wiley & Sons, New York.

Lindberg, W., J.A. Persson, S. Wold (1983) "Partial Least-Squares Method for Spectroflourimetric Analysis of Mixtures of Humic Acid and Ligninsulfonate", *Anal. Chem.*, 55, 4, 643-648.

Lorber, A., L.E. Wangen, B.R Kowalski (1987) "A Theoretical Foundation for the PLS Algorithm", *J. of Chemometrics*, 1, 19-31.

Lorber, A., B.R. Kowalski (1988) "A Note on the Use of the Partial Least Squares Method for Multivariate Calibration", *Appl. Spectrosc.*, 42, 8, 1572-1574.

Manne, R. (1987) "Analysis of two partial-least-squares algorithms for multivariate calibration", *Chemometrics and Intelligent Lab. Systems*, 2, 187-197.

Martens, H., T. Næs (1984a) "Multivariate Calibration: I. Concepts and Distinctions", *Trends in Analytical Chem.*, 3, 8, 204.

Martens, H., T. Næs (1987) "Multivariate Calibration by Data Compression" in Williams and Norris.

Martens, H., T. Næs (1984b) "Multivariate Calibration by Data Compression", in Martens (1985), 167-286.

Martens, H.A. (1985) *Multivariate Calibration: Quantitative Interpretation of Non-Selective Chemical Data*, Dr. techn. thesis, Technical University of Norway, Trondheim.

Martens, H.A., L. Izquierdo, M. Thomassen, M. Martens (1986) "Partial Least-Squares Regression on Design Variables as an Alternative to Analysis of Variance", *Anal. Chim. Acta*, 191, 133-148.

Maxim, L.D., A. Klein, M.D. Meyer, C.H. Kuist (1969) "Particle Size Distribution by Turbidimetry", *J. Polymer Sci. Part C*, 27, 195-205.

Miller, C.E., (1989) "Analysis of EPDM Terpolymer by Near-Infrared Spectroscopy and Multivariate Calibration Methods", *Appl. Spectrosc.*, 43, 8, 1435-1443.

Miller, R.G., H.A. Willis (1956) "Quantitative Analysis in the 2μ Region Applied to Synthetic Polymers" *J. Appl. Chem.*, 6, 385-391.

Mittlefehldt, E.R., J.A. Gardella Jr. (1989) "Quantitative Fourier Self-Deconvolution and Fourier Transform Infrared Analysis of Bisphenol-A-Polycarbonate/Poly(dimethylsiloxane) Random Block Copolymers", *Appl Spectrosc.*, 43, 7, 1172-1179.

Næs, T., T. Isaksson (1990) "Locally Weighted Regression and Scatter Correction for Near-Infrared Reflectance Data", *Anal. Chem.*, 62, 664-673.

Næs, T., H. Martens (1985) "Comparison of Prediction Methods for Multicollinear Data", *Commun. Statist. - Simula. Computa.*, 14, 3, 545-579.

Nicoli, D.F. (1987) *NICOMP Model 370 Submicron Particle Sizer Version 5.0: Instruction Manual*, Pacific Scientific Instrument Division, Silver Spring, MD.

Nomura, M., M. Harada (1981) "On the Optimal Reactor Type and Operation for Continuous Emulsion Polymerization", in D.R. Basset and A.E. Hamielec, 121-143.

Nyquist, R.A. (1987) "Infraared Study of Styrene-Acrylonitrile Copolymer at a Variable Temperature" *Appl. Spectrosc.* **41**, 5, 797-800.

Olsen, E.D. (1975) *Modern Optical Methods of Analysis*, McGraw-Hill, New York.

Penlidis, A. (1986) *Polymer Reactor Design, Optimization and Control in Latex Production Technology*, Ph.D. Thesis, McMaster University, Hamilton, Ontario.

Provder, T., Ed. (1987) *Particle Size Distribution; Assessment and Characterization*, ACS Symposium Series, no. 332, Washington, D.C.

Pollock, M.J. (1983) *Modelling and Control of Sustained Oscillations in the Continuous Emulsion Polymerization of Vinyl Acetate*, Ph.D. Thesis, McMaster University, Hamilton, Ontario.

Ramelow, U., Baysal, B.M. (1986) "Copolymer Analysis by UV Spectroscopy", *J. Appl. Polymer Sci.*, 32, 7, 5865-5882.

Rowell, R.L., J.R. Ford, J.W. Parsons, D.R. Bassett (1980) "Wide Angle Light Scattering Investigation of the Interval Structure of Polymer Latexes", in Fitch, 27-37.

Rowell, R.L., J.R. Ford (1981) "Characterization of Latex Particles by Light Scattering", in Bassett and Hamielec, 85.

Sauer, B.B., R.S. Stock, K.-H. Lim, W.H. Ray (1990) "Polymer Latex Particle Size Measurement through High Speed Dielectric Spectroscopy", *J. App. Polymer Sci.*, 39, 2419-2441.

Schork, F.J., W.H. Ray (1981) "On-Line Monitoring of Emulsion Polymerization Dynamics", in Bassett and Hamielec, 505-514.

Sharabash, M.A., R.L. Guile (1976) "Determination of Copolymer Composition by Quantitative Infrared Analysis", *J. Macromol. Sci. - Chem.*, **A10**, 6, 1021-1038.

Sharaf, M.A., D.L. Illman, B.R. Kowalski (1986) Chemometrics, John Wiley & Sons, New York.

Shashidhar, G.V.S., K.R. Rao, N. Satyanarayana, E.V. Sundaram (1990) "Spectroscopic Methods for the Determination of Composition in Styrene-Methacrylate Copolymers", *J. Polymer Sci. C*, **28**, 157-161.

Smith, C.L., R.E. Klie (1976) *On-Line Process Measurements*, Notes for AIChE Continuing Education Course, AIChE, New York.

Stark, E., K. Luchter, M. Margoshes (1986) "Near-Infrared Analysis (NIRA): A Technology for Quantitative and Qualitative Analysis", *Appl. Spectrosc. Reviews*, **22**, 4, 355-339.

Stevenson, A.F., W. Heller, M.L. Wallach (1961) "Theoretical Investigations on the Light Scattering of Colloidal Spheres. XI. Determination of Size Distribution Curves from Spectra of the Scattering Ratio or from Depolarization Spectra", *J. Chem. Phys.*, **34**, 5, 1789-95.

Stock, R.S., W.H. Ray (1985) "Interpretation of Photon Correlation Spectroscopy Data: A Comparison of Analysis Methods", *J. Polymer Sci: Polymer Physics*, **23**, 1393-1447.

Stock, R.S., W.H. Ray (1987) "Measuring Particle Size Distribution of Latex Particles Using Dynamic Light Scattering", in Provder.

Taboudoucht, A., H. Ishida (1989) "Diffuse Transmittance Spectroscopy of Polymeric Fibers", *Appl. Spectrosc.*, **43**, 6, 1016-1021.

Tenge, B., B.R. Buchanan, D.E. Honigs (1987) "Calibration of Fiber Optic Region of the Near-Infrared", *Appl. Spectrosc.*, **41**, 5, 779-785.

Thomas, E.V., D.M. Haaland (1990) "Comparison of Multivariate Calibration Methods for Quantitative Spectral Analysis", *Anal. Chem.*, **62**, 1091-1099.

Thomas, J.C. (1987) "The Determination of Log Normal Particle Size Distribution by Dynamic Light Scattering", *J. Colloid Interface Sci.*, **117**, 1, 187-192.

Urban, M.W., J.L. Koenig, L.B. Shih, J.R. Allaway (1987a) "Structure of Styrene/Acrylic Acid Copolymer in Aqueous Solution Determined by Fourier Transform Infrared Spectroscopy", *Appl. Spectrosc.*, **41**, 4, 590-596.

Urban, M.W., J.L. Koenig (1987b) "Spectroscopic Studies of Interaction between Styrene/Acrylic Acid Copolymer and Sodium Dodecyl Sulphate", *Appl. Spectrosc.*, **41**, 6, 1028-1032.

van de Hulst, H.C. (1957) *Light Scattering by Small Particles*, John Wiley & Sons, New York.

Wallach, M.L., W. Heller, Stevenson, A.F. (1961) "Theoretical Investigations on the Light Scattering of Colloidal Spheres. XII. The Determination of Size Distribution Curves from Turbidity Spectra", *J. Chem. Phys.*, **34**, 5, 1796-1802.

Wasmund, E.B. (1991) Personal Communication. Data from M.Eng. Thesis, McMaster University.

Weast, R.C., Ed. (1980) *CRC Handbook of Chemistry and Physics*, 60th edition, CRC Press, Inc., Boca Raton, Florida.

Weiner, B.B, W.W. Tscharnuter (1987) "Uses and Abuses of Photon Correlation Spectroscopy in Particle Sizing", in Provder.

Weyer, L.G. (1985) "Near-Infrared Spectroscopy of Organic Substances", *Appl. Spectrosc. Review*, **21**, 1 & 2, 1-43.

Weyer, L.G., K.J. Becker, H.B. Leach (1987) "Remote Sensing Fiber Optic Probe NIR Spectroscopy Coupled with Chemometric Data Treatment", *Appl. Spectrosc.*, **41**, 5, 786-790.

Williams, P., K. Norris (1987) *Near-Infrared Technology in the Agriculture and Food Industries*, Ammerican Assoc. of Cereal Chemists, St. Paul, Mimmesota.

Williams, R. (1989) "Applications of Fourier Transform Spectrometry in the Ultraviolet, Visible, and Near-IR", *Appl. Spectrosc. Reviews*, **25**, 1, 63-79.

Wiscombe, W.J. (1979) *Mie Scattering Calculations; Advances in Technique And Fast, Vector-Speed Computer Codes*, Near Tech Note Tn-140+Str, National Center For Atmospheric Research, Boulder, Colorado.

Wiscombe, W.J. (1980) "Improved Mie Scattering Algorithms", *Appl. Opt.*, **19**, 1505-1509.

Wiscombe, W.J. (1988) "Further Improvements in Mie Scattering Algorithms", *Appl. Opt.* (In Preparation)

Wold, H. (1966) "Estimation of Principal Components and Related Models by Iterative Least Squares", in P.R. Krishnaiah, Ed., *Multivariate Analysis*, Acedemic Press, New York, 391-420.

Wold, H. (1982) "Soft Modeling: the Basic Design and Some Extensions", in Jöreskog and Wold.

Wold, S. (1978) "Cross-Validatory Estimation of the Number of Components in Factor and Principal Components Models", *Technometrics*, 20, 4, 397-405.

Wold, S., H. Martens, H. Wold (1982) "The Multivariate Calibration Problem in Chemistry Solved by the PLS Method", *Lecture Notes in Mathematics*, Springer Verlag, Heidelberg.

Wold, S., C. Albano, W.J. Dunn III, U. Edlund, K. Esbensen, P. Geladi, S. Hellberg, E. Johansson, W. Lindberg, M. Sjöström (1984) "Multivariate Data Avalysis in Chemistry" in B.R. Kowalski, Ed., *Chemometrics: Mathematics and Statistics in Chemistry*, D. Reidel, Dordrecht.

Wold, S., M. Sjöström, R. Carlson, T. Lundstedt, S. Hellberg, B. Skagerberg, C. Wikström, J. Öhman (1986) "Multivariate Design", *Anal. Chim. Acta*, 191, 12-32.

Wold, S., S. Hellberg, T. Lundstedt, M. Sjöström, H. Wold (1987) "PLS Modeling with Latent Variable in Two of More Dimensions", manuscript prepared for the Frankfurt PLS meeting, Sept, 1987.

Wold, S., N. Katteneh-Wold (1989), Personal Communication.